TEM/EDXS STUDIES OF PHASE SEPARATION IN BLOCK AND GRAFT COPOLYMERS

by

GREG ALLEN YORK

Thesis submitted to the Faculty of the

Virginia Polytechnic Institute and State University

in partial fulfillment of the requirements for the degree of

MASTER OF SCIENCE

in

MATERIALS ENGINEERING

APPROVED:

David W. Dwight, Chairman

James E. McGrath

Jack L. Lytton

19 May, 1987

Blacksburg, Virginia

ABSTRACT

The relationships between molecular parameters and microdomain formation of a variety of block- and graft-copolymers were studied by Transmission Electron Microscopy (TEM). Molecular variables included chemical composition: dimethyl-, fluoropropyl and diphenyl-siloxane, sulfone styrene, paramethylstyrene, t-butylstyrene, arylester and methyl methacrylate, as well as molecular weight and distribution. Effects of the kinetics of phase-separation were also determined. Thick (approximately 1mm) films cast from solvent showed more complete phase separation than either thin (about 10nm) cast films or compression-molded specimens.

Spherical domains formed in alternating poly(ester/siloxanes), and phase mixing seemed to correlate with the solubility parameters of the three siloxane types. Shear-stresses during molding changed domain shapes and eliminated short-range ordering. In the PMMA-graft-dimethyl siloxane system, 5K, 10K and 20K $\langle M_n \rangle$ siloxanes were incorporated at 16% and 45% by weight. At 16 %, spherical siloxane domains formed in both thick- and thin-cast films. The domain sizes and interdomain distances scaled with siloxane molecular weight and total block molecular weight respectively to a 2/3 power law in excellent agreement with

theoretical predictions for di- and triblock copolymers. Thin films cast from the 45 % siloxane graft copolymers also showed spherical domains with sizes dependent on molecular weight. However, the thick films showed phase transitions from disordered bicontinuous (M_n = 5K) to lamellar (M_n = 10K) to cylindrical (M_n = 20K). Qualitative TEM/EDX analysis of other systems was used to identify oligomers, homopolymers, and contaminants, thus monitoring the effects of novel reaction conditions and work-up procedures.

ACKNOWLEDGEMENTS

I wish to thank Dr. D. Dwight and Dr. J. E. McGrath for their support during the conception and completion of this project.

I would like to extend my thanks to Steve Smith for many insightful discussions, providing the majority of the polymers utilized in this study and his exceptional cooperation in completing the essential link between the macromolecular chemist and engineer.

I also want to thank Dr. G. L. Wilkes for some useful suggestions and Steve Mcartney for his help in maintaining instrumentation in peak operational condition.

TABLE OF CONTENTS

LIST OF FIGURES

LIST OF TABLES

CHAPTER I

INTRODUCTION

1.1 Objectives

In the past, electron microscopy has played an important role in the evaluation of solid state microstructure of many polymer materials. With the advent of hybrid AEM machines (combining TEM, STEM, SEM and EDX) and increased operator friendliness, electron microscopy has increased its importance as a standard analytical technique for polymers morphology determination. Unfortunately, the body of literature dealing with electron microscopy of polymers is not as extensive as it is for many other types of materials. Additionally, many studies that utilize TEM analysis on a variety of polymer systems, deal with well established polymer systems often with no mention of any problems incurred during TEM analysis. It is from this aspect that some basic guidelines to aid the evaluation of the solid state microstructure of a variety of multiphase polymers by TEM/EDX analysis are proposed.

There are several basic objectives for the studies performed in this dissertation, which may be divided into

three basic categories. The first is to serve as a guide to the microstructural analysis of novel copolymer systems through standardization of qualitative analysis techniques. Qualitative analysis may be loosely defined as TEM/EDX analysis of thin-cast films for the purpose of gaining insight into the microstructural behavior of multiphase systems. The ease and quickness in which qualitative analysis may be performed allows it to be used as a precursor to subsequent microstructural analysis under the desired processing conditions. The various uses and limitations of qualitative outlined in this thesis are applicable to variety of multiphase polymer systems.

Another objective is to demonstrate the utility of quantitative image analysis of TEM micrographs as a less subjective method of determining the interdomain spacings, domain size and distribution of sizes. Historically these type of quantitative measurements from TEM micrographs are obtained measurement made by hand.

The last objective is to use SAXS data, qualitative and quantitative analysis coupled with compositional and molecular weight analysis to help delineate the nature of the microphase separated behavior of methacrylate-siloxane macromer graft copolymers with different compositions and varying graft molecular weight. In addition, the microstructural behavior of arylester-siloxane perfectly

alternating copolymers with varying siloxane character under various processing conditions will be studied.

CHAPTER II

LITERATURE REVIEW

2.1 Phenomenological Aspect of Multiblock Systems

2.1.2 Diblock and Triblock Systems

The theoretical and phenomenological aspects of the morphological behavior of pure multiblock polymers has been thoroughly covered in the literature. However with the advent of new synthesis techniques, and therefore novel multiblock systems, there is a growing need to further correlate real system behavior to theory. This section will cover the phenomenological aspect of multiblock polymers and the theoretical facet will be treated in the following section.

The potential of multiblock systems has been realized as early as Alfrey's[1] book on copolymerization. He theorized that the presence of long sequences of a certain monomer in a copolymer could result in incompatibility on a submicroscopic level. And further theorized that such material may have properties different than either a random polymer or a blend of two homopolymers of the same chemical nature.

The possibility of periodic arrangements of microphases were recognized in early work on soap gels[2,3]. In these systems it was concluded from SAXS, that the soap molecules took up lamellar, cylindrical and spherical states of aggregation, which could then give rise to one, two or three dimensional periodic sequences. These studies laid the foundation for the classification of the three basic morphologies of regular block copolymers.

Skoulios et al.[4] was the first to observe these structures by SAXS in block copolymers of polystyrene and polyethylene oxide. But not until the advent of anionically polymerized Styrene-Butadiene (SB or SBS) block copolymers that well controlled block length and distributions were made possible. With this very precise control over block chemistry it was possible to systematically vary the volume fraction of each block over the full range of compositions. One of the first commercially important block copolymers was marketed by Shell Chemical Company under the trade names THERMOLASTIC and KRATON[6-8]. With the commercial significance of these systems growing they became the topic of intense scientific investigations. Hendus et al.[9] were among the first to work with SBS systems. Using TEM of both microtomed sections and thin cast films as well as SAXS, IR and torsional braid analysis they were able to recognize the transitions from spherical to cylindrical to lamellar

morphology as a function of composition. And that the molecular weight for the same block ratio determined the scale of the structure. A generalized scheme for the solid state morphology of copolymers as a function of block composition is shown in Figure 2.1. Comparable results were attained by Lewis and Price[10], Beecher et al.[11,12], Inoue et al.[13,14] and Matsuo[15].

In what perhaps was one of the most comprehensive work in this field at the time, Kampf et al.[16] while confirming the previous results, also noticed that the annealed specimens revealed a long range order that could extend over very large areas. These areas appeared to have various orientations much like grains of crystallinity and exhibited amazing uniformity (Figure 2.2 and 2.3).

In these systems, convention dictated the minor component as A and was always present as the dispersed phase. The morphological dependence on weight fractions of A (W_A) found from these studies is as follows:

1. If $W_A < Ø.3$, then discrete spherical domains of A in a B matrix were found.
2. If $Ø.15<W_A<Ø.4$, then cylinders of A were observed in a matrix of B.
3. If $Ø.4<W_A<Ø.5$, then a lamellar structure was observed.

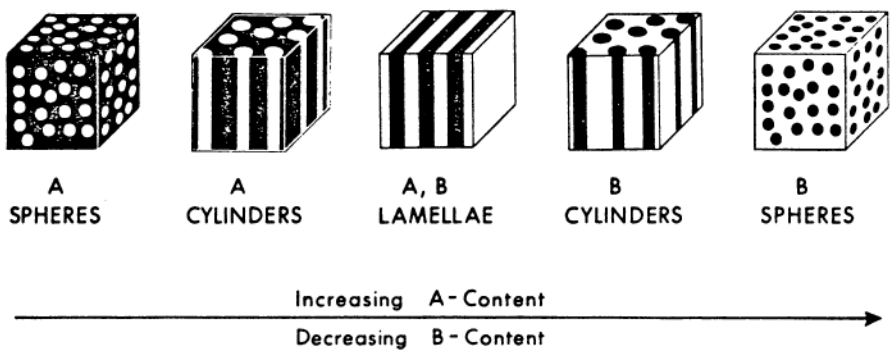

Figure 2.1 Generalized scheme of block copolymer morphology as a function of composition (reference 5).

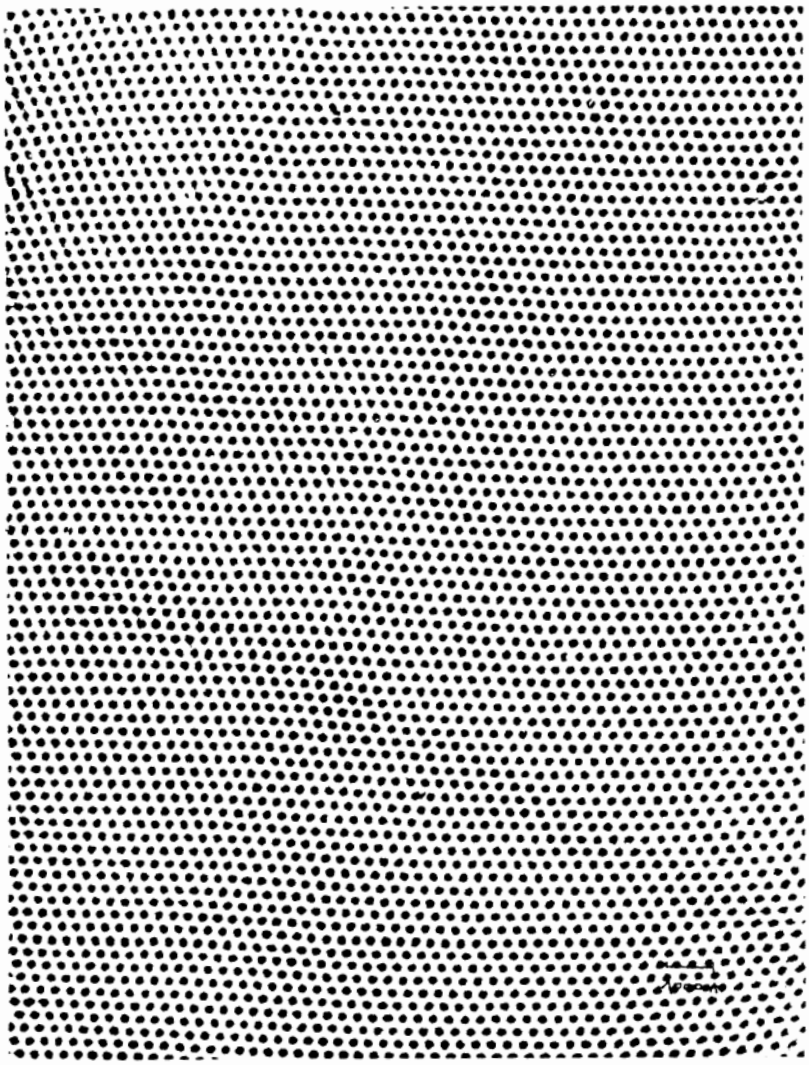

Figure 2.2 TEM micrograph of SB block copolymer containing 68 Wt. % Styrene showing various structural orientation (Kampf et al.[16]).

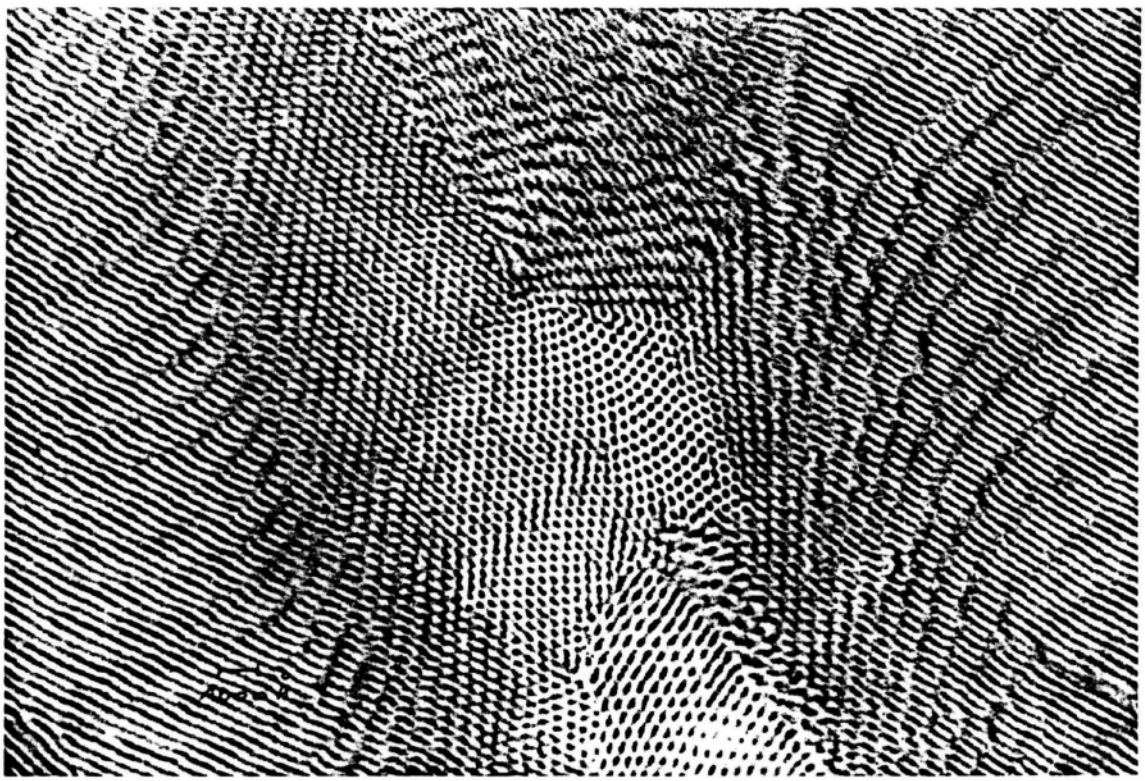

Figure 2.3 TEM micrograph of SB block copolymer containg 68 Wt. % styrene, demonstrating long range ordering (Kampf et al.[16]).

As these research efforts concentrated on the composition dependence of morphological texture others have looked at processing conditions as a variable. In the most liberal terms, a processing condition can be thought of as the parameters surrounding history of the formation solid state microstructure. Which typically involves both the thermodynamic and kinetic aspects of the formation of the solid state. Lewis and Price[17] performed TEM studies of the solid state structure of SBS cast from benzene at various evaporation rates. They found that the films exhibited a very regular morphological texture, with the exception of those cast at a very high rate of evaporation. Fischer[18] also showed by TEM analysis of thin cast films, that by slowing the evaporation rate, the SBS was able to form a hexagonal lattice of styrene cylinders.

Inoue et al.[16] studied both the effect of initial concentration of the solution on domain structure and the change of domain structure with various casting solvents. The results indicate that no significant microstructural differences observed when the solution concentration was kept below the critical concentration value of about 1Ø %. Also as the solvating power of the solvent was changed sufficiently to preferentially favor one component that component was favored as the continuous phase. This is

further supported by the milky white appearance of the solution caused by the suspension of the unfavored precipitated phase.

One of the most striking examples of how processing conditions affect the morphological texture is by Keller and associates[19]. In this study SBS samples were extruded then annealed and sectioned in directions perpendicular and parallel to the direction of extrusion. Results demonstrated complete orientation of the hexagonally packed polystyrene rods in the extrusion direction.

Juliano et al.[46] reported on the synthesis and characterization of a series of Polymethylmethacrylate-polysiloxane (PMMA-b-PSX) diblocks. In this study, TEM analysis of thin cast films revealed that siloxane formed discrete spherical domains (Figure 2.4) for compositions of approximately 22 and 34 wt.% siloxane. Though it should be noted that due to the presence of various side reactions common in the anionic polymerization of PMMA-b-PSX system the molecular weight distributions are not as narrow and defined as in the S-I or S-B systems.

Other historical perspectives of Diblock and Triblock systems include Aggarwal[20], Folkes and Keller[21] and Block and Graft Copolymers edited by Burke and Weiss[22].

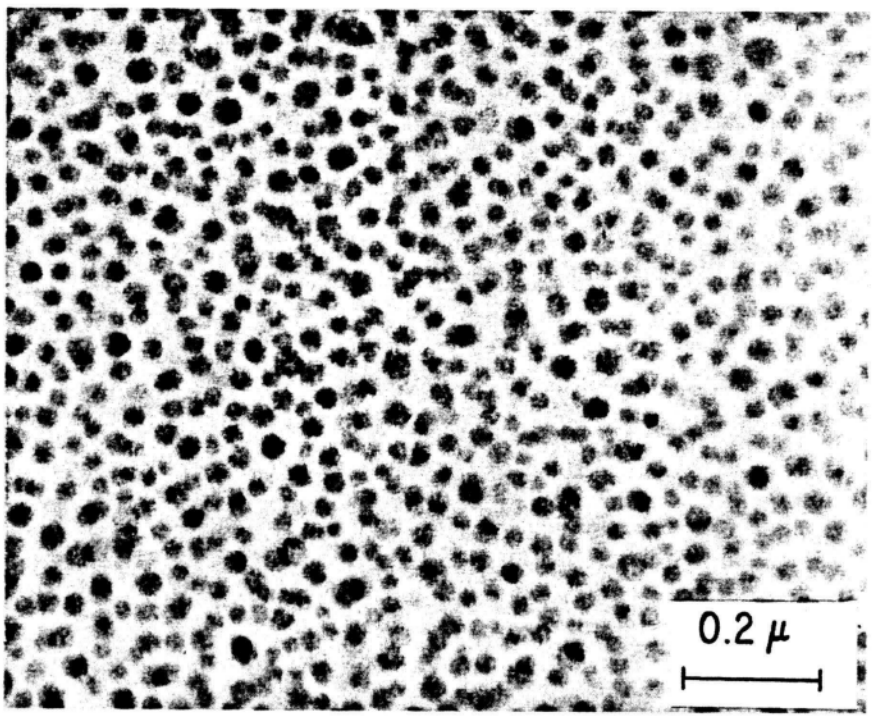

Figure 2.4 TEM micrograph of PMMA-b-PSX 22 Wt. % PSX thin-cast film (reference 46).

2.1.2 Star Blocks

The number of publications on the solid state behavior of star block copolymers is very small compared the number of studies published on linear block copolymers. However, some of the most dramatic effects on the texture of the domain structure through changes in the molecular architecture have been observed in comparisons of star blocks vs their linear counterparts (diblocks and triblocks). A schematic representation of various types of block architectures are illustrated in Figure 5a.

The first investigation into the molecular architectural effects on microdomain structure was conducted by Price et al.[23] on a series of diblock, triblock, three- and four- armed star block copolymers of styrene and isoprene (keeping volume percent constant at about 24 % styrene). TEM analysis revealed that solvent cast films exhibited hexagonally packed styrene cylinders in a isoprene matrix for all arm numbers. Support for this result came from Alward et al.[24] by reexamination of data from Bi and Fetters[25] who concluded on a basis of volume fraction calculations on six and nine-armed SI star blocks containing approximately 25 vol % polystyrene, that the microstructure consisted of a BCC array of styrene spheres in an isoprene matrix. The reexamination revealed that the proper interpretation of the results were that of hexagonally

A-B Block Copolymer

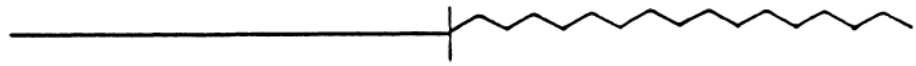

A-B-A Block Copolymer

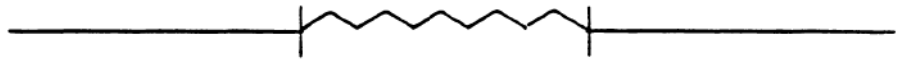

$(A-B)_n$ Block Copolymer

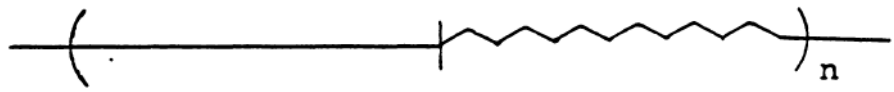

Radial Block Copolymer

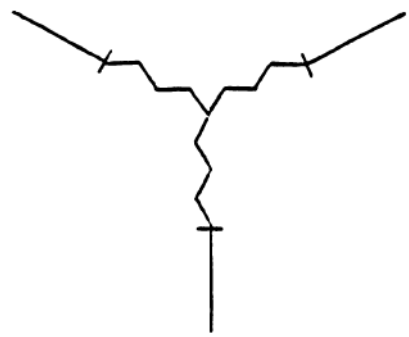

Figure 2.5a Schematic of various block copolymer architectures.

packed cylinders of styrene in an isoprene matrix, which is in agreement with Price[23].

Other studies on the solid state structures of star blocks include Bi et al.[26,27], Pedemont et al[28], Meyer and Widmaier[29] and Leblanc[30]. However, in these studies there is often ambiguous results and very little systematic work on the effect of molecular weight and number of arms has on the nature of the morphological texture, and therefore they do not provide a complete analysis of the solid state properties of star blocks.

Nevertheless very recent studies[24,31-33] have undertaken this issue and provided a very complete picture of the solid state behavior of star blocks. Alward et al.[24] studied samples consisting of about 30 Wt. % polystyrene (at the free end of the arm). The star blocks investigated had 2, 4, 8, 12, or 18 arms and total arm molecular weights of 2.3×10^3, 3.3×10^4 and 1×10^5.

This study showed that star blocks exhibit a transition from hexagonally packed polystyrene cylinders in a poly-isoprene matrix to a new ordered bicontinuous morphology, dependent on both the molecular weight of the arm and the number of arms per star. This transition to the ordered bicontinuous structure is thermodynamically favored if either the number of arms per star or the molecular weight of the arms is increased. A subsequent supporting study by

Thomas et al.[34], showed that a nonpreferential solvent-cast sample exhibited the same transitions to the ordered bicontinuous structure as the annealed specimens, and thus it was concluded that the annealing procedure did not transform the morphology. Further discussion on the nature of this new equilibrium morphology are also given. In Figure 2.5b a schematic representation of the ordered bicontinuous double-diamond structure is given. The supporting TEM micrographs for each projection are shown in Figure 2.6.

2.1.3 Macromer Graft Copolymers

Macromers are linear macromolecules that typically contain a polymerizable function at either one or both chain ends. These macromonomers can be copolymerized with a vinyl or acrylic species and with incorporation of each macromonomer unit into the chain a graft is formed. Siloxanes macromers were among the first to be prepared and synthesized in 1962[36]. But not until recently have macromers begun to received proper attention[37-39]. A great deal of interest in siloxane containing macromers has been due to the well defined PMMA-PSX and PS-PSX systems prepared by Yamashita et al.[40-42]. Who subsequently studied the preferential segregation of the siloxane component to the surface, which prompted other studies stressing the

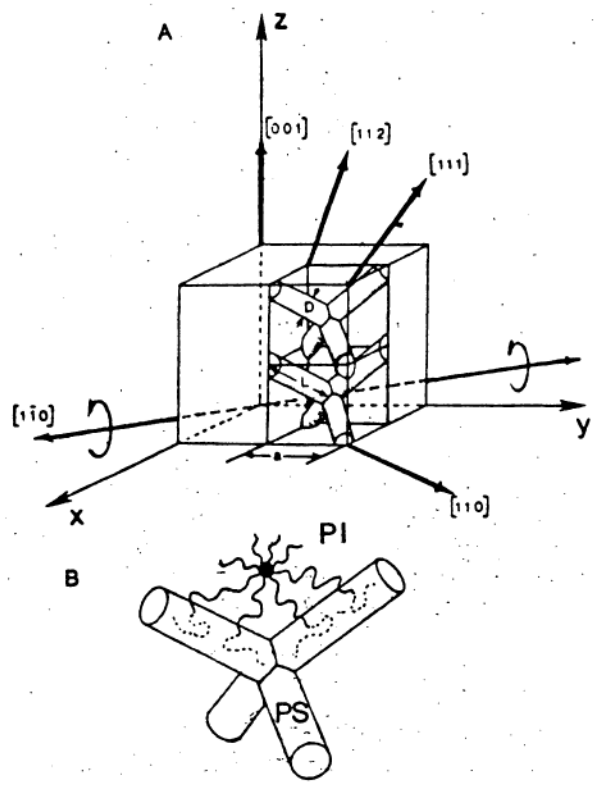

Figure 2.5b Schematic illustration of the ordered bicontinuous morphology (reference 35).

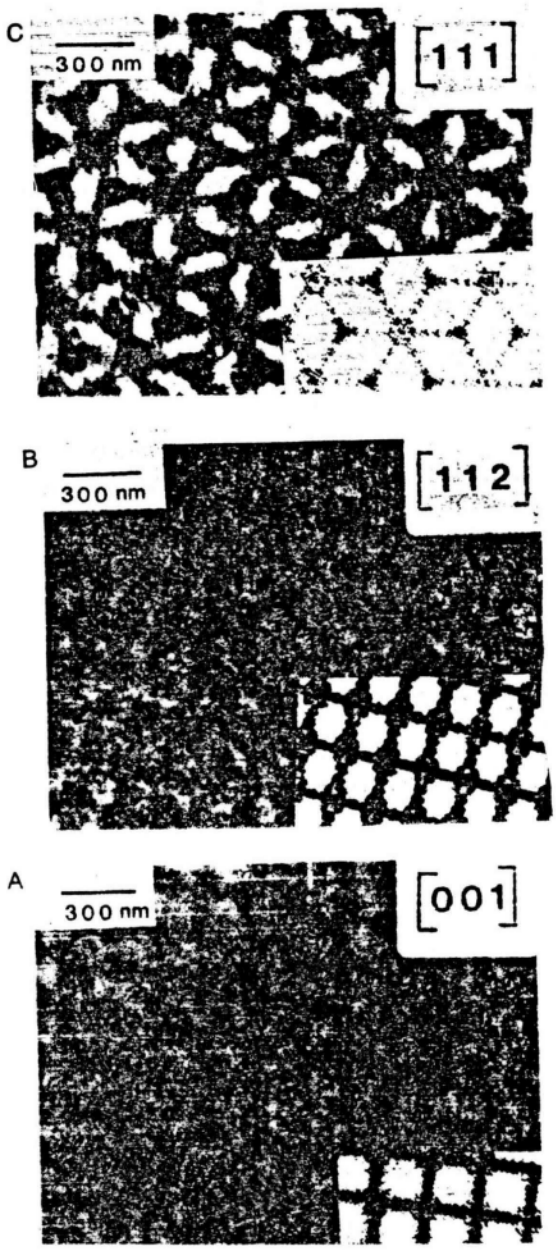

Figure 2.6 TEM micrographs of (A) [1ØØ] projection (B) [112] and (C) [111] projections of the ordered biconituous microstructure (reference 35).

possibility of surface modification[43]. Other research on PMMA-PSX macromers has been reported by Cameron[44] and Kawakami[45]. Nevertheless there have really been no detailed systematic study of the nature of the phase separated solid state behavior of these systems. It is from this viewpoint that the study of PMMA-PSX macromer graft systems has been undertaken in this thesis.

2.2 Theory of Phase Separation in Block Copolymer

2.2.1 Criteria For Phase Separation

When blended, two dissimilar homopolymers are usually incompatible and typically exhibit macrophase separated behavior. In thermodynamic terms, the state of mixing in polymer blends is determined by the free energy of mixing G_M, which consists of the following terms:

$$\Delta G_M = \Delta H_M - T\Delta S_M \qquad (1)$$

where ΔH_M is the change in enthalpy upon mixing and ΔS_M is the entropy change on mixing. In Flory's treatment ΔH_M takes the form of a Van Laar type expression and is related to the Hilderbrand solubility parameter δ of the polymers via χ the Flory interaction parameter as follows:

$$\Delta H_M = X \, \phi_1 \, \phi_2 \qquad (2)$$

and

$$X = (\delta_1 - \delta_2)^2 / kT \qquad (3)$$

This expression for the enthalpy of mixing is always positive (endothermic) and is valid for only species whose interaction are nonspecific in nature (only Van der Waals forces present). Consequently, in this treatment the only driving force toward miscibility is the entropy of mixing. Miscibility may be induced by an exothermic enthalpy of mixing created by the presence of specific interactions or volume change that occur during mixing.

The first insight into the quantification of the entropy term came from Flory's fixed volume lattice model[47]. In this treatment Flory formulated his expression for the combinatorial contribution to the entropy of mixing as:

$$\Delta S_M^{(c)} = -R(\phi_1 / V_1 \ln\phi_1 + \phi_2 / V_2 \ln\phi_2) \qquad (4)$$

where ϕ_i is the volume fraction of component i and V_i is the molar volume of component i which is directly proportional to the molecular weight. From this it is clear that under

the limits of high molecular weights the combinatorial entropy associated with mixing is quite small (approximately Ø). Since most practical polymer application use high molecular weights (above 3Ø,ØØØ) it is quite reasonable to assume that the combinatorial entropy does not contribute to the miscibility of most homopolymer blends. Assuming no volume change occurs upon mixing, this is the primary reason for the observed incompatibility of most dissimilar polymer pairs.

Substitution of equations 2, 3 and 4 into equation 1 and solving for the product of the degree of polymerization and interaction parameter at the critical point (where phase separation is no longer favored $\Delta G_M > Ø$) yields the critical characteristic parameter shown below:

$$(\chi N)_c = 4 \qquad (5)$$

where N is the degree of polymerization. Equation 5 is calculated on the basis that equal volume fractions of each component are present in the system (each homopolymer has N/2 monomer units and the same density).

Although block polymers may have the similar thermodynamic driving forces toward incompatibility they are prevented from separating by a chemical bond. The covalent bond between unlike blocks considerably changes the nature

of phase separation in the system. The microphase separation transition phenomena has been treated by Leibler[48] for the case of diblocks and by Sanchez et al. [49] for the case of simple graft and star block copolymers. It was found that f (the fraction of component A in an AB copolymer chain) and the product χN were the only relevant parameters needed to describe critical phase behavior. An additional parameter τ (the fractional position along the A backbone in which a B graft is attached) is required to describe the phase behavior a graft copolymer. The parameter τ is defined such that when τ is Ø or 1 it degenerates to a diblock copolymer.

In this treatment of the theory of the phase separation transition it is assumed that the correlation length (proportional to the polymer chain length) is sufficient that the mean field theory is applicable to the compositions studied. Correlation length is proportional to the area of the phase diagram in which the mean field theory may be applied. Essentially the system is characterized by concentration fluctuations (in the form of the Fourier transforms of an order parameter $\Delta p_A(r)$) and a static structure factor S(q) (the monomer density-density correlation function) which is determined from scattering experiments and is the link that relates theory to experiments. The static structure factor is defined as follows:

$$S(q) \equiv 1/V\langle p\rangle^2 \int [\exp(iq\cdot r)]\ \langle \Delta p_A(r)\Delta p_A(\emptyset)\rangle\ dr \qquad (6)$$

where V is the system volume, $\Delta p_A(r)$ is the difference between the monomer density of component A $\langle p\rangle$ at point r ($\langle p_A\rangle(r) + \langle p_B\rangle(r) = \langle p\rangle$) and the canonical average of the local density (f $\langle p\rangle$). The value for q, the reciprocal space scattering vector, is given as $q = (4\pi/\Gamma)\sin(\theta/2)$. And is subsequently determined from parameters in the scattering experiments, where Γ is the wavelength of the radiation source and θ is the scattering angle. The contribution of the density fluctuation to the free energy is given as

$$F/kT = F_0/kT + 1/2V\langle p\rangle \Sigma\ (\Delta p_{A_q}\ \Delta p^*_{A_q})/S(q) + \qquad (7)$$
$$\text{higher order terms in } p_{A_q}$$

where Δp_{A_q} is the Fourier transform of $\Delta p_A(r)$ and p^*A_q is its complex conjugate, this assures that real values are obtained from the product. At the critical point (a second order transition) the higher order terms will drop out.

The most probable concentration fluctuations occur when S(q) is a maximum. Density fluctuations tend to increase the free energy of phase separation. For large values of q, S(q)

scales as q^{-2} and scattering values approach that of a single chain (miscible system). In macrophase separated systems (e.g., blended hompolymers), the maximum S(q) occurs at q = Ø and represents concentrations fluctuations of infinite wavelength. Generally S(q) will pass through a maximum at q*. At the spinodal point S(q*) approaches infinity, and the characteristic value of χN at this point is defined as $(\chi N)_s$. The disorder-order transition occurs at $(\chi N)_T$ with $(\chi N)_T \geq (\chi N)_s$. The critical value occurs when $(\chi N)_T = (\chi N)_s$ and is as previously defined by $(\chi N)_c$. At the critical value the phase transition is second order and is first order anywhere else.

Subsequent calculations by Liebler yielded a value of $(\chi N)_c$ = 1Ø.5 for a diblock of 5Ø:5Ø composition (f = Ø.5). This composition was found to be the only transition at which diblocks exhibit a second order transition, all other transitions are first order. For other compositions Ø.3 < f < Ø.7, values for $(\chi N)S$ range from 1Ø-15. In contrast, at composition f = τ = Ø.5 for graft copolymers, $(\chi N)_s$ = 13.5 and no second order transitions are observed throughout the full range of compositions. Comparison of $(\chi N)_s$ values for homopolymer blends, diblocks and graft copolymers reveal several important aspects of critical phase behavior. From classical treatments χ has been shown to be proportional to 1/T (T is temperature). Comparison of

$(\chi N)_s$ or $(\chi N)_c$ for a diblock of f = Ø.5 to corresponding homopolymers of 5Ø:5Ø composition, shows that the degree of polymerization needed for phase separation increases or the critical temperature required for phase separation decreases by a factor of 2.6 for the diblock copolymers. This implies that the phase separation is more difficult for diblocks than for homopolymers of comparable compositions. Again comparison of the graft (f = τ = Ø.5) and diblock (f = Ø.5) $(\chi N)_s$ values suggests that the phase separation is more difficult in graft than diblock copolymers. These findings are quite reasonable when considering the entropic origins of microphase separation discussed in the next section. The equilibrium theories of Helfand[53-68], Meier[49-51] and Henderson[75,76] may also be used to calculate characteristic parameters at critical points. Helfand estimates a value of $(\chi N)_c$ of about 8 for similar conditions. Depending on the boundary conditions of the different theories these critical values will be slightly different. However, the trends for the difficulty of phase separation are consistent.

2.2.2 Theory of Microphase Separation

When separation occurs in block copolymers, rather than exhibit macrophase separation as in the case of homopolymers, they typically form microphases of well defined

size and shape. There have been many statistical thermodynamic theories[47-64] proposed that predict such various aspects of the domain morphology as morphological texture as a function of composition, minimum molecular weight for domain ordering, thickness of the interphase region, the temperature at which domains become thermodynamically unstable, size and shape of domains, and interdomain spacing. Meier[58] was the first to correctly identify the underlying thermodynamic terms involved in microphase separation. Leary and Williams[63,64] extended this treatment to triblocks and incorporated a mixed region at the interface which is assumed to show single phase behavior. Krause[61,62] has treated the phase separation of linear block copolymer systems from a macroscopic view rather than the microscopic view of others. Subsequent modifications to theory advanced by Meier[48-52] and Helfand[53-60] appear to be the most detailed and proficient in quantitatively predicting experimental data on linear diblocks and triblocks. What follows is a general synthesis of Helfand's statistical thermodynamic treatment of microdomain structures in linear block copolymers. In these derivations the basic assumptions involved are that the mean field theory properly describes the phase separation phenomena and no volume change occurs upon mixing. The essential thermodynamic properties of the system are incorporated in

the in an expression for free energy per molecule, $\Delta G/N$, relative to a homogeneous system. The formula for this expression of free energy (for the case of the formation lamellae structures) is shown in Eq. 8

$$\Delta G/NkT = 2\Gamma/kT\ (Z_A/p_{oA}+Z_B/p_{oB})\ 1/d - \ln(2a_1/d) + \qquad (8)$$
$$\emptyset.141\{[(Z_A^{1/2}/b_A p_{oA})^{2.5} + (Z_B^{1/2}/b_B p_{oB})^{2.5}]/$$
$$[(Z_A/p_{oA}) + (Z_B/p_{oB})]^{2.5}\}\ d^{2.5}$$
$$-\alpha[(Z_A/p_{oA})(Z_B/p_{oB})]/[(Z_A/p_{oA}) + (Z_B/p_{oB})]$$

The bulk interfacial tension Γ is usually determined experimentally, but values for many common polymer pairs have not been established. Thus the alternative is to use the formula for the interfacial tension used by Helfand and Sapse.[53]

$$\Gamma = k_b T\alpha^{1/2}[\beta_A+\beta_B/2 + 1/6\ (\beta_A-\beta_B)^2/(\beta_A+\beta_B) \qquad (9)$$

and

$$\beta_k^2 = p_o K b_k^2/6, \quad b_k^2 = \langle R_k^2\rangle_o/Z_K \qquad (10,11)$$

b_K is the Kuhn's statistical segment length, p_{oK} is the number density of the segments and Z_K is the degree of polymerization of the k block chain. α is the interaction parameter which is equivalent to X as defined in the previous section and follows the same relationship stated

equation 4. In the formulation of equation 8 for simplification, it is assumed the degree of polymerization Z_k is high and a_i the interfacial thickness (usually about 1.Ø to 2.Ø nm) is small relative to the size of domains (typically 1Ø nm). The above assumptions are embodied in what is known as the narrow-interface approximation. In the context of the narrow interface approximation, the free energy associated with domain formation separates into terms to which a physical meaning may be attached.

The first expression in equation 8 is attributable to the domain interface. This term is proportional to Γ, the interfacial tension, and the surface to volume ratio which scales as 1/d. Consequently, the interfacial term decreases as the size of the domain increases, and would tend to increase domain size infinitely. However, in copolymers the chemical bond between the polymers places two constraints on domain growth which balance the interfacial term.

The first arises from the fact that the joints are confined to an interfacial region of thickness a_i. Any excursions out of the interface would excessively pull one blocks chain into the domain of the other, and is therefore energetically unfavorable. Consequently, the chain end has only a fraction of the volume available to it, relative to the volume it could have if it were freely placed anywhere. Thus the second term of equation 8 represents the loss of

entropy due to this localization of the joint in the interface and has been shown to be proportional to log d.

The third term in equation 8 represents the other effect of localization of the joint between chains in the interface. If the polymer were to obey random walk statistics there would be a tendency for a higher density at the interface and a subsequently lower density toward the center of the domain. However, there is a prohibitively large free energy, originating from the strong cohesive forces of the system, that strongly disfavors the development of an inhomogeneous density pattern across the domain. Therefore the system statistically suppresses chain conformations that lead to these inhomogeneous density patterns and obtain rarer conformations that will uniformly fill the center of the domain. This suppression of chain conformation is associated with a loss in conformational entropy which increases as $d^{2.5}$.

An equilibrium domain size is found solving for the d value which achieves the minimum free energy. The contribution of each of these components to the free energy and the sum expressing where the minimum free energy occurs is depicted in Figure 2.7.

Even though both Helfand and Meier use diffusion-type equations to solve for the probability of finding a free chain end at a distance r from the interface, they apply

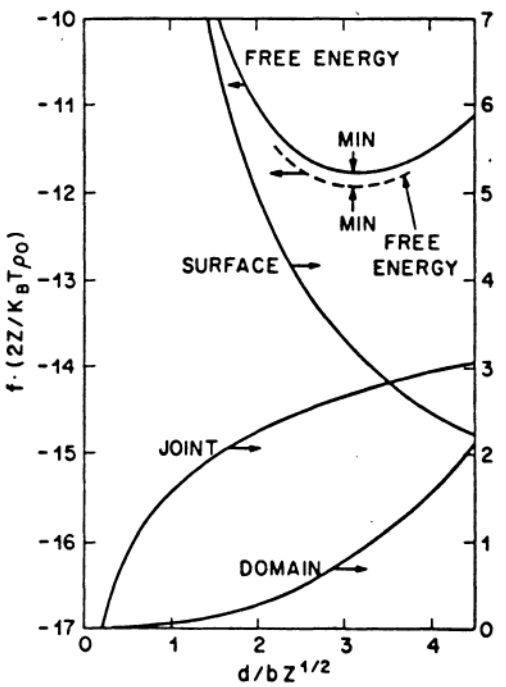

Figure 2.7 Free energy vs. periodicity distance, demonstrating the contribution of various facets to the free energy (χZ = 37) (reference 57).

different boundary conditions to the probability. Helfand adds a self consistent external field to the equation that embodies the repulsive forces of the second phase, the tendency to pull polymer into regions of lower density than the pure phase and push polymer out of regions of higher density than the pure phase. This results in a total uniform density pattern or self consistent density pattern for zero compressibility as opposed to the uniform expansion hypothesis of Meier[49], whereby density fluctuation are minimized through uniform expansion. Meier also neglected the conformational entropy loss associated with the maintaining uniform density throughout the interfacial area. Meier assumed that this contribution is negligible, in contrast to Helfand who includes a rigorous treatment of this effect in his derivation.

Later models by Meier[50-52] did incorporate an interfacial composition profile based on a sinusoidal wave function. Helfand et al.[53-60] chose a hyperbolic tangential function (based on their density gradient model) as the basis for the composition profile. Recent hypothesis by Henderson and Williams[75,76] have studied the effect of different density distributions used to evaluate the equilibrium domain theory. In these studies evidence was shown for the presence asymmetric interfacial composition profiles in various polymer systems. Using a modified form

of the theories of Leary and Williams[63,64], they show that in these systems the choice of interfacial profile affects the free energy equations and subsequent critical phenomena. However, the underlying physical factors governing equilibrium phase behavior, as previously described, remain intact for all copolymer systems.

Although these theories were derived for the case of diblock copolymers, it has been found that a triblock behaves equivalently to a diblock that is half of the molecular weight of the corresponding triblock copolymer[63,64].

2.2.3 Domain Size

A characteristic dimension such as the size or periodicity of domains, typically reflects scaling relationships of the individual chains, and can be related to molecular weight by a simple power law relationship described by

$$d = kM^{z} \qquad \text{and} \qquad R = kM_A^{z} \tag{12}$$

where M is the total molecular weight of the chain, d is the interdomain spacing, M_A is the molecular weight of the spherical domain forming block, R is the domain radius for

spherical domain and K is a constant. For a chain that follows random walk statistics (the unperturbed dimensions in the bulk) Z = Ø.5. A random coil with excluded volume effects has d scaling as $M^{Ø.6}$. From Meier[58] the exponent Z in the power law relationship was found to be Ø.56. Krömer et al.[65] found Z=Ø.58 from SAXS and TEM data. A compilation of TEM and SAXS data on spherical, cylindrical and lamellar structures by Roovers[66] gave a value of Ø.56 for Z. Helfand and Wasserman[55] have theoretically predicted a value of Z = Ø.64, which is more commonly referred to as the 2/3 power law. Hashimoto et al.[67,68,77] have compared lamellar and spherical morphologies for an S-I system and found excellent agreement with the 2/3 power law.

In a more recent publication, Hashimoto et al.[69] have compared their experimental values of d and that of others, for well defined diblock copolymers, to theoretical values of Helfand and Wasserman[56]. It was found that the spherical, cylindrical and lamellar domains were in agreement with the molecular weight scaling relationships dictated by the equilibrium theories of Helfand and Wasserman. The absolute values of d for cylindrical and lamellae domains were within the experimental error of the estimation of the surface tension values. However absolute d and R values for spherical domains were found to be consistently about 1/2 that of the predicted equilibrium values, even though the

spherical domains still maintained the equilibrium molecular weight scaling relationship of the 2/3 power law. This phenomena may be attributed to nonequilibrium effects encountered during domain formation from solution. As the solvent leaves the system, domains equilibrate by changing size. For spherical domains this involves transport of A (the spherical forming component) chains through a matrix of B chains. On the other hand, cylindrical and lamellar domains can change size by shrinking along the interface and effectively decrease the distance between chemical junctions at the interface. The energetic barrier associated with the transport of the A chains through a B matrix is larger than that involved with the equilibration of cylindrical and lamellar domains. This energetic barrier increases as solvent content in the system decreases. Therefore at some point during the evaporation process (at less than 100% polymer concentration) this energetic barrier becomes sufficient to inhibit the transport of A through the B matrix. The equilibrium domain size at this point will be the domain size observed in the system. Consequently, the molecular weight dependence is close to that predicted by equilibrium theory, but the absolute values for domain size are below equilibrium values. This also suggest that the solid state spherical domain structure formed from solution are in a metastable state, containing excess free energy

associated with the excess interfacial area present in the system. Other results[69] indicated that this deviation decreased when the domain forming component had low molecular weight and were present in high concentration (weight %).

2.2.5 Domain Formation From Solution

In 1966 Vanzo[70] observed that the reflectance of visible light from solution (polystyrene-polybutadiene diblock in ethylbenzene) demonstrated an sharp increase in the maximum reflectance at a concentration of about 9% (Figure 2.8 b). Shifts in the maximum reflectance as a function of concentration indicate that the identity period decreases as a function of concentration (Figure 2.8 a). These results suggest the presence of a critical concentration above which some degree molecular ordering exists which increases with concentration. Sardon and Gallot[71] studied the microstructure of polymer solutions through the use of a post polymerization technique. In this method a monomer, which is readily polymerized via UV radiation is used as a preferential solvent.

Figure 2.9 presents typical results for a polystyrene-polybutadiene diblock in which styrene monomer was used as the preferential solvent for PS block in a PS-PB diblock.

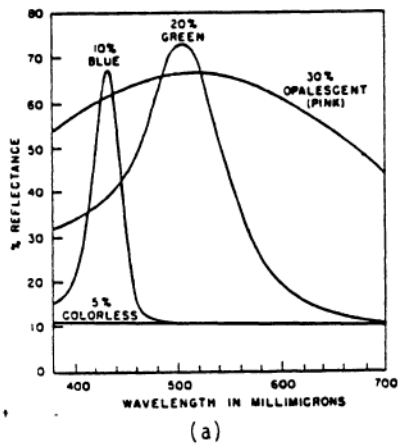

(a)

Figure 2.8a reflectance of visible light for PS-PB solutions at 5, 1Ø, 2Ø and 3Ø% concetrations. (Ref. 7Ø)

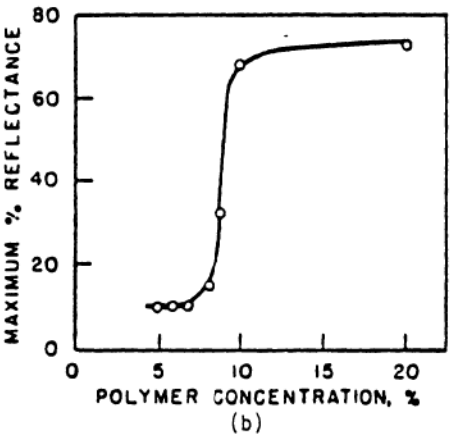

Figure 2.8b plot of maximum reflectance vs. polymer concentration (Ref. 70).

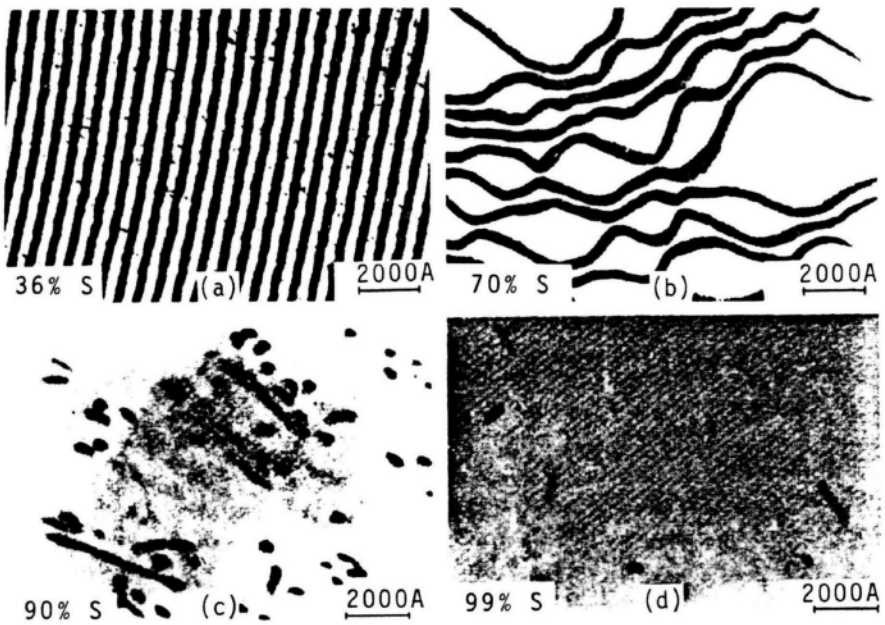

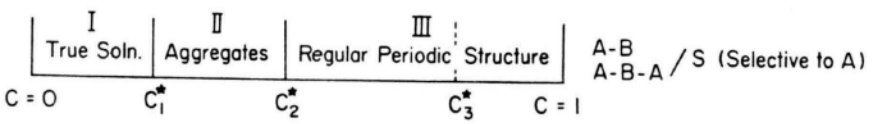

C_2^* : critical concentration for the microphase separation

C_3^* : concentration at which the T_g of the hard segment reaches to ambient temperature

Figure 9a and b Solidified structures of solutions of PS-PB diblocks in styrene as a solvent at styrene concentrations of (a) 36%, (b) 70%, (c) 90% and (d) 99% (top) and proposed isothermal diagram for solution formation (bottom) (reference 71).

In this study an isothermal phase diagram was proposed for A-B diblock and A-B-A triblock copolymers as illustrated in Figure 2.9b.

In region I of the diagram, the concentration of polymer is very low and the solution exhibits the properties of a true solution. As the concentration of the solution concentration exceeds C_1^*, molecules begin to aggregate and form micelles. Although the micelles themselves do not exhibit any long range ordering.

A further increase in the concentration past C_2^* results in the formation of a regular periodic structure. This concentration coincides with the onset of microphase separation and is thought to be the origin of the abrupt increase in the maximum reflectance pointed out by Vanzo.

Hashimoto et al.[69] have modified the original phase diagram by adding an additional critical concentration C_3^*. Above C_3^* equilibrium morphologies become difficult to obtain and no significant changes in the either size or shape of the structure are possible. This more aptly applies to hard and soft block systems where the T_g of the hard block is above the temperature at which the microstructure is observed (typically ambient temperatures), since at 100% polymer concentration two blocks with T_g's well below room temperature are highly mobile and may still be able to attain there equilibrium structures. However, in the case

where one or both blocks have a T_g above the temperature at which the microstructure is observed, a concentration C_s^* will exist, above which the mobility is sufficiently hindered as not to allow any large scale cooperative chain motions. This results from the plasticization effects (suppression of the T_g) by the solvent on the polymer system. The solvent effectively increases the free volume available to the polymer chains. As polymer concentration increases the free volume available to the polymer chains is reduced, eventually to the point where large scale molecular motion is no longer possible. At this point the T_g of the hard block is near the observation temperature and the resulting glassy behavior does not allow sufficient mobility to pursue further equilibrium structures. In other words, there may be other equilibrium states thermodynamically favored, but are kinetically impossible to achieve in a reasonable time frame. It is this effect that is thought to be the cause of the nonequilibrium values of the absolute dimensions of the spherical domains and interdomain spacings as discussed earlier.

Both Sardon and Gallot[71] and Skoulios[72] have studied transitions in region III of Figure 2.9b. Sardon and Gallot proposed that two types of systems exists. In the first type, only one type of morphology exists throughout the entire concentration range of region III. The second type

exhibits either the spheres-to-cylinders or cylinders-to - lamellae morphological transitions as concentration is increased. However, the fact that in the post-polymerization method, the solvent is polymerized before observation, suggests that it is possible that the observed structure may be more representative of a blend rather than a true solvent-polymer solution. It has been show by Inoue, et al.[74] that the addition of a soluble homopolymer to a copolymer system can result in phase transitions.

2.3 TEM Analysis of Polymers

2.3.1 TEM Optics

Before reviewing the transfer theory of imaging, it will be useful to describe a various feature in the standard TEM. Thomas[85] and Thomas[84] both offer good general descriptions of the TEM optical systems.

Figure 2.1Ø illustrates the first integral part of the TEM, the illumination system consisting of the electron gun and the first and second condenser lenses and apertures. In most instruments electrons are produced via thermionic emission form a heated V shaped tungsten filament held at

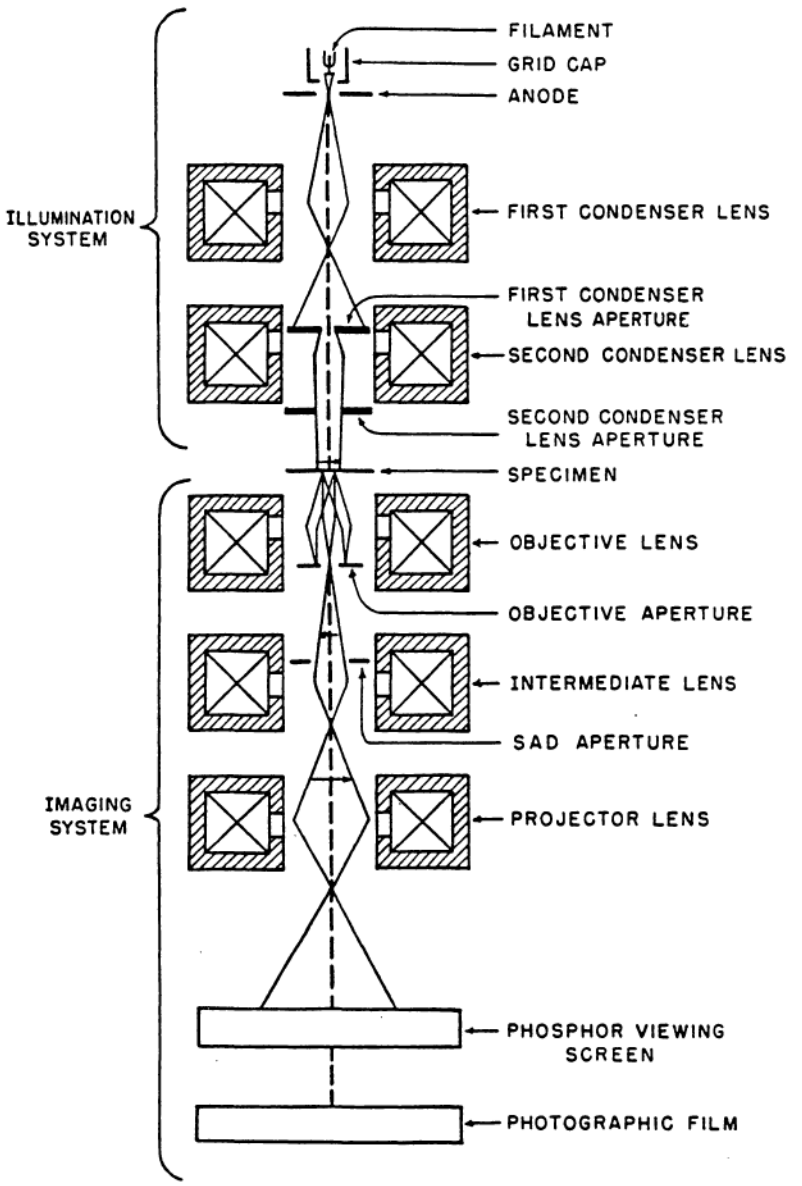

Figure 2.1Ø Schematic diagram of a transmission electron microscope imaging system (reference 85).

-100 kV relative to the ground. The operating or accelerating voltage is adjustable, where higher voltages typically offering better resolution and an increased sample penetrating power. Other types of sources such as LaB_6 and field emission guns that offer some distinct advantages primarily increased brightness, are also available (at significant cost). The condenser lenses are used to regulate the electron beam. Adjusting the lens current alters the electron density impinging onto the specimen to cover the range of different magnifications employed. The condenser apertures serve to collimate the electron beam.

The second part illustrated in Figure 2.10 is a typical imaging system. The imaging system is composed of the objective lens, projector lens, intermediates lenses phosphor screen and camera. The initial image is first magnified by the objective lens and is then further magnified by subsequent lenses in the imaging system. The use of intermediate and projector lenses allow for multiple stage magnification control. The electrons then impinge on the phosphor screen, where the electron intensities are converted into degrees of light intensities by the photoemission properties of the phosphor screen. This allows the operator to check for sufficient contrast and properly focus the image. Once properly focussed, tilting the

phosphor screen forward, allows the image to be photographed onto a electron sensitive emulsion that has better contrast and resolution than the phosphor screen.

2.3.2 Phase Contrast Imaging

The purpose of this section is not to provide a rigorous derivation of the transfer theory of imaging, but rather to provide basic insight into some important aspects of the transfer theory and practical applications of the theory. Detailed derivations of the transfer theory of imaging have been provided by Handlin[78], Hanzen[79], Erickson[80], Misell[81] and Cowley[82]. A simplified versions for applications to polymers has been given by Thomas[83].

In the this section a simplified treatment of transfer theory of imaging is applicable to the case of polymers specimens that behave as pure phase object (basically a synthesis of treatment already given by Thomas[83], Roche[84] and Handlin[78,87]) is presented.

The manner in which an image is formed in the electron microscope, based upon Abbe wave theory of imaging[82], is illustrated in Figure 2.11. The phase shift incurred by incident electron wave as it passes through an object, with a mean inner potential of $\emptyset(r_o)$, is represented by the

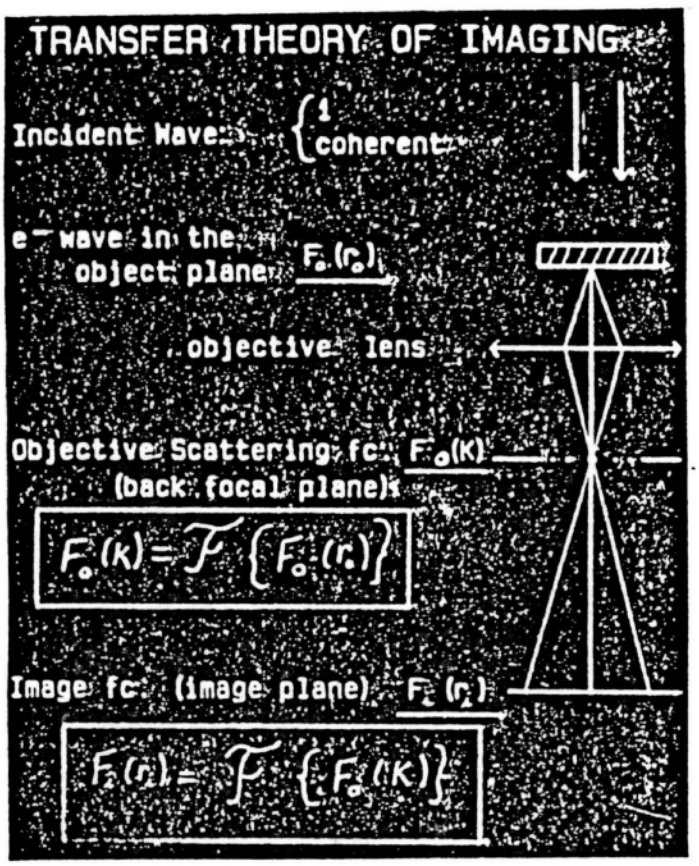

Figure 2.11 Illustration of TEM image formation (the script F indicate Fouier transform) (reference 78).

object function $F_o(r_o)$. The Fourier transform of $F_o(r_o)$ is the Fraunhofer diffraction pattern F(S) ($F_o(K)$ in Figure 2.11) formed in the back focal plane of the objective lens. The function F(S) is modulated by the apertures and aberration of the microscope. These effects are embodied in the pupil or transfer function and produce a modified scattering function F'(S). The Fourier transform of this modified scattering function then becomes the image function $F_i(r_i)$ formed in the image plane. Consequently, any differences between the electron wave in the object plane $F_o(r_o)$ and the final image plane $F_i(r_i)$ are due to the pupil function. Mathematically, the image formed is determined by only the pupil and object functions.

As previously stated the object function is the phase shift of the incident electron wave passing through the object. Electrons are scattered by the electrostatic potential originating from the electron cloud and the nuclei of the atom. In contrast to the nuclei, the electrons are distributed in space about the atom, such that the absolute value of their potential is less than that of the positively charged nuclei. This results in a positive net potential about the atom. Consequently, under the context of the weak phase approximation, the object function may be directly related to the mean inner potential of the specimen via the following relationship[84]

$$F_o(r_o) = \pi / \nu V_o \ \langle \emptyset \rangle (r) \qquad (13)$$

where ν is the wavelength of the electron, t is the specimen thickness and V_o is the accelerating voltage. The mean inner potential difference is given in equation 14.

$$\langle \emptyset \rangle = 28.83 \ [p/M \sum_i n_i f_i^{(1)}] \quad \text{(volts)} \qquad (14)$$

where p is the density in g/cm^3, M is the molecular weight in g/mole, f_i is the electron scattering factor at zero scattering angle for the ith type of atom in the repeat unit, n_i is the number of ith type atoms in the repeat unit. The mean inner potential for electrons is analogous to an index of refraction for light. It follows, that in a two phase system, it will be the difference in the mean inner potential as well as the shape and distribution of the phases that will determine the relative projected phase change.

The pupil function basically consists of a phase shift term and an aperture function as follows:

$$P(S) = A(S) \sin X(S) \qquad (15)$$

where A(S), the aperture function, essentially truncates the scattering pattern at a finite angle. When any part of the electron wave is scattered at a larger angle they are blocked by the objective aperture and do not contribute to the image. Thus at this point A(S) is equal to zero. When the electrons are scattered below this finite scattering angle, they are unaffected by the aperture and A(S) becomes unity.

A phase shift in the electron wave occurs due to the different path lengths taken by electrons when focused through electromagnetic lenses. The magnitude of the phase shift is given by $X(S)$

$$X(S) = \pi/2\ C_s\, \nu^3 S^4 - \pi\, Z\nu S^2 \qquad (16)$$

where Z is the defocus, defined as the distance between the focal plane of the lens and the object plane. C_s is the spherical aberration coefficient, S is the modulus of the reciprocal space scattering difference between the incident and scattered wave vectors and ν is the wavelength.

When the relative phase shifts are small compared to unity (weak-phase object approximation), the bright field

image contrast can be expressed in terms of Fourier optics as follows:

$$(I(r_o)-I_{av})/I_{av} = F^{-1}\{2A(S)\ \sin X(S)\ F[F_o(r_o)]\} \quad (17)$$

where F denotes a Fourier transform, and S is the reciprocal scattering vector.

It is important to note that sin $X(S)$ function is very sensitive to changes in defocus as given by equation 16. The underlying importance of this term is that it alternately selects or subdues the contribution of various object spacial frequencies to the final image. Consequently, a weak phase object (such as a single phase homopolymer with a uniformly varying $F[F_o(r_o)]$ distribution) will exhibit the so called "salt and pepper" structure that is so often mistaken as evidence for microphase separation. The microscope conditions under which the "salt and pepper" structure or phase contrast structure is observed determines the size of the structure. An approximation for the size of the largest phase contrast structure is represented by

$$d = (2\nu Z)^{1/2} \quad (18)$$

where at a typical defocus value (3 microns) and 100kV operating voltage the size of the phase contrast features

are approximately 5ØØ nm.

The function sin $X(S)$ is almost antisymmetric at medium defocus values and higher, such that when the image is viewed at a series of defocus values (through focus series) going through true focus (+ to - values), the "salt and pepper" structure will reverse contrast (dark will become light and visa versa). This is a common way for the operator to distinguish phase contrast from real amplitude contrast resulting from a two phase system, while observing the structure before any permanent recording of the image.

If a question still exists to whether or not the image on a micrograph is due to phase contrast, optical transforms of the micrographs will allow determination of defocus values and determination of the size of the phase contrast features[78,87].

When under proper defocus conditions, it is possible to image well defined multiphase systems that would normally require staining, without staining, using phase contrast techniques[78]. Under slight underfocus condition, phase contrast tends to enhance other primary imaging contrast mechanisms (amplitude contrast), making the observed structure sharper and more appealing to the eye. Phase contrast imaging has even been proposed as a routine method for microstructure analysis of polymers[88].

2.3.2 Amplitude Contrast

Amplitude contrast results from the scattering of electrons outside the objective aperture and therefore are lost and do not contribute to the image. This scattering of electrons typically results from either diffraction, or mass thickness effects or a combination of the two.

Diffraction contrast will vary with the orientation and thickness of the crystals. The orientations will determine which crystalline lattice planes will diffract (ones that satisfy the Bragg condition) the incident wave, resulting in coherent scattering of electrons outside the objective aperture. Thus, contrast will result from small scale deviations of the crystal lattice planes from the Bragg condition. The diffracted intensity is given as

$$I(S) = F_{hkl}^2 \sin^2 \pi st / \sin^2 \pi s \qquad (19)$$

where F_{hkl} is the structure factor for the (hkl) plane, whose magnitude is equal to the ratio the amplitude of the wave scattered by all the atoms of the unit cell to the amplitude of the wave scattered by one electron. The thickness of the crystal is t and s is a parameter that measures the degree of deviation from the Bragg condition. Since diffraction contrast is very sensitive to orientation,

changing specimen orientation by only a few degrees will effectively decrease the diffracted intensity to approximately zero. Hence, the operator may determine the presence of diffraction contrast by varying specimen orientation and observing contrast fluctuations in the image.

Mass thickness (scattering) contrast arises from samples that incoherently scatter electrons. This is generally true for only noncrystalline materials. For the bright field image, the intensity in the image plane is given as

$$I = I_0 \exp(-S_p(V_0,)\ pt) \qquad (20)$$

where I_0 is the incident electron beam intensity, p is the density of the object and αt is the sample thickness. $S_p(V_0,\alpha)$ is the effective mass scattering cross section, which encompasses plural, elastic and inelastic scattering phenomena. $S_p(V_0,\alpha)$ has been shown to be nearly independent of Z (the atomic number), but strongly dependent the accelerating voltage V_0 and the half angle of the objective aperture α^{88}. Differentiation of equation 20 yields an expression for the bright field contrast shown in equation 21

$$C^2 = S_p(V_0, \alpha)\ (p\,\Delta t^2 + t^2 \Delta p^2) \qquad (21)$$

where C ($\Delta I/I$) is the contrast in the image. The minimum detectable contrast for the human eye is 6% (C = Ø.Ø6).

2.3.4 Film Restrictions

For imaging a multiphase polymer (assuming sufficient differences in primary contrast mechanisms are already exist between the two phases) there are basically two geometric constraints placed on the TEM specimen.

One constraint is on the on sample thickness. As the name transmission electron microscopy implies, the film must allow electrons to readily pass through the sample. Although the degree of transmission is a function of the accelerating potential, as a general rule at 1ØØ kV, metal (gold) and hydrocarbon films should be less than 2Ø nm and 1ØØ nm respectively. In addition, increases in specimen thickness have several adverse effect on the image[78]. First, resolution decreases with thickness as $(t\nu)^{1/2}$, where sample thickness and ν is the wavelength of the incident beam. Secondly, the ratio of inelastic to elastic scattering (inelastically scattered electrons do not contribute to image contrast) increases rapidly with increases in thickness. And lastly, a thick sample will have different

planes at zero defocus for different values of defocus, rendering zero defocus for the specimen indeterminate.

The second geometric constraint, involves the variation of projected phase change. If the morphology consist of randomly ordered domains, whose spacing or size is small as compared to the thickness of the film (Figure 2.12b), the projected potential will resemble that of a pure noise object (random fluctuations). In comparison, the well ordered structure in Figure 2.12a that produces variations in the projected phase that are consistent with the structures geometry. Another restriction deals with the scale of the structural features. If domains are expected to be on the order of 10-30 angstroms it will be difficult to determine phase contrast effects from amplitude contrast. For medium resolution conditions (near zero defocus) the contribution of the phase contrast is negligible. However, under high contrast conditions, the transition from predominantly scattering contrast to phase contrast is not well defined and the fine detail in the observed structure will be dependent on both scattering and phase contrast.

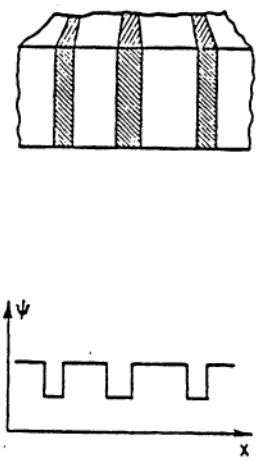

Figure 2.12a The projected potential of geometry A can be interpreted (reference 87).

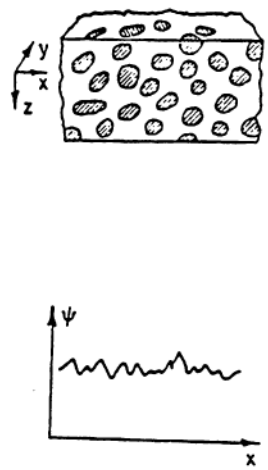

Figure 2.12b Geometry B appears as random noise and cannot be interpreted (reference 87).

CHAPTER III

EXPERIMENTAL

3.1 Synthesis and Purification

3.1.1 Polymethylmethacrylate-Polysiloxane

Macromers were prepared by initiation of dried sublimed D_3 in Cyclohexane with s-BuLi, followed by the addition of purified tetrahydrofuran to promote propagation of the siloxanolate species. Termination with 3-methacryloxy propyl dimethyl chlorosilane produced the macromer which was then precipitated in methanol and dried under vacuum. The free radical copolymerizations of the alkyl methacrylate were carried out with 20 wt% monomer in toluene at 60°C using 0.1 weight percent (based on monomer) AIBN initiator. Methacrylate polymerization were carried out at 20 wt. % solids. The resulting copolymers were extracted extensively with hexane or isopropanol, depending on the polymer solubility, to remove and unreacted siloxane homopolymer. Under appropriate conditions, these values were typically low. Further detail on the reaction conditions, preparation of the macromer and characterization are presented in Steve

Smith's Ph.D. dissertation [reference 90]. The generalized chemical structure of a PMMA-g-PSX macromer copolymer is illustrated in Figure 3.1.

3.1.1 Polyarylester-Polysiloxane

A brief summary of the synthesis and characterization of the high molecular weight perfectly alternating polyarylester-polysiloxane copolymer is given here. Details on the starting materials, synthesis of intermediates, solvents used in the polymerization and all of the characterization of the structure, molecular weight and thermal transitions have already been presented in detail in Patricia Brandt's Ph.D. dissertation (reference [91]). The amino propyl terminated polysiloxane oligomers were produced in the bulk by anionic equilibration of the aminopropyl disiloxane with D4 alone or with either octaphenylcyclo-tetrasiloxane or trifluorpropylmethylcyclotrisiloxane added depending on the character of the siloxane desired. The polyarylesters were synthesized by reacting Bis A with a 50:50 mixture of tetraphthaloyl chloride-isophthaloyl chloride in tetrahydrofuran (THF) at room temperature. Molecular weight was controlled by use of stoichiometric imbalance of reactants according to the Corother's equation. The three different types of siloxane oligomer used in the synthesis and studied in this thesis are shown in Figure

3.2. The structure of the arylester oligomer and arylester-siloxane copolymer is illustrated in Figure 3.3. The silylamine terminated siloxane oligomers were reacted with hydroxyl terminated arylester oligomers via condensation reaction in solution. The hydroxyl terminated polyarylester was placed in a reaction flask containing distilled chlorobenzene. Under inert gas flow, the system was refluxed at 132°C to remove water. The silylamine terminated polysiloxane terminated oligomer was then added dropwise through an addition funnel into the reaction mixture over a period of about 2 hours. The reaction produce a dimethyl-amine by-product that can be detected by pH paper. The reaction was considered complete when the by-product was no longer detected and the reaction mixture was subsequently cooled and precipitated in an excess of methanol-/isopropanol. Residual cyclics are expected to be extracted during this procedure. The resulting white fibrous material was filtered and dried under vacuum at 80°C overnight. The recovered yield was expected around 95%.

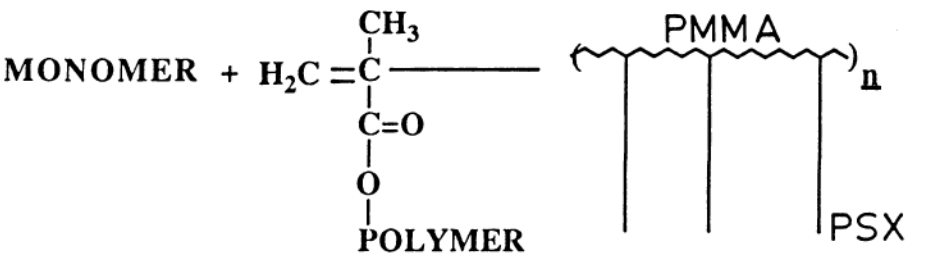

Figure 3.1 Structural scheme of a PMMA-g-PSX macromer polymerized free radically.

Dimethylsiloxane Oligomer

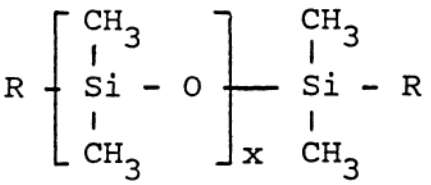

(Dimethyl-diphenyl)siloxane Oligomer

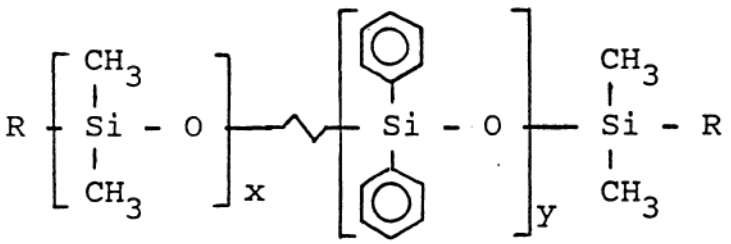

(Dimethyl-trifluoropropylmethyl)siloxane Oligomer

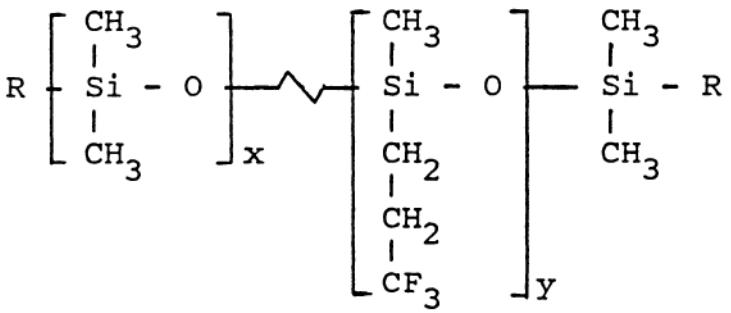

Silylamine-terminated : R = $-N(CH_3)_2$

Aminopropyl-terminated: R = $-(CH_2)_3NH_2$

Figure 3.2 Difunctional siloxane oligomers

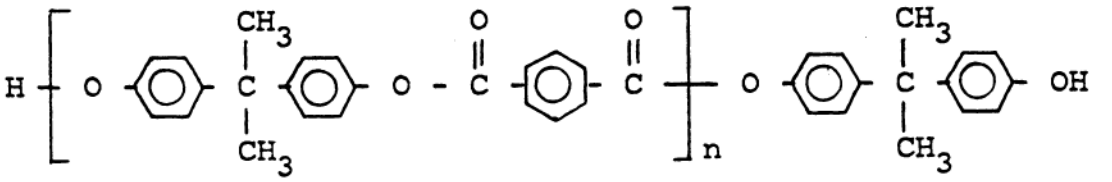

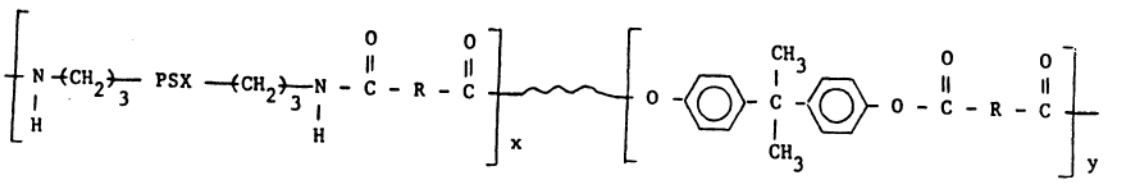

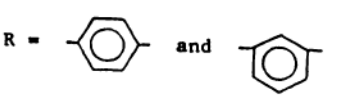

Figure 3.3 Hydroxyl functional arylester oligomer (top) and arylester-siloxane perfectly alternating copolymers (bottom)

3.2 Characterization of Arylester-Siloxane Copolymer

3.2.1 Molecular Weight

a) Titration

The number average molecular weights of the amine terminated siloxane oligomers and the hydroxyl terminated arylester oligomer were determined by titration using a Fisher Titrimeter II automatic titration system. The polysiloxanes were dissolved in isopropanol and titrated with a Ø.1N solution of hydrochloric acid in isopropanol. The polyarylesters were dissolved in THF and titrated with a Ø.2N solution of tetramethylammonium hydroxide in methanol.

b) Intrinsic Viscosity

Intrinsic viscosity measurements were performed in methylene chloride at 25°C using a Cannon-Ubbelohde dilution viscometer.

c) Size Exclusion Chromatography

Size Exclusion Chromatography (SEC) was used to qualitatively check molecular weight distributions. Data was obtained with THF solutions using a Waters SEC instrument with 5Ø, $1Ø^2$, $1Ø^3$ and $1Ø^5$ nm microstyrogel columns. The flow rate was fixed at 1.Ø ml/min. Differential refractive index and UV detectors were used in the analysis. The characterization results presented in reference 9Ø.

3.2.2 Thermal Analysis

a) Differential Scanning Calorimetry

Differential Scanning Calorimetry (DSC) analysis was performed on a Perkin-Elmer Model DSC-2. Scans run at $10_{\circ}$/min with a sensitivity of 5 mcal/sec. Values for the second scans are reported in Table 3.1 and 3.2.

3.3 Characterization of PMMA-PSX Graft Copolymers

3.3.1 Molecular Weight

a) Size Exclusion Chromatography (SEC)

These polymers were analyzed by Gel Permeation Chromatography (GPC) with a Waters 105-c GPC fitted with microstyrogel columns of 50, 10^2, 10^3, 10^4 and 10^5 nm porosity in THF. PMMA standards were used to determine equivalent number and weight average molecular weights. Direct comparison is difficult, since the graft polymers are branched, the hydrodynamic volumes are different from those of their linear counterpart at the same molecular weights. Both refractive index and UV detectors were utilized in the analysis. Absolute molecular weights were obtained by combining the GPC techniques with the differential viscometer detector. Comparing the detector responses to standards used for determining the universal calibration

TABLE 3.1

Perfectly Alternating Copolymers

Sample	25°C [ ] CH_2Cl_2	% Yeild	Copolymer T_g (°C)
PE-PSX	2.34 dl/g	91	-123,135
PE-PPSX	Ø.51 dl/g	86	-61,156
PE-PFSX	Ø.71 dl/g	81	-1Ø2,138

PE-PSX are 1ØØ wt. % CH_3

PE-PPSX are 5Ø wt.% diphenyl and 5Ø wt. % CH_3

PE-PFSX are 5Ø wt. % fluoroprpyl and 5Ø wt. % CH_3

TABLE 3.2

Characterization of Oligomers

Sample	Siloxane Block		Ester Block	
	$\langle M_N \rangle$	(T_g °C)	$\langle M_N \rangle$	T_g (°C)
PE-PSX	6000	-123	5100	171
PE-PPSX	5400	-74	5100	171
PE-PFSX	5650	-105	5060	171

curve generates number and weight averages for each fraction. Subsequently, the number and weight average molecular weights of the entire fraction can be calculated. Super Critical Fluid Extraction was performed on PMMA-g-PSX samples and these fractions were subsequently analyzed to determine compositional distributions among the fractions. All compositional and molecular weight analysis are discussed and listed in the sections 4.2 and 4.3.

b) Super Critical Fluid Extraction (SCFE)

Super Critical Fluid Extraction was used to separate fractions on the basis of solubility, which is dependent on both compositional and molecular weight variations. The resulting fractions were analyzed by NMR and GPC to determine compositional and molecular weight. Comparison of the composition and molecular weight of each fraction allows insight into the composition variations of the total sample. SCFE separations were performed by Dr. Val Krukonis on approximately ten grams of sample using butene as a carrier with a starting pressure of 1500 psi. The samples were typically fractionated into 5 or 6 distinct fractions.

c) Membrane Osmometry

Number average molecular weights were determined by membrane osmometry on a osmometer in toluene to compare with other previously determined values from differential viscometer and NMR results.

3.2.3 Thermal Analysis

a) Differential Scanning Calorimetry

DSC thermograms were obtained on a Perkin Elmer DSC-2 run at 10°C per minute heating rate.

b) Dynamic Mechanical Thermal Analysis

Dynamic Mechanical Thermal Analysis (DMTA) spectra were obtained on a Polymer Labs DMTA at 1Hz frequency with a temperature range from -150°C to 150°C at a scan rate of 5°C per minute. The results are presented in Table 3.3.

3.4 Processing Conditions

3.4.1 Compression Molding

The polymer, in the form of a white fibrous powder, is placed between two Ferro-type photographic plates coated with a mold release agent. The ferro-type plates were then placed in a previously heated hydraulic press. The temperature to which the platens were heated was set at about 50°C above the T_g of the block with the highest T_g as determined by DSC. The pressure was increased to 10,000 psi as the polymer began to flow easily (usually after several minutes). Additional pressure was applied until the polymer stopped flowing, indicated by a constant pressure reading. The press was subsequently cooled by an air flow through the

Table 3.3

Thermal Analysis of PMMA-g-PSX Copolymers

(approximately 16 wt.% PSX)

Macromer Mn	T_g by DSC	T_g by DMTA
1000	111	110
5000	123	123
10000	125	126
20000	127	---
control PMMA	127	---

platens to 500°F and then water cooled to room temperature, then the pressed film was removed from the plates.

3.4.2 Thick-Cast Films

Two slightly different methods of solution casting were employed for the arylester-siloxane and PMMA-PSX systems. The arylester-siloxanes were dissolved in chloroform solution at a concentration of approximately 5 wt.%. The solution was placed into a top of a petri dish (about 10 cm in diameter) and covered by the larger bottom of the dish to allow slow evaporation of solvent. The films were allowed to form overnight and then placed in a vacuum at room temperature for about a day. Care was taken in the removal of the film from the dish so as not to induce any plastic deformation.

The PMMA-PSX system was dissolved in chloroform, at a concentration of 5 wt.%. About 0.1 g of solution was deposited into a disposable glass sample jar (about 2 cm in width), where the top was loosely placed onto the top of the jar. 0.1 g was chosen because it formed a film thickness of the order of several millimeters, which were ideal thicknesses for microtome preparation. The films were allowed to form at room temperature overnight. Exceptional care was taken in the removal of the film, especially in the stiffer

low wt.% PSX samples, where plastic deformation occurred more easily.

3.5 Film Preparation for TEM Analysis

3.5.1 Cryo-ultramicrotome

Samples were sectioned on the Reichert cryo-ultramicrotome. Films were trimmed, such that the face of the film had an area of about Ø.1 mm by Ø.1 mm. After trimming, the samples are placed in the sample holder and secured. The cryo-ultramicrotome (MC)has three adjustable temperature controls. These controls adjust the temperature of the incoming nitrogen gas, sample holder and knife temperature and are monitored by digital displays that receive input from thermocouples. Since the thermocouples are not in direct contact with the knife and specimen there is expected to be a small temperature differential between the true temperature of the knife and specimen and the temperature of read by the thermocouples. The temperature in the system was decreased and equilibrated at about -1ØØ°C for the sample holder, -1Ø5°C for the nitrogen gas and -9Ø°C for the knife. The sample temperatures used were slightly above the T_g of the siloxane blocks contained in all of the materials studied. Typical cryo-ultramicrotome procedure is

to decrease the sample temperature below the T_g of the block with the lowest T_g . However, if the temperature is too far below the hard block, the higher T_g material can become to brittle and craze during sectioning. Therefore the temperatures employed were found to yield good sections with little evidence of deformation of the siloxane phases, while still allowing sectioning onto a liquid substrate. The liquid used in the knife boat was methanol, a non-solvent for the systems studied. The advantage of sectioning onto a liquid substrate (wet sectioning) rather than a solid substrate (dry sectioning) is that the liquid allows for easier removal of the sections from the knife edge. Once the systems temperature is stabilized, the knife is positioned as close as possible to the sample without making contact. The cutting stroke is adjusted to start before (a couple of mm) the bottom of the sample is parallel to the knife edge and end as soon as the top of the sample passes below the plane of the knife edge. Both glass and diamond knives were employed in the sectioning of the samples. The length of the cutting stroke was adjustable to accommodate various sample dimensions. The sample advance was placed on the maximum (90 microns) and the cutting rate was changed accordingly. As sectioning a continuous ribbon of sections form. The sample advance and cutting rate steadily decreased while maintaining the continuous ribbon. This continued until

almost every cutting stroke generates a sections when the sample advance settings are that of the sample thickness required for electron transparency. The thicker sections generated earlier are usually brushed away so as not to interfere with the desired thinner sections. When enough sections were obtained at this setting, they were ready for removal. The sections were lifted from the liquid surface onto a TEM grid. The excess liquid was drained from the grid by contact with a Kimwipe. Rather than using an electron microscope, which are not always available, the electron transparency may be determined using an optical microscope. Since the thickness of the section are typically within the wavelength of visible light the color is also indicative of thickness. Color and corresponding thickness charts are available for epoxy resin materials. Since most glassy polymers have similar indices of refraction these charts may be extended to many other materials.

3.5.2 Thin-Cast Films

Thin films were prepared by first dissolving the polymer in chloroform at about 5 wt.% concentration. This concentration was found to give good specimen thicknesses for TEM analysis. A disposable syringe was used to draw several ml from the solution. A drop a solution was deposited onto a liquid (distilled water) substrate, where

the solution spread on the surface and readily formed a film. This method may be extended to other solvent systems, provided the solvent system is not soluble in the liquid substrate and that the solution spreads onto the substrate. Once the film was formed, the color corresponding to the desired sample thickness (usually gold or silver for TEM of glassy polymers) were selectively lifted onto TEM grids. These grids can either be placed in a vacuum or stored at room temperature to allow drainage and evaporation of the excess liquid picked up by the grid. Again optical microscopy may be used to determine the degree of electron transparency.

3.6 TEM Analysis

A Philips EM-420 Scanning Transmission Electron Microscope (STEM) was operated in the transmission mode at 100 kV. Objective and condenser apertures of 50 and 30 microns were used in the analysis of TEM specimens.3.6 Quantitative Image Analysis

3.7 Quantitative Image Analysis

Quantitative image analysis was performed on the Zeiss 380-A and Tracor Northern TN-500 image analyzers. A video

camera was used to transfer positive images into the memory of the analyzer. Once the image was digitised in the memory, grey levels were selected to give what appeared be the best representation of the original micrographs (Grey levels are grades of intensity between white and black, white being the lowest and black the highest). The portion of the micrograph, as represented by pixels in the digitised image, with a grey level below that of the selected level are turned off and those pixels higher than that of the selected level remain on. This creates the binary image for analysis of the domain size and shape. The accuracy is determined by the magnification of the micrograph used and subsequent enlargements of the digitised image, since these factors control the area each pixel represent in the real image. At low magnifications (on the order of 60,000 times) each pixel may represent several nanometers. If pixels (several nm) in domains (of the order of 10 nm) are determined lower that of the selected grey level, and are subsequently turned off in the conversion to a binary image, a significant portion of the domain are eliminated upon the binary conversion and would result in skewing the data toward smaller sizes. Therefore, for very small microstructures (about 10 nm) it is desireable to use high magnification photomicrographs (approximately 200,000 times) with a fairly consistent background to maximize the efficiency of this method. In

either case the information obtained from this method is considerably less subjective than measurements made by hand. Which, aside from optical diffraction of negatives, has been the typical protocol historically used for quantitative TEM micrograph analysis.

Information on approximate circular diameters, maximum and minimum diameters, and interdomain spacings can be computed. The approximate circular diameter takes the area of the domain and solves for the diameter based on the equation for the area of a circle. This may compensate for small deviation in spherical structures caused by deformation during sectioning. 32 diameters of each domain are taken and averaged over all the measured domains to give mean values. The ratio maximum and minimum mean diameters provide information on the shape of the domains. The geometrical center of each domain can be taken on the basis of center of mass type calculation. From this measurements of the interdomain distances are provided.

3.8 Energy Dispersive X-ray Spectroscopy

EDX analysis was performed on the Tracor Northern TN-5ØØ. All analyses were performed on electron transparent TEM samples. This allows for accurate analysis of composition of microscopic areas (4Ø-1ØØ nm) since the electron transparent

films do no produce the scattered electrons generated in thicker bulk specimens that severely limit resolution. In this case the size of the volume analyzed by EDX is essentially limited by the electron beam size selected. However, beam sizes too small may increase collection time significantly, so as to make the sizes generally beam diameters (< 40 nm) impractical. Collection time is very important in electron beam sensitive specimens, where prolonged exposure to electron beams may induce changes in the chemical structure. Therefore exposure times were minimized, sometimes at the expense of resolution.

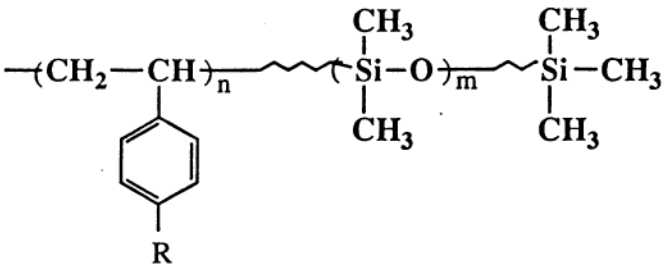

R= H, CH_3, t-C_4H_9

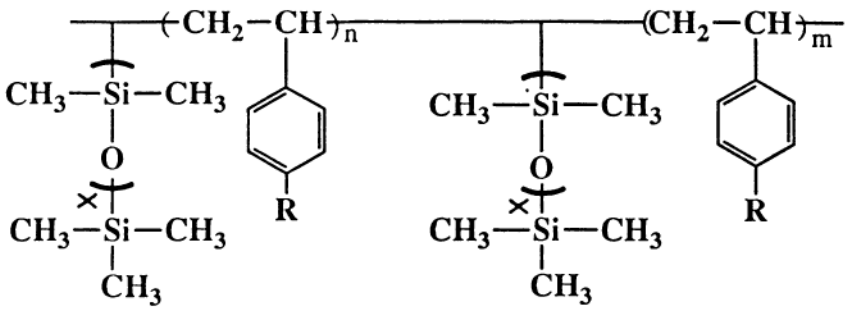

Figure 3.4 Chemical structure of styrene-siloxane copolymers studied in qualitative analysis.

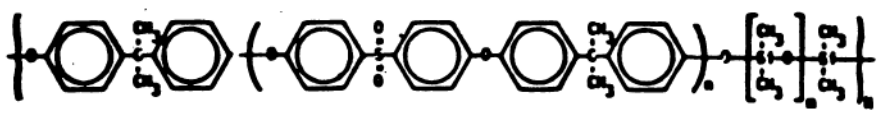

Figure 3.5 Chemical structure of sulfone-siloxane perfectly alternating copolymer utilized in qualitative analysis.

CHAPTER IV

RESULTS AND DISCUSSION

4.1 Use of TEM/EDX in Qualitative Analysis

In most copolymerization reactions, even at high conversions, there is typically some amount of unreacted species present. For example, in the macromer type copolymerization of the PMMA-g-PSX system, any macromer not incorporated into the backbone is present as oligomeric impurities. Also PMMA chains, not incorporating a macromer unit, may exist as homopolymer. In anionic copolymerizations (e. g., polystyrene-b-PSX system), impurities introduced through the addition of the siloxane monomer, can terminate the living styrene carbanions, Thus creating a homopolymer impurity for each living end terminated. For most anionic copolymerizations, 1Ø to 15% homopolymer is typical. Furthermore, the nature of the copolymerization reaction will determine what type of molecular weight distributions exist in the polymer system.

Although it will depend on the properties of interest, the presence of unreacted species is usually undesirable. In

the case of a surface-active species (like siloxanes), less than 1% in a system can contaminate the entire surface. Therefore, the presence of a surface active oligomer will significantly affect, among other surface properties, the plasma and ion etch resistance important in semiconductor and aerospace applications. Furthermore, any surface analysis results used to characterize the surface will not represent the true copolymer surface. By surface-active species, it is meant that the surface energy of one of the components is sufficiently low, in comparison to the other component, the surface active component is thermodynamically favored at the surface.

Homopolymer present in the system that is of equal or less molecular weight, than the corresponding block incorporated into copolymer chain, should be completely miscible with the copolymer. This may have several effects on the observed microstructure that will be discussed in following sections.

The presence of such species proposes several problems in the evaluation of microstructure features through TEM analysis. Although, before discussion of these problems it will be useful to cover typical TEM film preparation techniques.

4.1.1 Preparation of Thin Films

It has been known for a long time that electron transparent films are easily prepared by dissolving the polymer in a volatile solvent and casting onto a solid or liquid substrate. Varying either the solution concentration or casting conditions will allow control of film thickness.

In the case of a solid substrate, if the film does not adhere to the solid substrate (glass is a common substrate), the cast film may be partitioned and floated off onto a liquid substrate, then removed from the surface onto a TEM grid for subsequent analysis. If adhesion to the substrate occurs, a substrate, soluble in a liquid substrate (a nonsolvent for the polymer, usually water) may be utilized. Dissolving the substrate, would allow for recovery of the residual polymer film for TEM analysis.

Direct recovery of the film is possible when casting onto a liquid substrate. Moreover, it is much less time consuming than casting onto the solid substrate. However, there are several criteria to follow when casting onto a liquid substrate.

First, is that neither the polymer or solvent should be soluble in the substrate. Failure to meet either of these conditions, usually results in films unsuitable for TEM analysis. Second, in order to form a film, the solution must

spread onto the liquid substrate. A trial casting onto the selected substrate is the simplest method of determining whether the solution will spread. Although, this may seem intuitive, PMMA-g-PSX and PS-b-PSX copolymers of similar PSX composition have shown quite different spreading behavior, when cast onto a water substrate. As stated before, a volatile solvent should be used. This permits the formation of thin electron transparent films. The use of a non-volatile solvent may result in complications, that will form films too thick for TEM analysis. If any compositional analysis, like Energy Dispersive X-ray (EDX) spectroscopy or X-ray Photoelectron Spectroscopy (XPS), the substrate has to be inherently free from impurities. When water is the chosen substrate, distilled water should be utilized. Impurities in tap water, like Fe from pipes, complicate the compositional analysis. When mercury is utilized as a substrate, residual mercury or its oxides, may adhere to the film. In some cases, XPS results have detected residual mercury at the mercury/film interface. Throughout this dissertation the thin films used for TEM analysis, formed by casting onto a liquid substrate from solution, will be referred to as thin-cast films (section 3.5.2).

Only types of casting methods have been discussed so far and no repercussion of this method on the polymer

morphology have mentioned. Subsequent sections will discuss the affect of thin-casting on morphology. But for now it will suffice to say that thin-cast films will not completely represent the morphology in most applications, where bulk structure-property correlations or duplication of a specific process influenced morphology is required. Hence, in situations where the thin-cast films do not represent the desired processing conditions for a specific application, microtoming may be the only recourse.

In microtoming, a sample is suitably oriented and trimmed to the proper dimensions (a cutting face of Ø.1mm by Ø.1mm is considered ideal) in preparation for sectioning. For samples with a low T_g, cryogenic conditions maybe utilized as described in the experimental section 3.5.1. In addition to the time consuming nature of microtomy, often with no guarantee of successfully obtaining good sections, it suffers from another deficiency. This deficiency arises from the small sampling volume utilized in the microtoming of sections.

As stated earlier, many polymer systems inherently contain oligomeric species or homopolymer, depending on the nature of copolymerization. In a polymer processed under nonequilibrium conditions, the morphological texture may vary throughout the volume of the film. Consequently, the

observed morphological texture will be dependent on the piece selected for sectioning. Even though under some circumstances the solution-cast microstructure may closely approach true equilibrium textures, all solution-cast morphologies essentially are metastable. An example of the dependency of the observed microstructure on sampling volume would be in the situation where surface-active oligomer were present. Sections taken near the surface would indicate a much higher concentration of unreacted species than the average value, due to the preferential segregation of that oligomer to the surface. Copolymers produced under condition where various side reactions are present, may exhibit several types of microstructural textures (even under equilibrium type processing conditions). Reflecting the presence of different block architectures, molecular weights or chemical composition. Sections taken from areas exhibiting only one type of morphology, when several types of structures actually exist, might be assumed erroneously to have a texture representative of the entire sample. For well-defined block copolymers (anionic multiblock copolymers), with a narrow molecular weight distribution, any homopolymer present would also have a narrow molecular weight distribution, and for the most part be solubilized into the microstructure. However, the solubilization of

homopolymer will change the absolute dimensions of some microstructural features such that they will not truly represent a pure copolymer system. In light of the possibility of system heterogeneities, it is suggested that qualitative analysis is performed before any other type of microstructural analysis is attempted.

Qualitative analysis may be defined as the TEM/EDX analysis of thin-cast films, for the primary purpose of obtaining qualitative compositional and morphological information about the polymer system of interest. This information will either reveal the need for further modification of synthesis techniques and subsequent work up procedures or provide preliminary insight into micro-structural behavior of the system. Consequently, using qualitative analysis preceding any definitive micro-structural analysis, via microtoming or some other method, should save time as well as provide a more complete and accurate picture of the systems microstructure.

Thin-film casting is utilized in qualitative analysis for several reasons. One is that thin-film casting is quick and easy. In a matter of a couple of hours a large number of sample (on the order of 2Ø or more) may be produced. This is particularly useful when many variations of a particular copolymers are synthesized. Another reason is that thin-film

casting is cheaper than cryo-ultramicrotoming, only a syringe, a beaker and several ounces of distilled water are needed. Finally, most of the cast films surface area can be utilized for TEM analysis (large sampling volume) when cast correctly. The film thickness should be relatively uniform and sufficiently thin to allow electrons to readily pass through the film. The increased sampling volume should more fully represent the system and increase the detection of heterogeneities present in the system.

4.1.2 Identification of Unreacted Oligomer

It would be naive to assume that chemists involved with the synthesis of polymers were not aware of the presence of a certain amount of unreacted species in the system. Therefore, various extraction techniques are employed, these techniques rely on differences in solubility between the unreacted species and the pure copolymer. However, there has been no sensitive methods of determining the effectiveness of such extraction procedures. Typical procedure is to weigh the material before and after extraction. For a surface active species like siloxanes, an amount undetected by the weighing procedure, could completely dominate the surface and control surface properties.

In the case studied here, a paramethylstyrene-siloxane (PPMS-b-PSX 2Ø Wt. % PSX) diblock copolymer, the unreacted species would be in the form of a low molecular weight siloxane, that was not incorporated into the chain by completion of the reaction. Figure 4.1 shows a typical TEM of a thin-cast PPMS-b-PSX film. The micrograph contains several important features. First, is the presence of discrete dark phases that vary over an order of magnitude in size. The size of some of the domains is on the order of a micron. Second is the well defined or sharp interface around the domain as depicted in the micrograph. In a pure copolymer the interfacial thickness of a relatively low molecular weight (5,ØØØ g/mol) domain forming component would be greater (3.2 nm for diblocks) than the corresponding homopolymer blend (about 1.7 nm as predicted from Helfand) of the same components. Any architectural effects that increase compatibility between the two blocks (relative to diblocks of the same composition) will tend to increased the interfacial thickness. Therefore, for a micro-phase separated system the interfacial region will appear more diffuse than a macrophase separated blend morphology. Only for domain forming blocks of high molecular weights will the interfacial thicknesses approach macrophase separated blend structures. Comparison with expected values

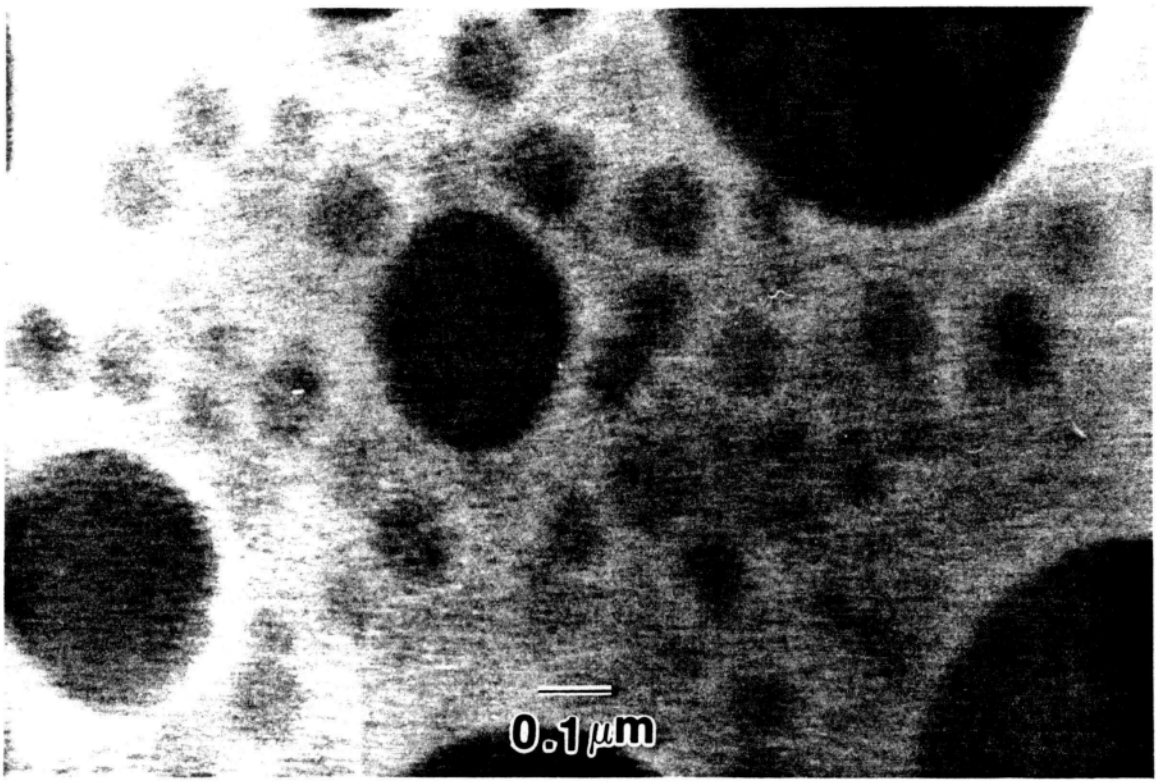

Figure 4.1 TEM micrograph of a PPMS-b-PSX (20K PSX-100K PS) thin-cast film.

of domain size (for a 20K block) indicates that these domains are several orders of magnitude higher than that expected by equilibrium theory. As will be shown later, even under the non-equilibrium conditions of thin film casting, the absolute size for spherical domains is not significantly altered. Coupled with the observed sharp interface and large size distribution the observed structure resembles the macrophase separated morphology of blends. This suggests that the dark phase is a species not incorporated into the copolymer structure. Although, elemental analysis is required for chemical identification of the structure.

The latter is provided by the EDX spectra generated during the analysis of the thin film. The advantage of EDX of thin films, in comparison to thicker bulk specimens, is that the sampling volume is approximately that of a cylinder. In bulk specimens scattered electrons effectively increase the analysis volume, to a drop shape micron in diameter for a beam diameter of only 100 nm. Unfortunately in EDX analysis, the generated x-rays must pass through a thin beryllium window before detection, and elements of lower atomic number than sodium are not detected due to absorption of the x-rays by the window.

Fortunately the PSX contains Si that is detectable, but the PPMS does not contain a detectable atom. Thus, a

comparison is made between spectra recorded at equivalent times, from a single domain and the continuous matrix adjacent to the domain. A balance must be struck between the desired beam diameter and spectral recording times. Even though a smaller beam diameter (10-40 nm) may be desirable due to the increased lateral resolution, the resulting longer recording times required to obtain a proper spectra are undesirable, because of radiation induced damage which may alter the spectra. Figure 4.2a and b indicate that the spectrum obtained from the domain has a significantly higher Si concentration than the matrix. We concluded that the dark domains observed in the PPMS-PSX copolymer, are an oligomeric siloxane not incorporated into the copolymer.

We found this method to be very sensitive to the detection of siloxane oligomer. Since low molecular weight siloxane is incompatible with the copolymer (exhibits macrophase separated behavior), thermodynamically favored at the surface and less dense, it will tend to migrate to the surface of a solution. It follows, that if the solution used in the in thin film casting is taken from the surface, will be very sensitive to the presence of oligomer.

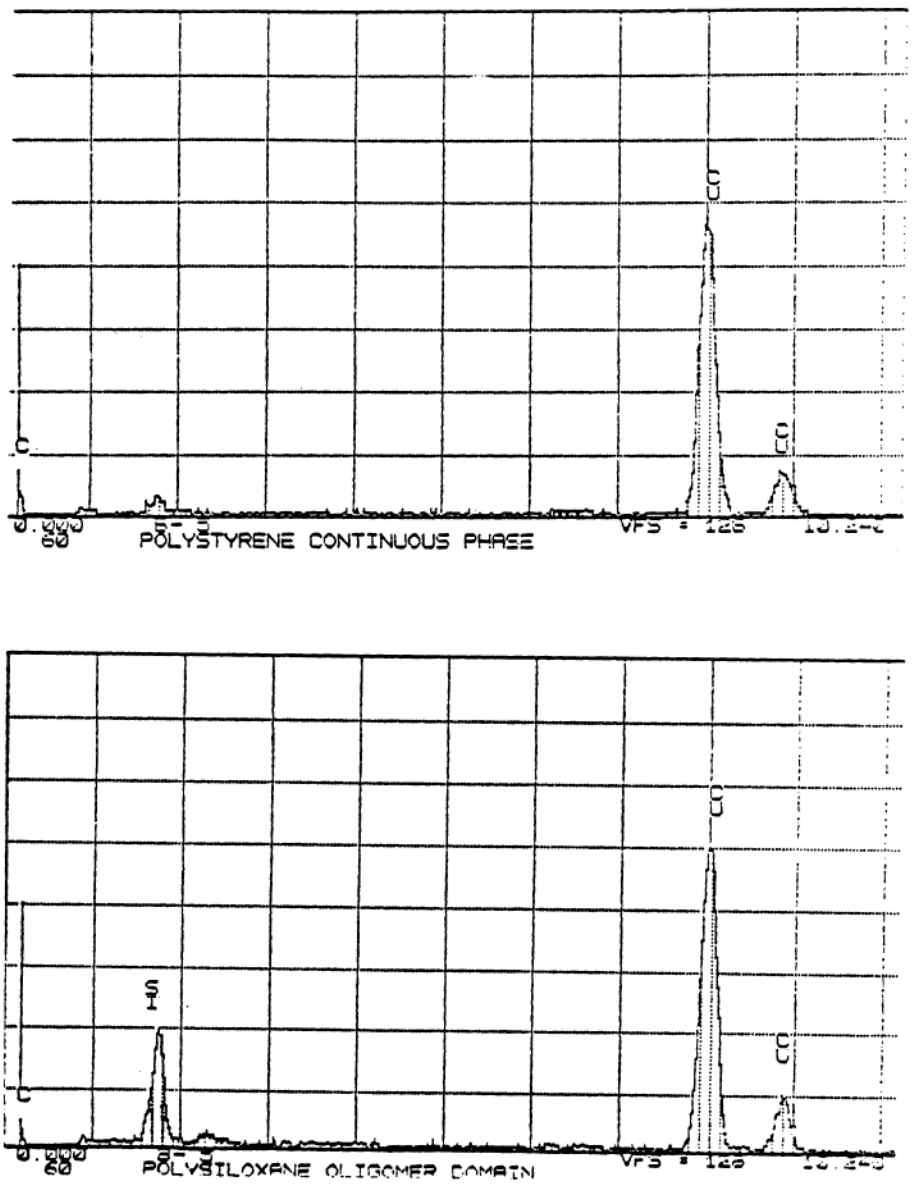

Figure 4.2a and b EDX spectra of PPMS-b-PSX matrix and domain structure.

4.1.3 Qualitative Analysis of Reaction Conditions and Work Up Procedures

If a significant amount of unreacted species is detected, further extractions or the use of another type of purification procedure may be warranted. The effectiveness of extraction is exemplified by qualitative analysis in the micrographs of PMMA-g-PSX (5K PSX graft at 16 Wt. % PSX) shown in Figure 4.3 (a and b). The micrograph of the thin-cast film before extraction, clearly shows unreacted siloxane present as the dark macrophases in Figure 4.3a. After three extractions in a siloxilate (isopropanol), qualitative analysis revealed a microstructure (Figure 4.3b), consistent in size and distribution of sizes with the microstructure observed for pure copolymers.

The fact that thin cast films are highly metastable is advantageous for determining the presence of homopolymer. When dissolved in a good solvent for both components, the homopolymer and copolymer are completely mixed. As the polymer concentration increases via evaporation of solvent, to a critical concentration defined by C_2^{69}, the solution phase separates. Since evaporation is quite rapid, $C_2^{\S}$ is soon reached, effectively trapping metastable morphological textures in the film.

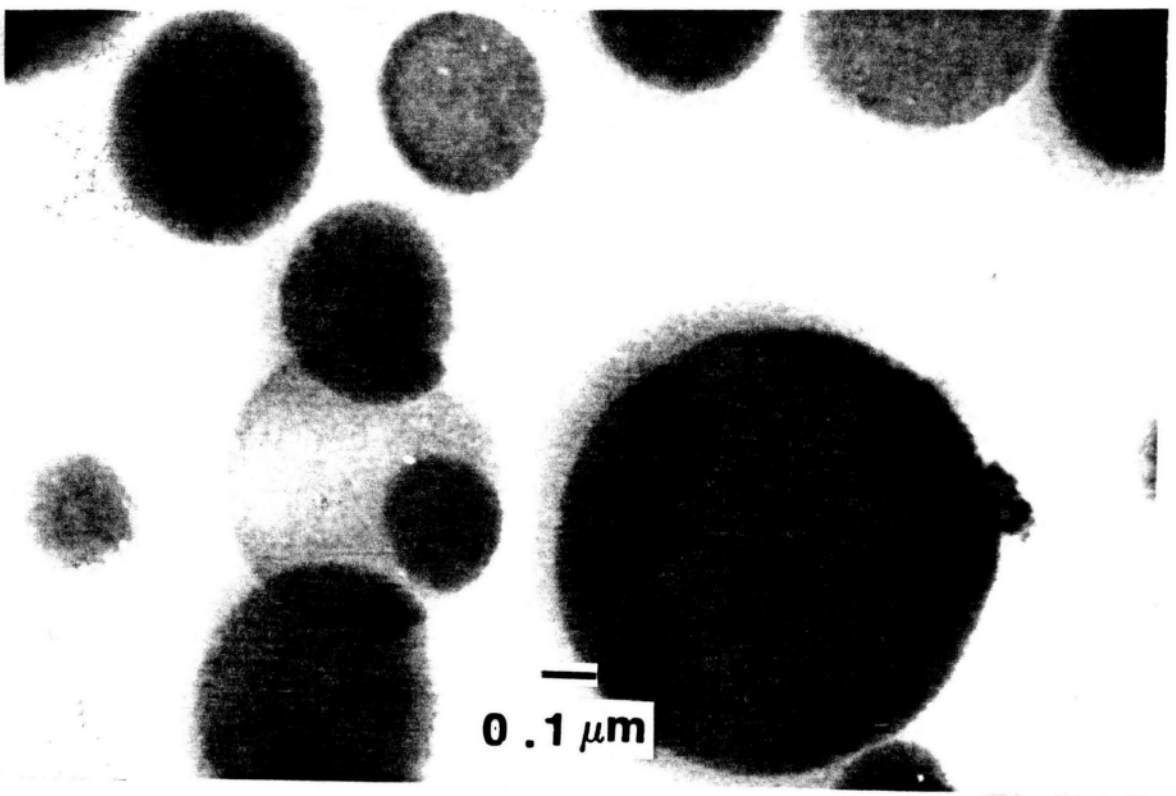

Figure 4.3a TEM micrograph of PMMA-g-PSX (16 Wt.% PSX) before extraction.

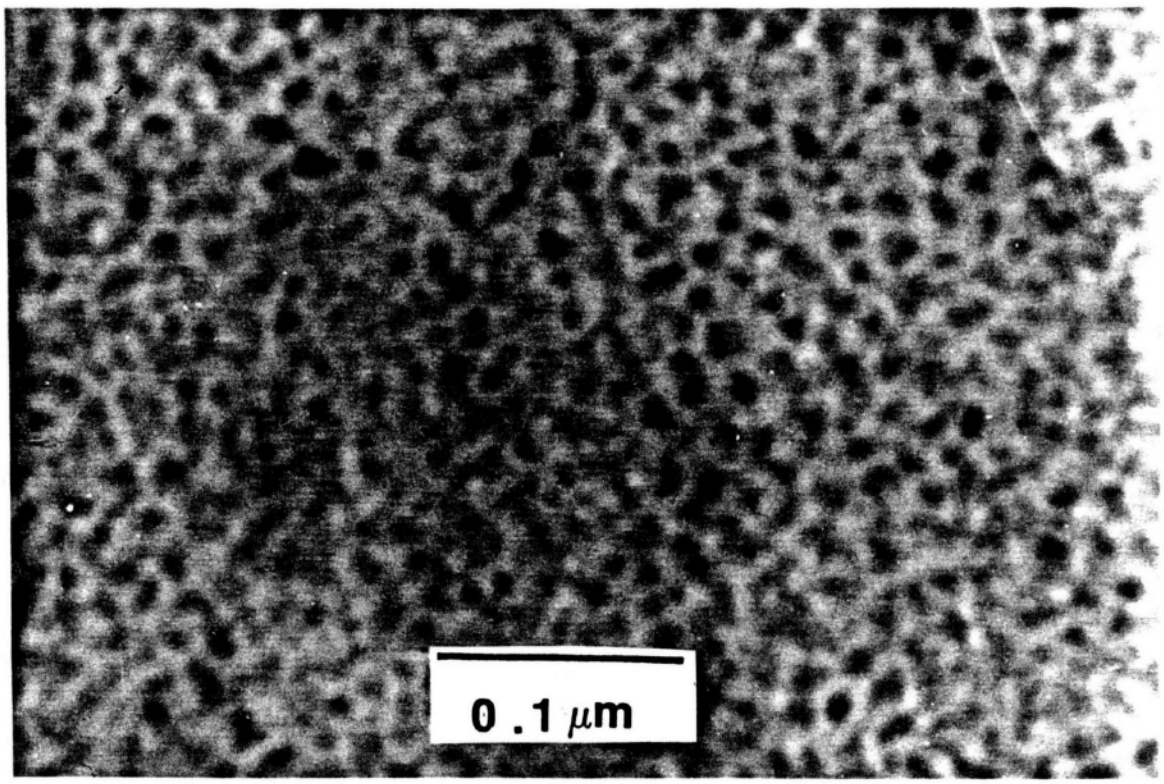

Figure 4.3b TEM micrograph of PMMA-g-PSX (16 Wt.% PSX) after extraction.

In a pure copolymer system, large deviations from the equilibrium structure are improbable because significant deviation from equilibrium structures require attaining highly energetically unfavorable chain conformations arising from the fact that a chemical bond exists between the blocks. Assuming some type of micellation can take place under these nonequilibrium conditions, (at concentrations between C_1^* and C_2^*) the pure copolymer system will attain some type of equilibrium structure for a composition of C_2^* or above. This is quite reasonable, since at concentrations below C_2^*, the system is still highly mobile due to the platicization effect of the solvent.

However, for the presence of homopolymer in the system, no covalent bond exists between the copolymer and homopolymer, therefore homopolymer concentrations can vary throughout the solution. Under highly nonequilibrium casting conditions (thin-casting), local compositional fluctuations may be trapped as the polymer concentration increases during solvent evaporation. Therefore, observed microstructure will contain the morphology obtained for that local composition, in addition that for pure copolymer it should be noted that in systems where the chemical structure is not well controlled, any resulting broad molecular weight distributions or variances in block architecture may

contribute to the heterogeneity of the thin-cast film morphology.

If the homopolymer is compatible with the copolymer, with the domain forming block (not the block corresponding to the homopolymer) is present in low concentrations (about 20 Wt.% or less), large areas of pure homopolymer (where no domains are present) are typically observed. At higher concentrations, variation in local concentration of the homopolymer may cause phase transitions resulting in several types of morphological textures being observed throughout the specimen. Incompatibility of the homopolymer will result in discrete macrophase-separated domains of either the homopolymer in a copolymer matrix or copolymer in a homopolymer matrix, depending upon the amount of homopolymer present.

Depending on the degree of heterogeneity observed in the thin cast films, the presence of homopolymer may be determined. This will allow insight into the interpretation of microstructural features of microtomed sections or the need for further purification. Figure 4.4a illustrates the presence of several morphological textures in a polystyrene-siloxane diblock (PS-b-PSX) at 50 Wt.% PSX composition. On the left side of the micrograph, the dark phase (siloxane) is present as spherical and lamellar structures. The right

side exhibits only a lamellar structure, which is the expected structure for this composition. This is indicative of homopolymer solubilized into the structure shown in the left side of the micrograph, resulting in local phase transitions and the observed heterogenous structure. In contrast, a system which was purified by various homopolymer extraction techniques (Figure 4.4b), shows a fairly consistent microstructure.

Qualitative analysis was also useful in the evaluation of polymer synthesis techniques. Figure 4.5 (a and b) depicts two microstructures of the PS-b-PSX system. Figure 4.5a demonstrates the microstructure of PS-b-PSX copolymer synthesized by typical anionic techniques[9,5], where approximately 1Ø to 15% of the growing PS homopolymer chains are terminated by impurities introduced through the addition of the PSX monomer. Altering the monomer addition method (adding the monomer in steps rather than all at once) reduces the amount of terminated homopolymer species resulting in the depicted microstructure in Figure 4.5b. NMR analysis shows that the composition of both polymers is approximately equal. However, the polymer synthesized by typical anionic methods has a PSX block molecular weight about 1Ø to 15% larger than the polymer synthesized by PSX monomer addition in sequential steps, but its overall

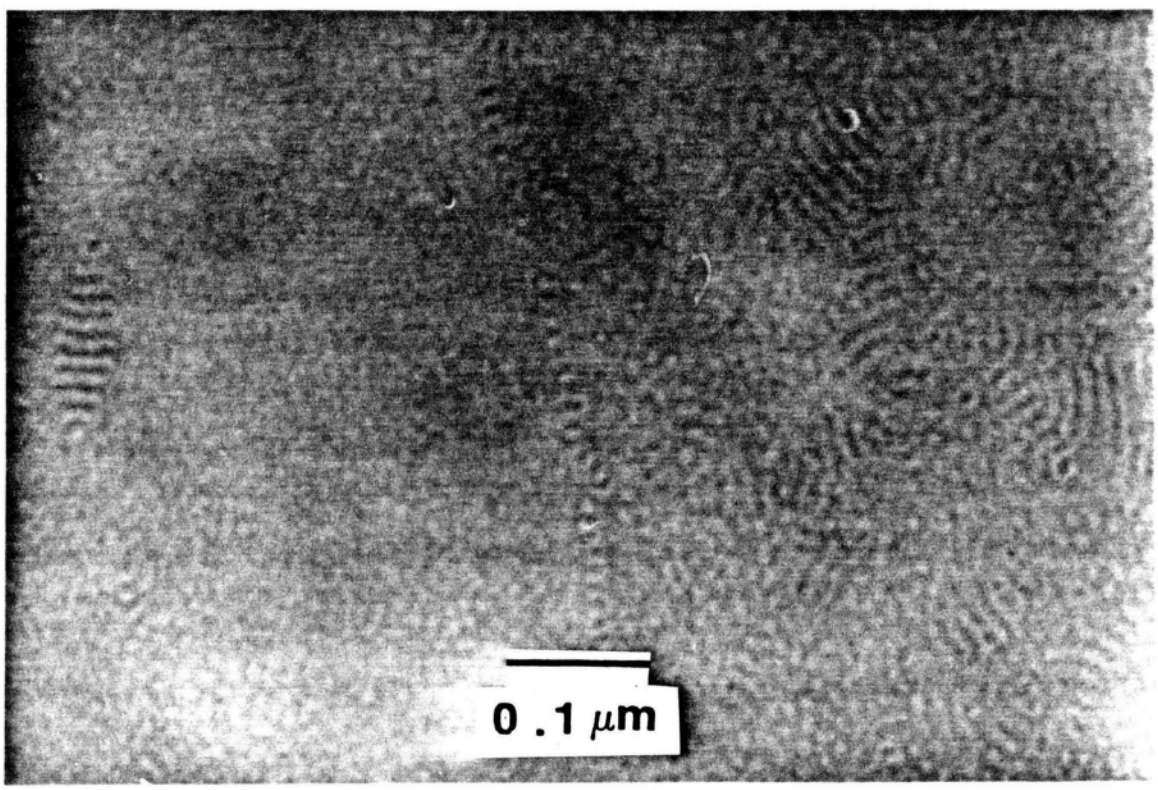

Figure 4.4a Unpurified PS-b-PSX [5Ø Wt.% PSX (1ØK-1ØK)] demonstrating the presence of several morphological textures.

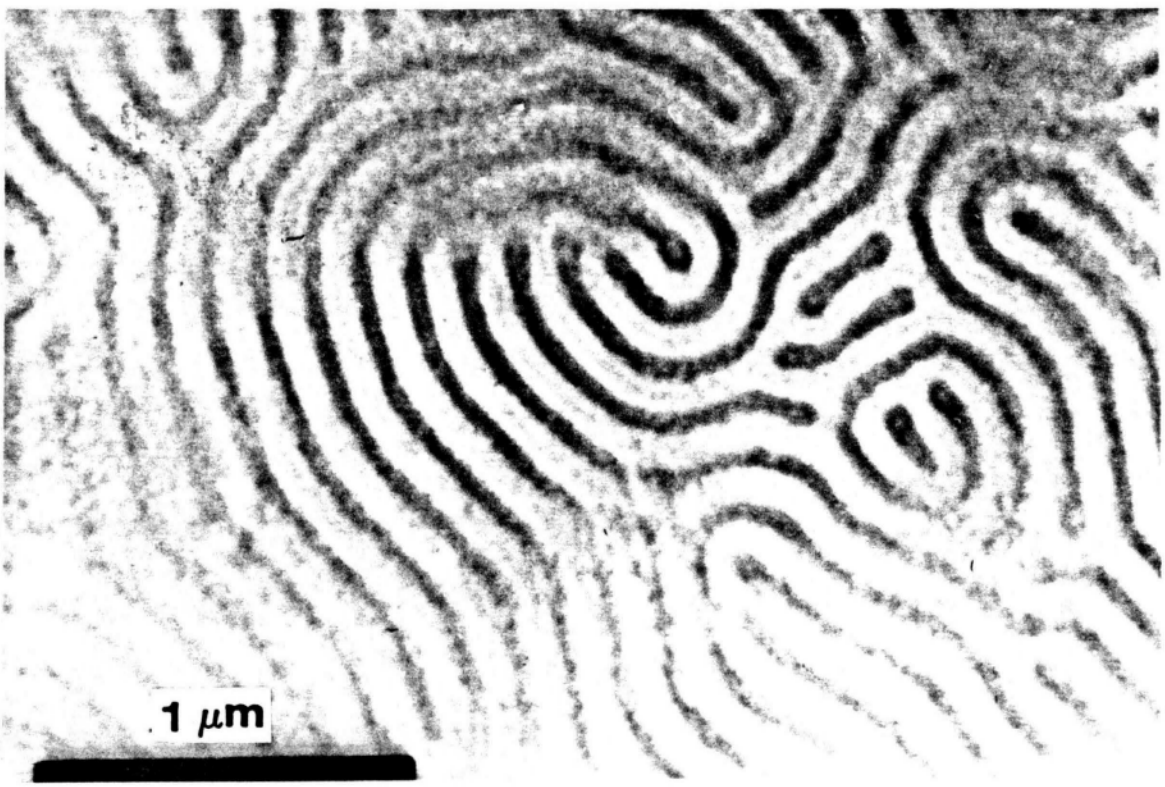

Figure 4.4b Extracted PS-g-PSX [50 Wt.% PSX (10K-10K)] showing a consistent microsructure.

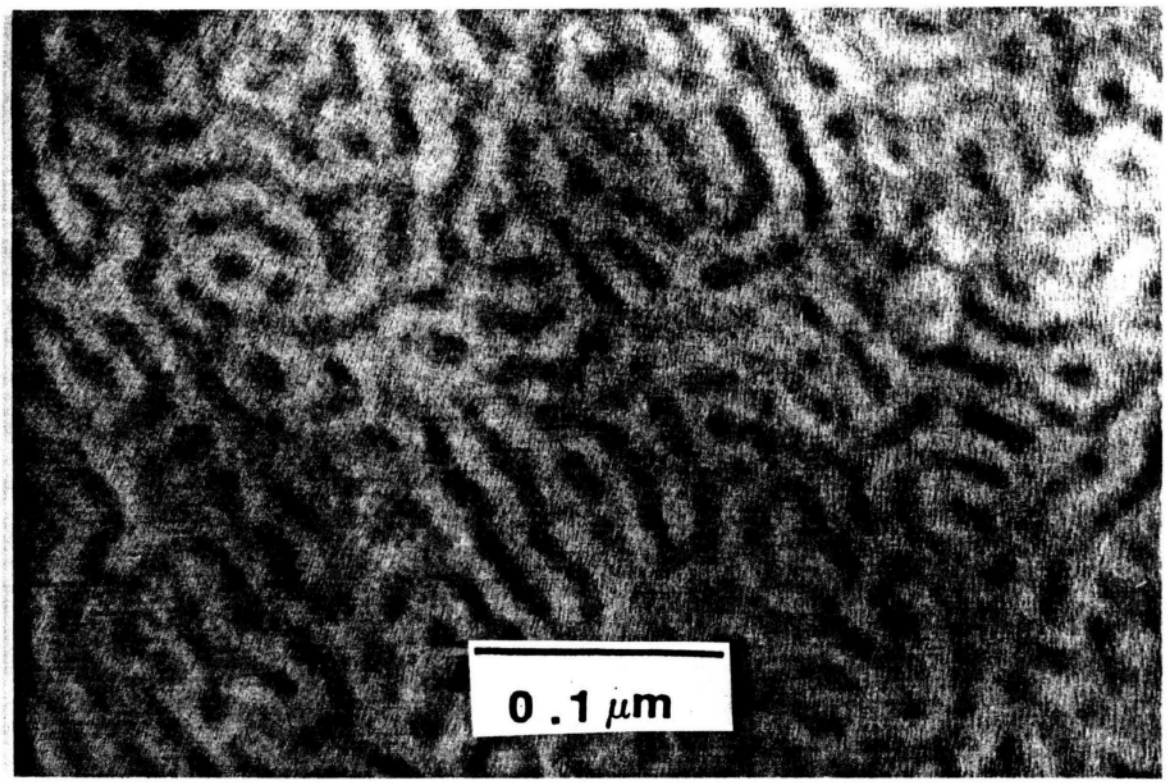

Figure 4.5a PTBS-b-PSX [50 Wt.% (10K-10K)] synthesized by standard anionic techiniques.

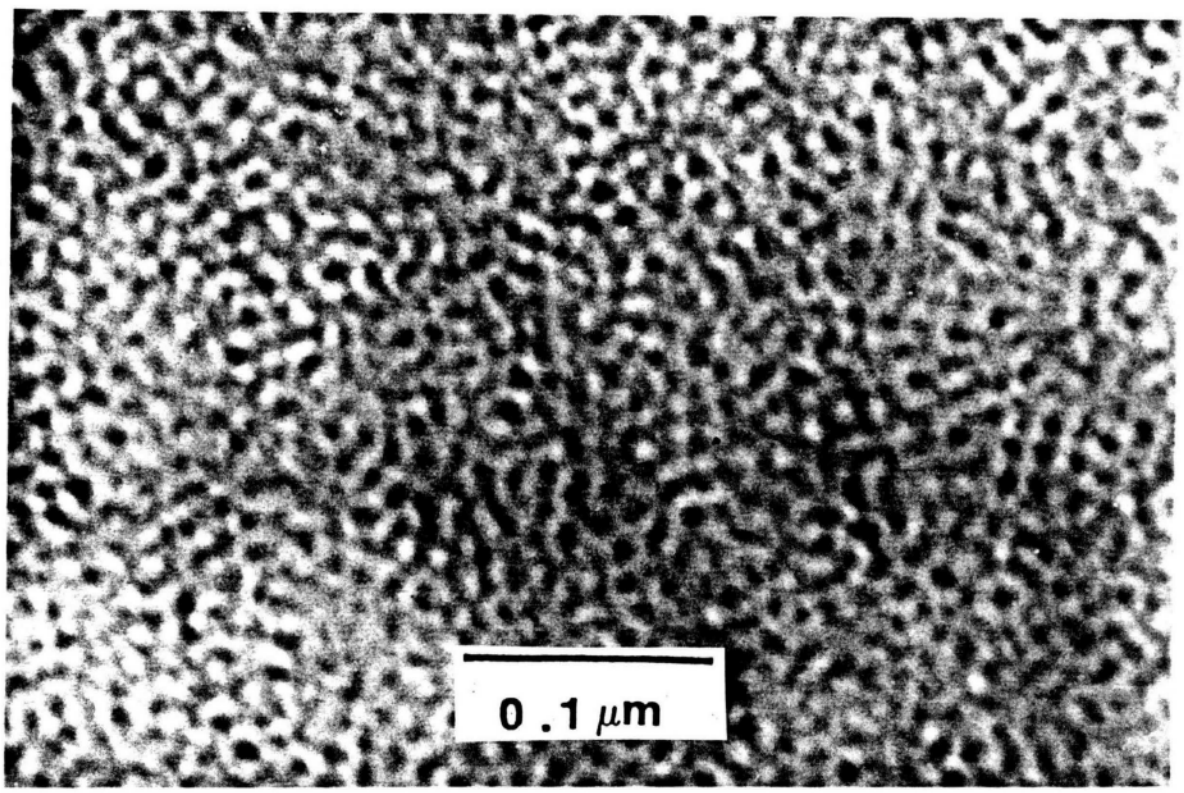

Figure 4.5b PTBS-b-PSX [50 Wt.% PSX(10K-10K)] with monomer added in sequential steps rather than at once.

composition is diluted to similar values by the PS homopolymer. Demonstrating qualitative analysis is very sensitive to changes in the chemical microstructures resulting from different processing conditions.

4.1.4 Characterize Phases in Blends.

In recent years, strong interest has been generated in the use of blending as a method to modify polymer properties to meet existing design criteria. Contingent on the properties of interest, the miscibility of the polymer species will strongly influence the resulting properties. Even though significant advancement toward the prediction of polymer pair miscibility has been made over the years, there is still a need to determine miscibility experimentally. Accordingly, qualitative analysis may be used as a method for easily determining miscibility of blended polymer pairs.

Quite simply, the presence of a macrophase separated structure in a thin-cast film indicates immiscibility of the blended polymers, providing that several criteria are met. First, a good solvent for both components or nonpreferential solvent is used in the casting. A preferential solvent can induce phase separation by favoring one component as the continuous phase. Secondly, when blending with a copolymer,

the copolymer should free of unreacted oligomer which could be mistakenly identified as macrophase separated copolymer.

Even when sufficient differences in a contrast mechanism(s) exist between the two phases, the microstructural evaluation by TEM of novel multiphase copolymer systems can pose a problem. It is sometimes difficult to distinguish which projected phase has a stronger operating contrast mechanism (which is the darker phase). Although theoretical calculations are possible, values for some of the critical materials parameters used in the calculation are not always available. Hence, it is suggested that a blend containing the copolymer and a homopolymer of one of the components contained in the block copolymer be used for calibration. The concentration of the copolymer should be sufficiently low (about 10 Wt.%), so that the copolymer will form the discrete phase. The homopolymer molecular weight should be relatively high, so as to assure incompatibility. The intensity of the background (the continuous homopolymer phase) relative to the copolymer discrete phase will determine which phase is the lighter and which is the darker.

Subsequent EDX analysis, can confirm the composition of the discrete phase, if an element in one or both components is within the limits of detection of EDX ($Z > 10$). In the

polysulfone-siloxane (50 Wt.% PSX) blend, the S and Si atoms were unique to each block respectively, and therefore were used for compositional analysis. From the EDX spectra (Figure 4.7a and b) of the lighter discrete phase and darker continuous phase (pictured in Figure 4.6b), the continuous phase was shown to have higher Si/S ratio of about 2:1 compared to the 1:1 Si/S ratio of the lighter phase. Higher magnification TEM micrographs (Figure 4.6a) a microphase separated structure representative of the copolymer microstructure. Hence, it was concluded that for the 50 Wt.% PSX blend of a polysulfone-PSX perfectly alternating copolymer and polysulfone homopolymer, the lighter discrete phase was the homopolymer and the darker continuous matrix was the PSF-PSX copolymer.

It should be noted, that in all of the polymer studied in this thesis, siloxane was present as the darker phase. Staining of the siloxane was not necessary, since the difference in mass thickness contrast between siloxane and the polymer of interest were sufficient to produce detectable contrast levels. If negligible contrast is present between the two components in a copolymer, staining may be employed. However, very little systematic studies have been done on staining with heavy metal containing reducing agents (like osmium tetroxide OsO_4). It is

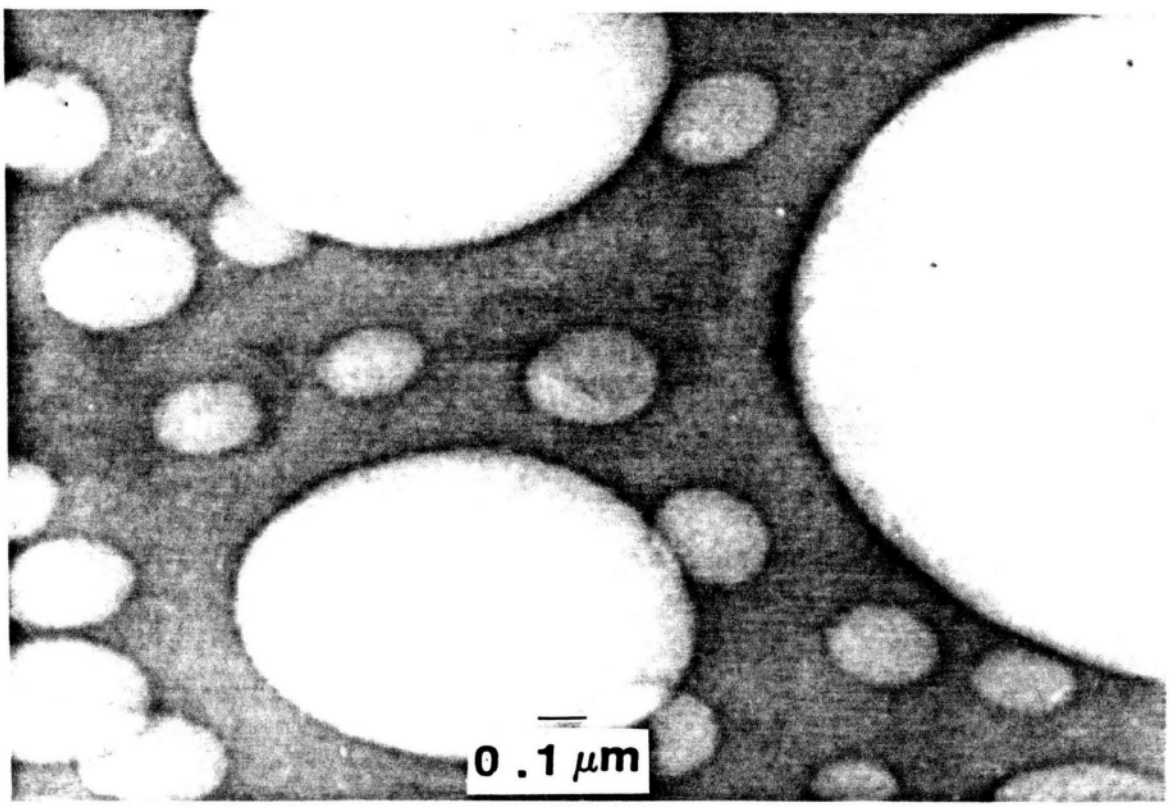

Figure 4.6a TEM micrograph of polysulfone(PSF)-PSX (12K PSX-5K PSF)perfectly alternating copolymer/PSF homopolymer blend (50 Wt. % PSX).

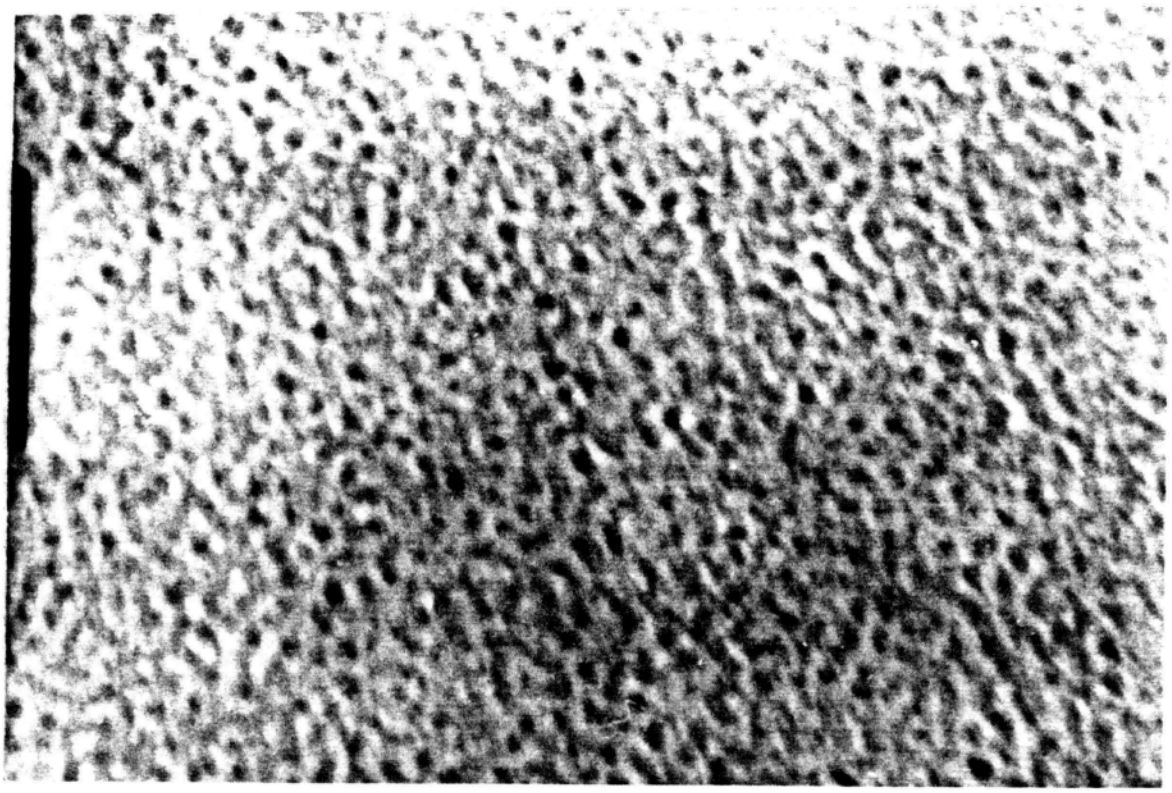

Figure 4.6b Higher magnification photomicrograph of the PSF-PSX/PSF (50 Wt. % PSX blend) martrix (Figure 4.6a).

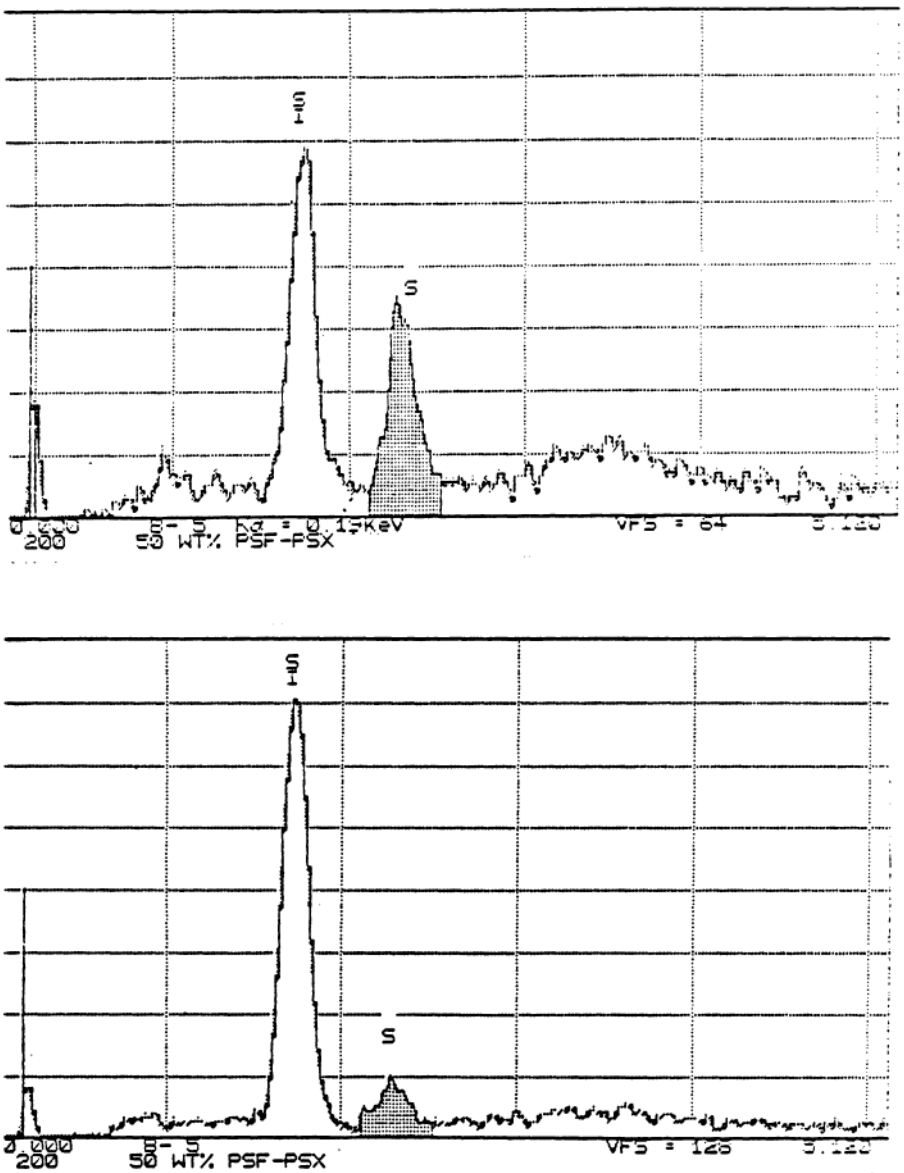

Figure 4.7a and b EDX spectra of the darker matrix (top) and the lighter discrete phase (bottom).

cautioned that staining butadiene with OsO_4 has been shown to increase in domain size proportional to log(ct), where c is the solution concentration and t is time[88].

4.2 PMMA-g-PSX 16 Wt.% Siloxane Series

4.2.1 Microstructural Difference Between Thin- and Thick-Cast Films

For simplicity, a standard nomenclature will be adopted to describe the difference in the graft copolymers. A macromer graft system consisting of a graft molecular weight 20,000 g/mol PSX at an approximate composition of 16 Wt.% PSX will be referred to a 20/16 graft copolymer.

Figures 4.8, 4.9 and 4.10 illustrates thin- and thick-cast microstructures for the 5/16, 10/16 and 20/16 copolymers respectively. Comparison of the thick- and thin-cast microstructures yields several interesting results. In general, the thin-cast spherical domains are not as well defined or as symmetric, and have a larger distribution of phase sizes than the thick-cast films. In the thin film forming process of the low (16) Wt.% PSX PMMA-g-PSX system, there seem to be two critical factors that determine the

nature of the observed microstructure. The first, is the rapid solvent evaporation rate (kinetics). As discussed in the literature review, the excess interfacial volume created by the nonequilibrium process, will increase interfacial mixing and result in less-defined phases observed in all of the thin cast structures. Secondly, the film forming process is dynamic in nature. In the thin-casting process, a drop of solution with a diameter on the order of a millimeter, forms a solid film about 50 mm in diameter and 50 nm thick in approximately one second. As the solution begins to spread onto the substrate, the surface area dramatically increases. The evaporation rate will subsequently increase, due to the increased access of the solvent to the atmosphere. In the plane parallel to the substrate, the leading edge of the advancing solution is the first part of the solution to increase its surface area and will accordingly be the first part of the film to reach C_s^*. In the plane perpendicular to the substrate, it is the air/film interface which will reach C_s^* first. Provided that solvent concentration below the surface is sufficiently low, such that the surface is not resolvated of by the solvent diffusing from the bulk through the surface. When any part of the film reaches C_s^*, the dynamic process turns into a essentially a static process. This is evidenced by the

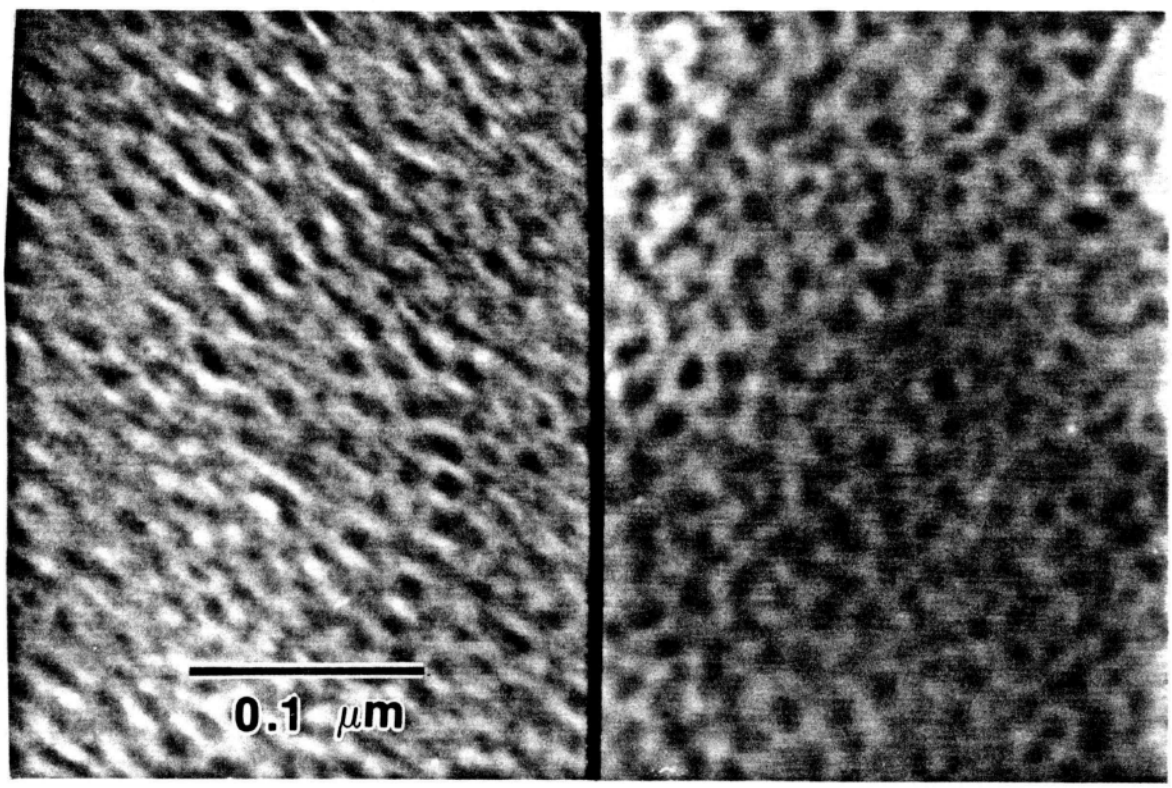

Figure 4.8 TEM micrographs of 5/16 PMMA-g-PSX thick-cast (right) and thin-cast (left) films.

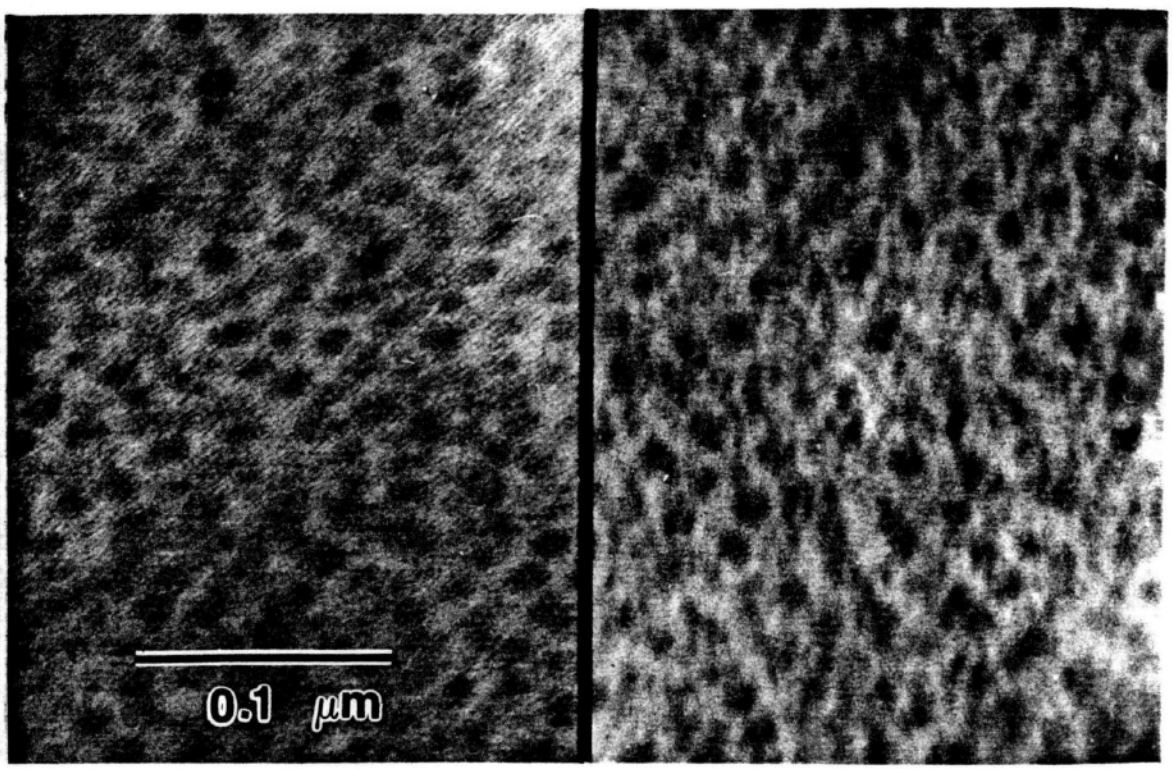

Figure 4.9 TEM micrographs of 10/16 PMMA-g-PSX thick-cast (right) and thin-cast (left) films.

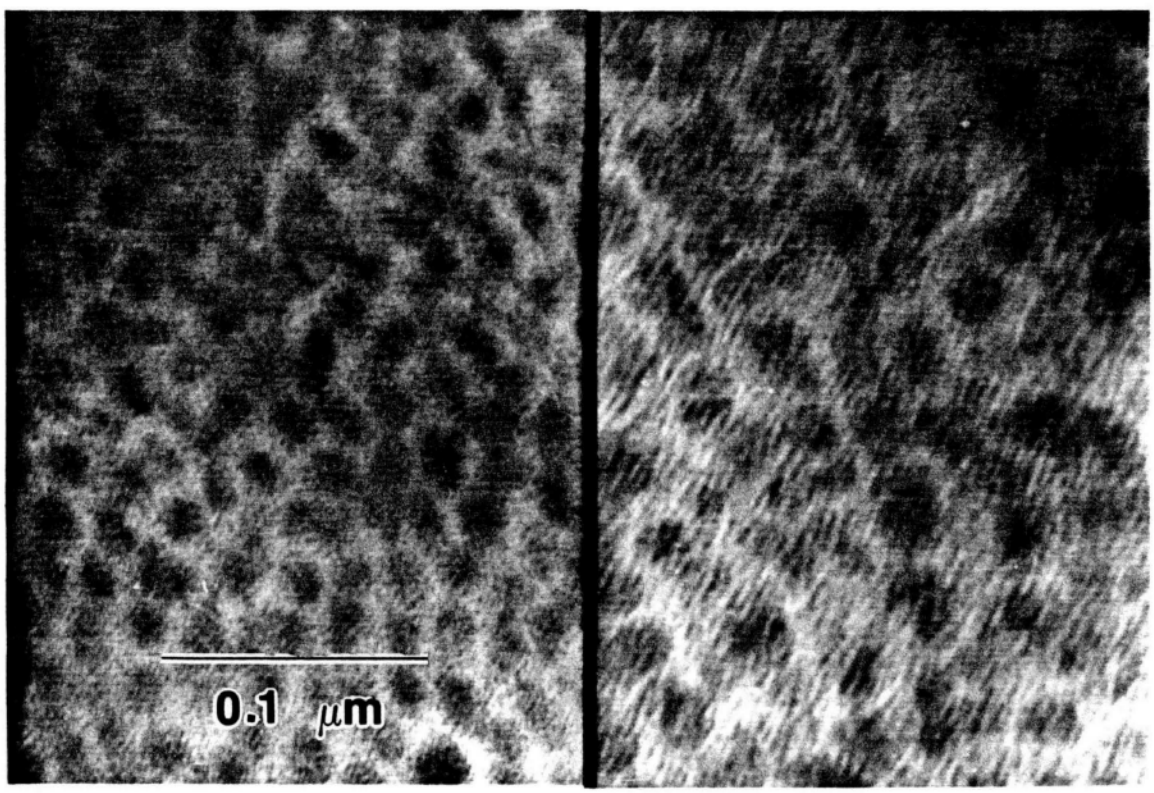

Figure 4.1Ø TEM micrographs of 2Ø/16 PMMA-g-PSX thick-cast (right) and thin-cast (left) films.

thinner outer edges observed, as determined from the color of the film, in the thin-cast films. The thin skin formed on the surface when casting onto a solid substrate supports the initial formation of a surface film.

It follows that when phase separation occurs (at C_2^*), the remaining viscous solution is still in motion. As the concentration increases (from C_2^* to C_3^*) some areas of the film solidify (reach C_3^*) before others. Hence, the part of the film that has not reached C_3^*, will be subjected to some type of shearing action. Consequently, domain symmetry in those regions will be affected. The result is the observed variation in the shape of the domains of the thin-cast films. A comparison of domain sizes of thick- and thin-cast films, measured by quantitative analysis (described in section 3.6), is presented Table 4.1. The size (mean circular diameter) of the thick- and thin-cast microstructures for 5/16, 10/16 and 20/16 system are within experimental error (typically ±0.6 nm) of the quantitative analysis. The experimental error is determined from the area a pixel represents in the digitised image (section 3.6). However, the standard deviations of the domain sizes are significantly larger in for the thin-cast films. A possible cause of the variation in spherical domain size in thin-cast films may be the thickness of the solution during film

Table 4.1

Quantitative Analysis Results of 16 Wt.% PMMA-g-PSX Series

Mean Circular Radius

Sample	Thick-Cast	Thin-Cast
5/16	4.Ø nm	4.3 nm
1Ø/16	7.5 nm	6.3 nm
2Ø/16	1Ø nm	1Ø.5 nm

formation. As mentioned before, when the solution spreads onto the substrate the it becomes thinner. When the solution concentration is between C_2^* and C_3^*, if the thickness is less than the size of a domain, the domain will flatten and become lens shaped. Since TEM is a two dimensional projection of a three dimensional structure, the apparent domain size will be larger. This effect is also clearly evidenced by the elliptical shape (radially oriented) of macrophases structures formed in blends (Figure 4.6b), where the thickness of the macrophase domain is larger that the thickness of the film. Interestingly, from thermodynamic and kinetic points of view one would expect larger domains in a highly metastable film cast from a solvent that slightly favors the continuous phase. Although, it is evident that even though there are differences, the size of the domains in thin-cast PMMA-g-PSX graft copolymer films may be used as an estimate of domain size in the thick-cast films.

In summary, analysis of thin-cast structures indicated the presence of discrete spherical domains and gave an accurate estimate of domain size. Additionally, a small scale grainy structure was observed in the background of some of the micrographs (especially Figure 4.12 the 2Ø/16 graft copolymer). This is thought to result from random thickness fluctuations, caused by PMMA degradation, enhancing the

phase contrast features structures. Since PMMA is very sensitive to degradation via electron beam exposure, precautionary steps outlined in reference 85 were employed. Even using great care in the examination of PMMA-g-PSX TEM specimens, during the initial exposure to the electron beam an increase in mass thickness contrast was observed, probably due to subsequent crosslinking of the PSX phase and degradation of the PMMA phase under exposure to the electron beam.

4.4.2 Quantitative Microstructural Analysis of Thick Cast Films

Before analyzing novel multiphase copolymer microstructural features, the various aspects of the compositional and molecular weight characteristics, must first be delineated.

In macromer graft systems synthesized free radically, there are not only molecular weight distributions present, but also compositional distributions. Figure 4.11 demonstrates the simultaneous variation of molecular weight and composition with concentration, typically observed for free radically synthesized macromers. Several techniques were employed in the compositional and molecular weight

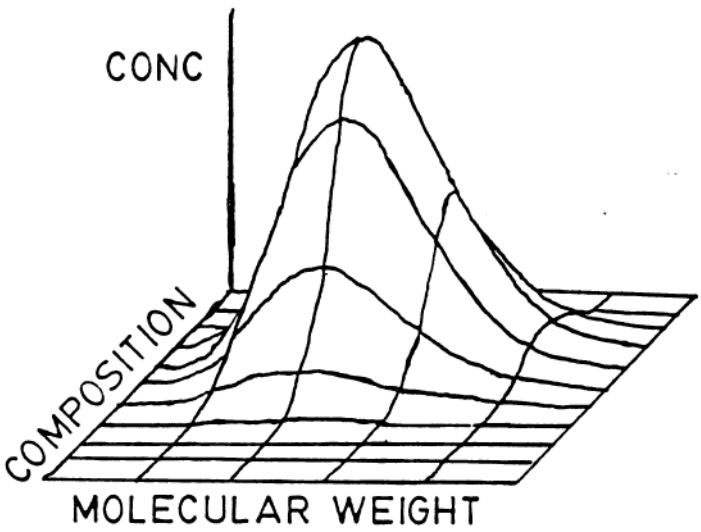

Figure 4.11 Schematic of the concurrent variation of composition and molecular weight in free radical macromer graft systems.

analysis of the PMMA-g-PSX polymers. A detailed discussion of the techniques and results obtained are provided in Steve Smith's Ph.D. dissertation. What will be presented here is brief description of the of the techniques and result important to the evaluation of the microstructure.

Super Critical Fluid Extraction (SCFE) was used to determine compositional heterogeneity. Fractions are obtained from polymer solution at the critical point, where pressure changes will induce a fraction of the copolymer to precipitate on the basis of solubility. These fractions are then analyzed by H^1 NMR and GPC to determine the composition and relative molecular weight distributions. The results of an extraction of a 1Ø/12 sample are tabulated in Table 4.2. As seen from Table 4.2, the percent of the total sample for each fraction is evenly distributed and a large distributions of compositions are present. The results indicate that this polymer has a heterogeneous or broad compositional distribution. In addition, no significant amount of homopolymer is detected when more than one backbone per graft exists. Hence, the siloxane grafts appear to be uniformly incorporated into the system. For a more in depth discussion of this analysis one is referred Steve Smith's Ph.D. dissertation[9,8].

Table 4.2

NMR Analysis of the SCFE Fractions

PMMA-g-PSX	Fraction					
Sample Analysed	1	2	3	4	5	6
10/12 Wt.% PSX by NMR	35	25	11	11	9	11
% of total sample recovered	6	19	14	17	16	28
10/27 Wt.% PSX by NMR	42	42	22	22	24	
% of total sample recovered	15	12	59	15	8	
10/43 Wt.% PSX by NMR	54	46	44	45	44	
% of total sample recovered	15	13	62	7	3	

GPC results indicate that the breadth of each fractions relative molecular weight distribution (MWD) are representative of the whole fraction, but that the Mn decreases as the weight percent PSX increases in each fraction. Membrane osmometry and isorefractive index measurements (Table 4.3) show that the MWD of the whole copolymer and PMMA backbone are quite broad as compared to typical anionic copolymerization values (typically 1.1), with the PMMA backbone generally having the broader distribution.

Other relevant information was provided by TGA analysis[9,5]. Free radical reactions may terminate by several different mechanisms. In the case of free radically polymerized PMMA, the predominate mechanisms are combination and disproportionation. Chains terminated by these mechanisms degrade at approximately 175°C and 220°C respectively. The copolymerization with siloxane has two pertinent effect on the degradation behavior. First, when the average number of grafts per backbone is unity or greater, no significant degradation occurs until 300°C. Secondly, pure copolymers are more stable than copolymers of higher PSX content blended with homopolymer PMMA to achieve similar PSX compositions. We believe that the presence of the macromer changes the termination mechanism, and

Table 4.3

Molecular Weight and Compositional Analysis

Graft MW	Wt.% PSX[1]	$\langle M_n \rangle$[2]	MWD	MWD(PMMA)
5K (5/16)	14.Ø	1ØØK[3]	-	-
1ØK (1Ø/16)	15.Ø	165K	-	-
1ØK	29.Ø	135K	2.75	3.88
1ØK (1Ø/45)	48.Ø	88K	3.95	5.15
2ØK (2Ø/16)	16.8	-	-	-
2ØK	25.Ø	96K	1.66	2.53
2ØK (2Ø/45)	42.Ø	75K	1.51	2.72

[1] values determined by NMR

[2] values determined by membrane osmometry

[3] values determined by differential viscometer

subsequently alters the nature of the end group, which is thought to be the initiator of degradation. The fact that when at least one backbone per graft is present, no degradation is detected at the degradation temperature for homopolymer PMMA, again suggests uniform incorporation of grafts into the system with preferential positioning at chain ends. The termination of a chain by a macromer unit is supported by the decreased reactivity of the propagating radical just after a macromer is incorporated.

Another important aspect to consider in the analysis of macromer graft copolymers is the number of grafts per backbone. Table 4.4 shows the average number of grafts per backbone calculated on the basis of a 100,000 g/mol total molecular weight. Although, in the real system some type of distribution of the number of grafts per backbone will exist, the number average is still representative in terms of observable phase behavior and is generally useful in discussion of this phenomena.

From the results discussed so far, the 16 Wt.% PSX PMMA-g-PSX series seems to have a broad molecular weight and composition distribution. Other data indicates that the macromer is uniformly distributed and may be preferentially located at the chain ends. Using these results as a criteria, examination of the number of grafts per backbone

Table 4.4

Model Calculations for the Number of Grafts/Backbone

Based on 100,000 g/mole Total Molecular Weight

	Wt. % PSX				
Graft M_n	10	20	30	40	50
1,000	10	20	30	40	50
5,000	2	4	6	8	10
10,000	1	2	3	4	5
20,000	0.5	1	1.5	2	2.5

gives some insight into the microstructural behavior of the 16 Wt.% PSX graft system.

Assuming the grafts are uniformly distributed and that a majority of the grafts are present at the chain ends, then at a specific composition, if the average number of grafts per backbone were unity, the system would essentially resemble a mixture of different diblock and graft copolymers. The chains with macromer located only at the chain (pseudo-diblocks) would contain a PSX block with narrow MWD (Poisson distribution for anionic polymerization) and a variable molecular weight PMMA block, most likely with a broad Gaussian distribution. A number average of grafts per backbone less than one would suggest the presence of homopolymer PMMA. Averages higher than unity, indicates further incorporation into of the graft into the backbone.

One way to gain insight into the heterogeneity of the chemical structure is to examine microstructural features such as domain size and interdomain spacings. Since no equilibrium theory predicting the absolute value and scaling relationships of domain size and spacings for graft copolymers have been established, one is forced to make comparisons to the relationships derived for diblock and triblock copolymers. The standard nomenclature used for an AB copolymer, that forms either a cylindrical or spherical

microstructure, is that the A component will always form the discrete phase and the B component the continuous phase.

From equilibrium theory it is found that the interdomain distance and domain size of well defined diblock and triblock copolymers, scale with molecular weight to the 2/3 power. In Table 4.1 values of the average circular domain radius, as measured from quantitative analysis for thick-cast films, are shown for 5/16, 10/16 and 20/16 samples, Figure 4.12 illustrates the TEM photomicrographs comparing each spherical structure. Domain radius measurements made by hand for 30/16 and 40/16 are also included in Table 4.1. The domain radius was found to vary with molecular weight to the 0.66 power, as determined from the slope of the log-log plot of domain radius vs graft molecular weight (Figure 4.13). The agreement with the 2/3 power law suggests that domain formation of the macromer graft copolymer is subject to the same underlying thermodynamic influences that determined the scaling relationships in the equilibrium theory derived for the domain formation for di- and triblock copolymers. The close correlation to the 2/3 power law is not unexpected. Since in the case spherical domain formation, the equilibrium domain scaling relationships are dependent only on the well defined graft molecular weight (domain forming component with a

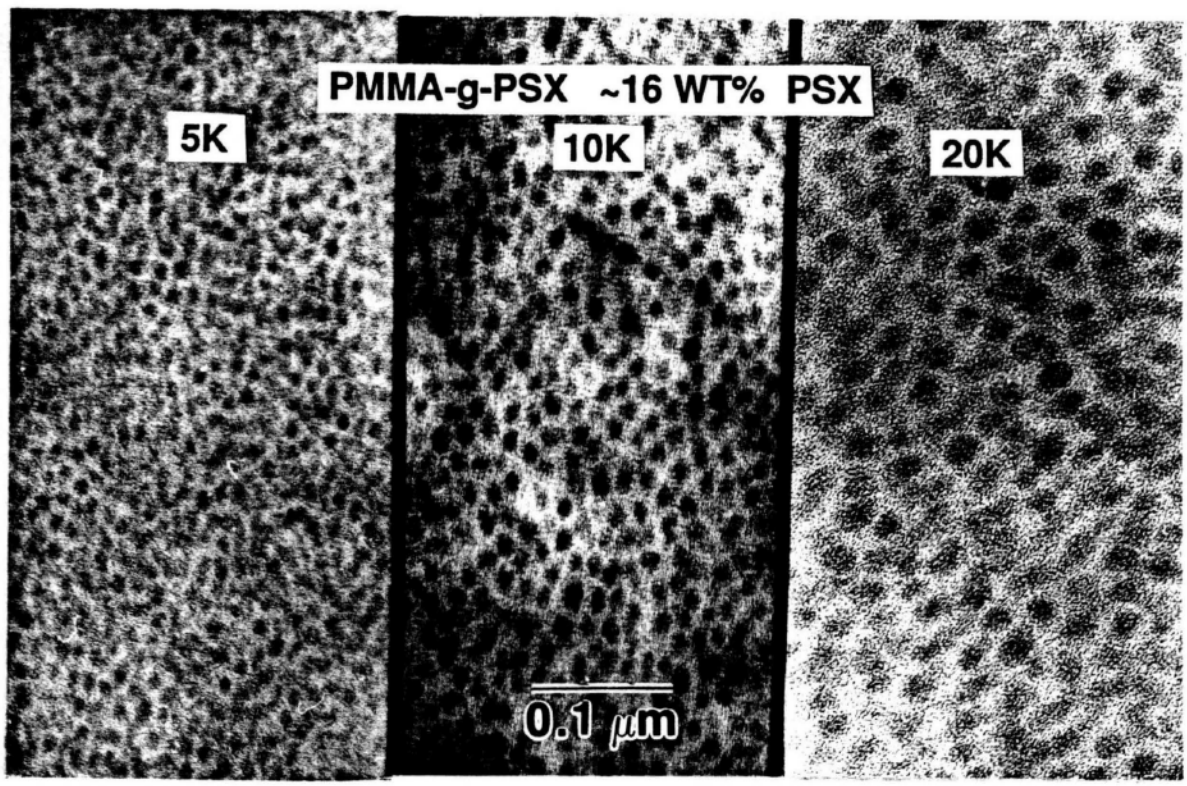

Figure 4.12 TEM microgaphs for the thick-cast films of the 16 Wt.% PSX series.

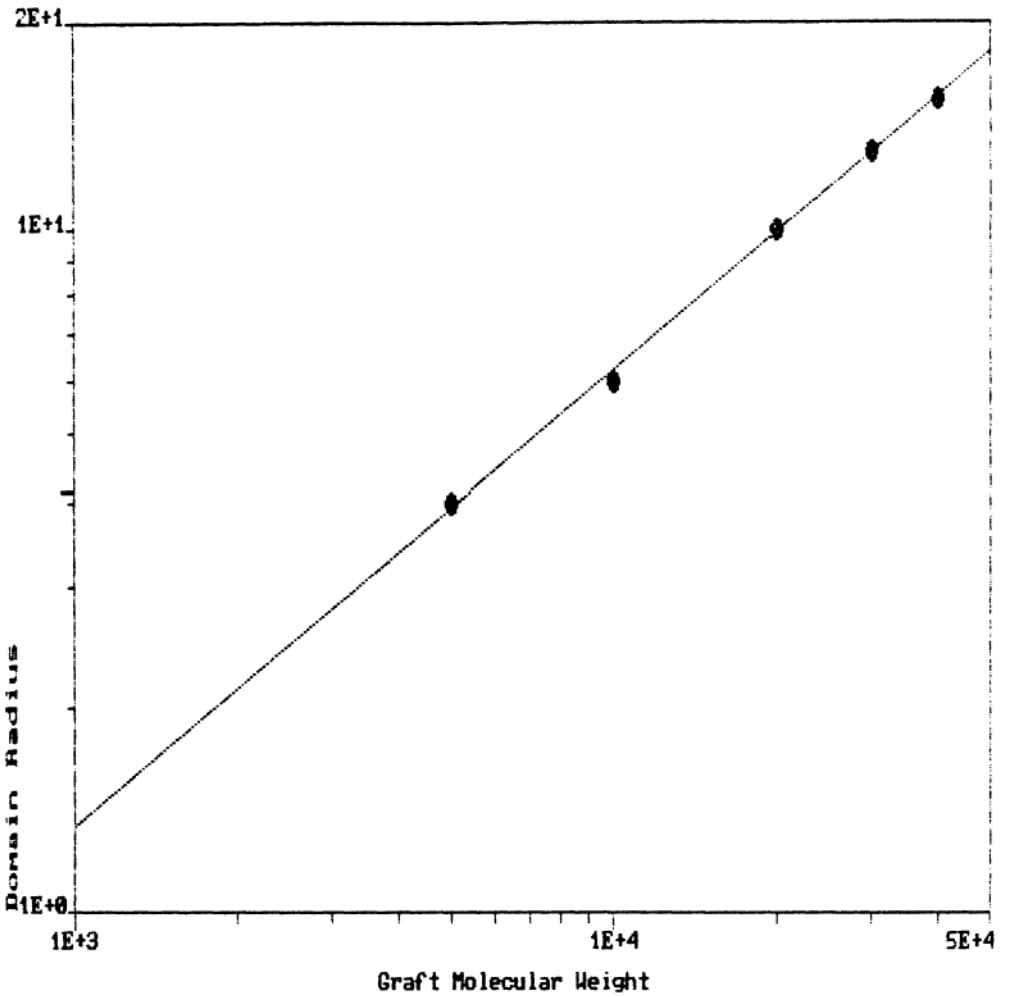

Figure 4.13 Log-log plot of domain radius Vs. graft molecular weight.

narrow molecular weight distribution) and not the heterogeneous PMMA continuous phase forming component.

Generally, the structural differences between an AB diblock and an AB macromer graft copolymer (where A is the graft) that will affect the phase behavior are the nature of the AB chemical junction, the chemical and structural nature of B phase and the number of grafts along the backbone. A graft copolymer with a single graft located at a position along the chain other than the chain end, would have three chains (two B's and an A) entering the junction point rather than two (an A and B) as in the case of diblocks. One effect of the different junction is a larger change in entropy associated with phase separation[4,8] for the graft copolymer, making phase separation more difficult. If enough grafts are present along the backbone, it may affect the equilibrium morphology, much the same way the number of arms affect the equilibrium textures of starblock copolymers (section 2.1.2). This type of effect is more prevalent in the 45 Wt.% series examined in the section 4.3.2, where the number of grafts per backbone is significantly higher. Another effect may be observed in the absolute values of the domain size and interdomain spacing. For example, a BAB triblock will behave as a (1/2A)B diblock and the size of the A domain will scale with 1/2 the molecular weight of A. However, due

to difficulties in obtaining some of the parameters required for equilibrium calculations, a comparison of these calculated values with experimentally determined values is not possible at this time. The comparison of such values will provide insight into whether the graft copolymer studied here behave as diblocks (AB), which would support the preferential positioning of grafts at chain ends, or triblocks (ABA and BAB) or another type of scaling relationship. Nevertheless, some insight into effect of the chemical and structural nature of the B or continuous phase on the phase behavior of macromer graft systems may be obtained from the interdomain spacing scaling relationships and domain ordering.

In well defined di- and triblock copolymer systems, not only do spherical domains obtain uniform dimensions, but the spatial arrangement of the spherical domains is usually quite regular and may be characterized by a basic type of lattice structure (hexagonal close packed (HCP), FCC, BCC or SC). This type of behavior is attributed to entropic repulsion between domains. That is, the domain space filled by the continuous phase is subject to the same homogeneous density and joint localization constraints that result in equilibrium sizes for the discrete domain forming component. Consequently, with a fairly narrow distribution of molecular

weight existing for both components, domains become arranged into a periodic array or lattice, that minimizes free energy. Any variation from this structure, leads to an entropically unfavorable situation of the matrix forming chains having to obtain more extended and energetically unfavorable conformations than those obtained in the equilibrium structure in order maintain a uniform density profile, while maintaining junctions in the domain interface. Thus, the well defined nature and narrow MWD of the di- and triblock chains results in uniform spacing between domains and the subsequent periodic ordering of the spherical domain structure. Employing the same concepts to the PMMA-g-PSX macromer graft systems, one would then expect that spherical domain ordering is sensitive to structural heterogeneities (molecular weight distributions) of the PMMA continuous phase. This appears to be the case for 5/16, 10/16 and 20/16 series.

TEM analysis revealed no apparent periodicity or long range ordering for all graft sizes in the 16 Wt.% series (Figure 4.12). This would concur with the broad molecular weight distributions present in the PMMA continuous phase. It is probable that local interdomain distances may equilibrate to local values of $\langle M_n \rangle$ between domains, where the nonperiodic or disordered array of domains will reflect

the polydisperse nature of the PMMA continuous phase.

Regardless of the local variation in the interdomain spacings, equilibrium scaling relationships of the average interdomain spacings and number average molecular weight $\langle M_n \rangle$ should still remain intact. Additionally, the magnitude of the average interdomain distance should be determined by the $\langle M_n \rangle$. To explore these possibilities, SAXS was utilized[8,9] to obtain information on interdomain spacing and domain ordering for several reasons. One reason is if any significant fluctuations in the interdomain distances existed, the small sampling volume of microtomed sections may not be totally representative of the spectrum interdomain distances present in the system. Possibly skewing the resulting measurements toward that either smaller or larger spacings. To assure a representative sampling would require analysis of a number of sections taken from different areas in the film, which is often time consuming. In addition, several other inherent problems in obtaining reliable interdomain spacing of spherical domains from these TEM micrographs exist. One problem arises from the fluctuation of the relative contrast (background relative to domain) throughout the photomicrographs. If the fluctuations are too great, a sufficient number of interdomain spacing measurements required for a statistical

sampling may not be obtained from quantitative analysis. When determining interdomain spacing of spherical structures by TEM one has to consider that the distances measured are from a two dimensional projection of a three dimensional structure, and will represent true spacing only when the film contains a single layer of domains roughly in the same plane or several planes of highly ordered domains oriented such that domains constructively overlap. SAXS on the other hand, does not suffer from these deficiencies and is more sensitive to the global order due to the larger sampling volume. SAXS analysis of an ordered structure will produce scattering maxima arising from the various different interdomain spacings present in the periodic structure of the unit cell. The smeared SAXS spectra for specimens 5/16, 10/16 and 20/16 (Figure 4.14), show one broad scattering maxima, but no higher ordered maxima. Desmearing the SAXS data revealed one weak higher ordered maxima in the 20/16 specimen, but no higher order maxima in the 5/16 and 10/16 samples. From this it was concluded the domains had no global periodic arrangement that would result in several higher the ordered scattering maxima. This is in accord with the TEM results which indicate the domains exhibited some localized packing fitting an hexagonal packed lattice, but had no long range periodic spatial arrangement.

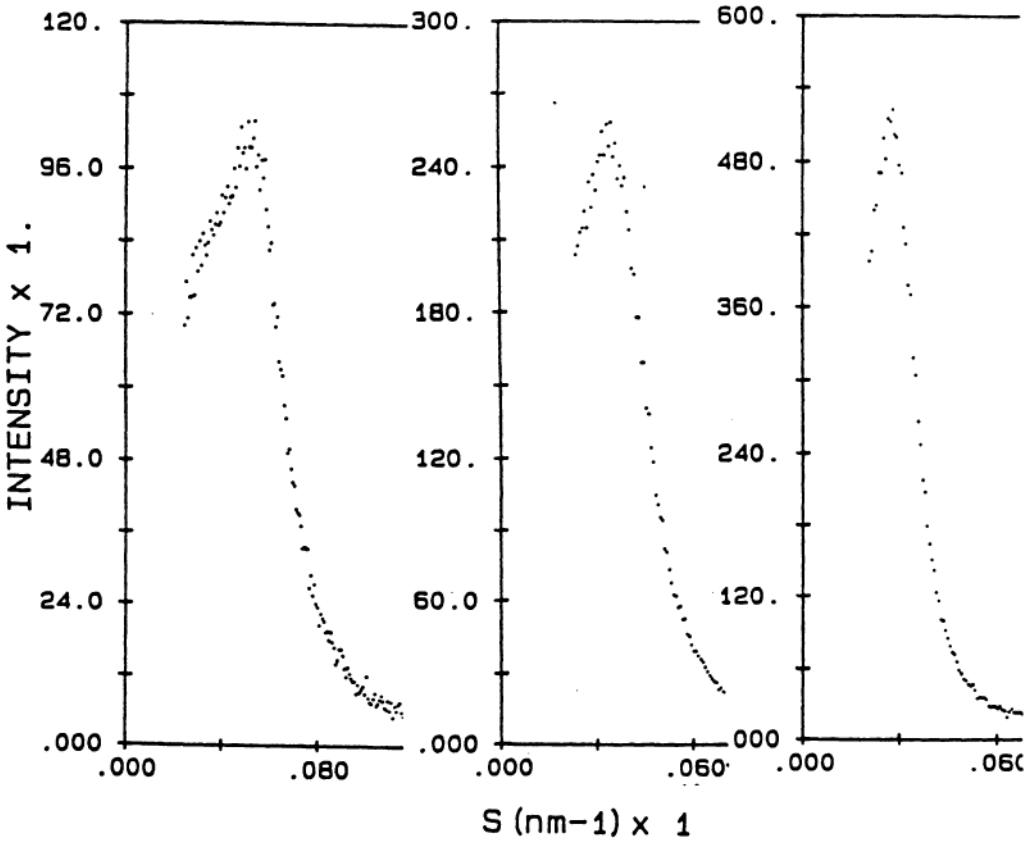

Figure 4.14 SAXS spectra for 5/16, 1Ø/16 and 2Ø/16 (respectively from right to left).

SAXS interdomain spacings, nearest neighbor distances of the SC, BCC, FCC and HP lattices based on volume fraction calculations appear in Table 4.5. Comparison of interdomain spacings show that values determined from SAXS are consistently larger than the calculated nearest neighbor distances (first order reflections) for the SC, BCC and FCC lattices. The measured interdomain distances more closely fit the calculated interdomain distances for a hexagonal packed lattice. As previously stated, no higher ordered maxima signifies that the 5/16, 1Ø/16 and 2Ø/16 systems does not exhibit any global or long range ordering of domains. From the SAXS and TEM results we concluded, that the domains locally pack into hexagonal lattices according to local PMMA backbone $\langle M_n \rangle$ values, and that the fluctuation of local the $\langle M_n \rangle$ due to the broad molecular weight distributions of the backbone results in the breakdown of any global ordering. Since SAXS interdomain spacings represent the average spacings of a large sampling volume, the proposed relationship between $\langle M_n \rangle$ and the magnitude of the interdomain distances can be confirmed by comparison to calculated values. To further explore relationship the graft copolymer was modelled by its structural equivalent AB diblock. This was done by taking the graft, with a known molecular weight (5K, 1ØK or 2ØK), as the A block size. From

Table 4.5

Measured and Calculated Values of Interdomain Distances

Sample	Experimental	Calculated using Volume Fractions			
	(nm)	SC	BCC	FCC	HCP
5/16	19.Ø*	11.2	12.2	12.5	17.Ø
1Ø/16	28.6*	2Ø.96	22.8	23.5	25.Ø
2Ø/16	36.5*	3Ø.5	33.3	34.2	31.2
2Ø/45	28.1**	--	--	--	26.9

* measured from desmeared SAXS spectra
** measured by quantitative image analysis of TEM micograph

NMR compositional data an equivalent molecular weight ($\langle M_n \rangle$) for the B block (PMMA) fitting a diblock is calculated. For example, a 20/16 graft copolymer has a graft 20,000 g/mol which is 16 Wt.% of the total copolymer molecular weight. In the case of a diblock, simple division yields a 20K PSX/97.6K PMMA diblock. Similar calculations were performed for the 10/16 and 5/16 specimens. Equations 4.1 and 4.2 (obtained from Hashimoto et al.[69]) were utilized for calculation of the interdomain distances assuming a hexagonal packed lattice.

$$4/3\ \pi R^3 = N_A\ V_A \qquad (4.1)$$

where R is the radius of the spherical domains, N_A is the number of A (PSX phase) blocks in the domain and V_A is the molecular volume of each A block.

$$D^3/(2)^{1/2} = N_A\ (V_A + V_B) \qquad (4.2)$$

where V_B is the molecular volume of the B block. Values for R were determined by quantitative image analysis and are listed in Table 4.1. Comparison of calculated and experimentally determined interdomain distances (Table 4.6) show surprising agreement between calculated interdomain

Table 4.6

Comparison of Calculated Interdomain Spacings and Experimentally Measured Interdomain Spacings in nm

Sample	Determined from Desmeared SAXS Spectra	Calculated from Equations 4.1 and 4.2	Measured from TEM Micrographs
20/16	36.5	31.2	31.6
10/16	28.6	25.1	21.0
5/16	19.0	17.0	15.7

spacings and those determined from TEM. The discrepancy between the SAXS and TEM interdomain spacings can be attributed to possible deformation during sectioning and measuring the prjected distance between domains that are not in the same plane. However, SAXS values are still larger than the calculated interdomain distances. This slight disagreement is thought to arise from several deficiencies associated with the determination of the domain radius. First, obtaining domain size information from a binary image assumes a sharp interface and excludes the mixed interphase region. Secondly, the observed increase in specimen contrast during initial exposure to the electron beam is thought to result from radiation induced crosslinking of the siloxane. Crosslinking will result in a small increase the density, slightly shrinking the domain. Back calculation of the domain radius (R) using interdomain spacings (D) measured from SAXS show that experimentally determined R values are approximately 1.5 nm smaller than the back calculated R values. It is believed that when the siloxane contained in the interphase thickness (2 nm for a 67K PS-13K PI diblock[69]) and the effect of electron beam radiation on the PSX domain are considered measured values will fall well within the experimental error (1 %) for the determination of

Wt. % PSX from NMR and the determination of domain sizes from quantitative analysis (±0.6 nm).

Interdomain spacing-molecular weight scaling relationships were determined from the log-log plot (Figure 4.14b) of the total molecular weight of the modelled diblock vs interdomain spacings measured by SAXS. From the linear regression fit the interdomain distances were found to vary with total molecular weight to the 0.56 power. Comparing the agreement of the graft copolymer to the 2/3 power law to PI-PS diblocks that were said to be in good agreement to the 2/3 power law[69,77], show the diblocks deviate from the 2/3 power law. A linear regression line fit to data within the molecular weight range of those used in this study (spherical domain forming PI blocks from 13,000 to 34,000 g/mol) yields a scaling relationship of interdomain spacings to the 0.45 power with molecular weight. Hashimoto et al.[77] attribute the scattering of data around the 2/3 slope line to variations in the chemical composition of the block copolymers. Figure 4.14c shows a close fit of a 2/3 slope line to the data fit by a linear regression line in Figure 4.14b. In the same context, the interdomain distance-molecular weight scaling relationships agree with the 2/3 power law as well as has been shown experimentally with PS-PI diblocks[69,77]. Additionally, the interdomain spacing-

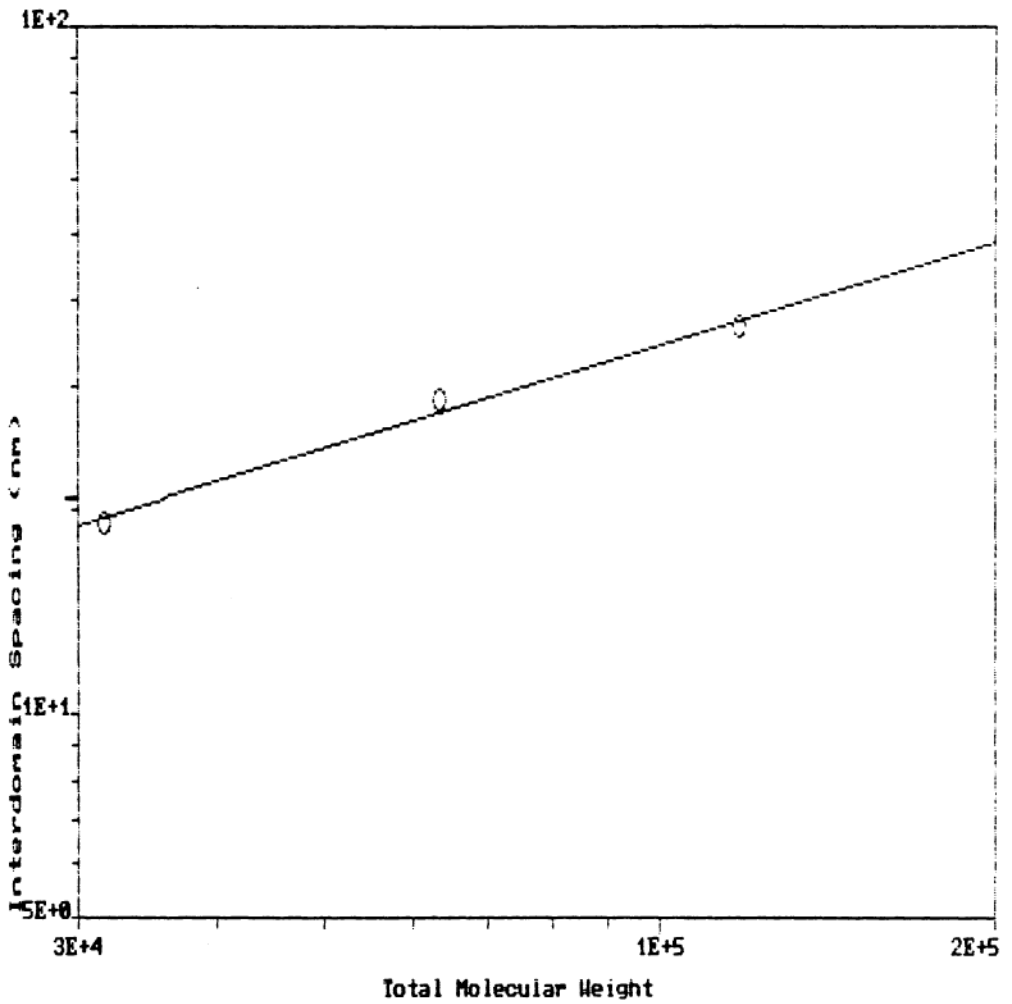

Figure 4.14b Log-log plot of interdomain distance vs total molecular weight with linear regression fit line.

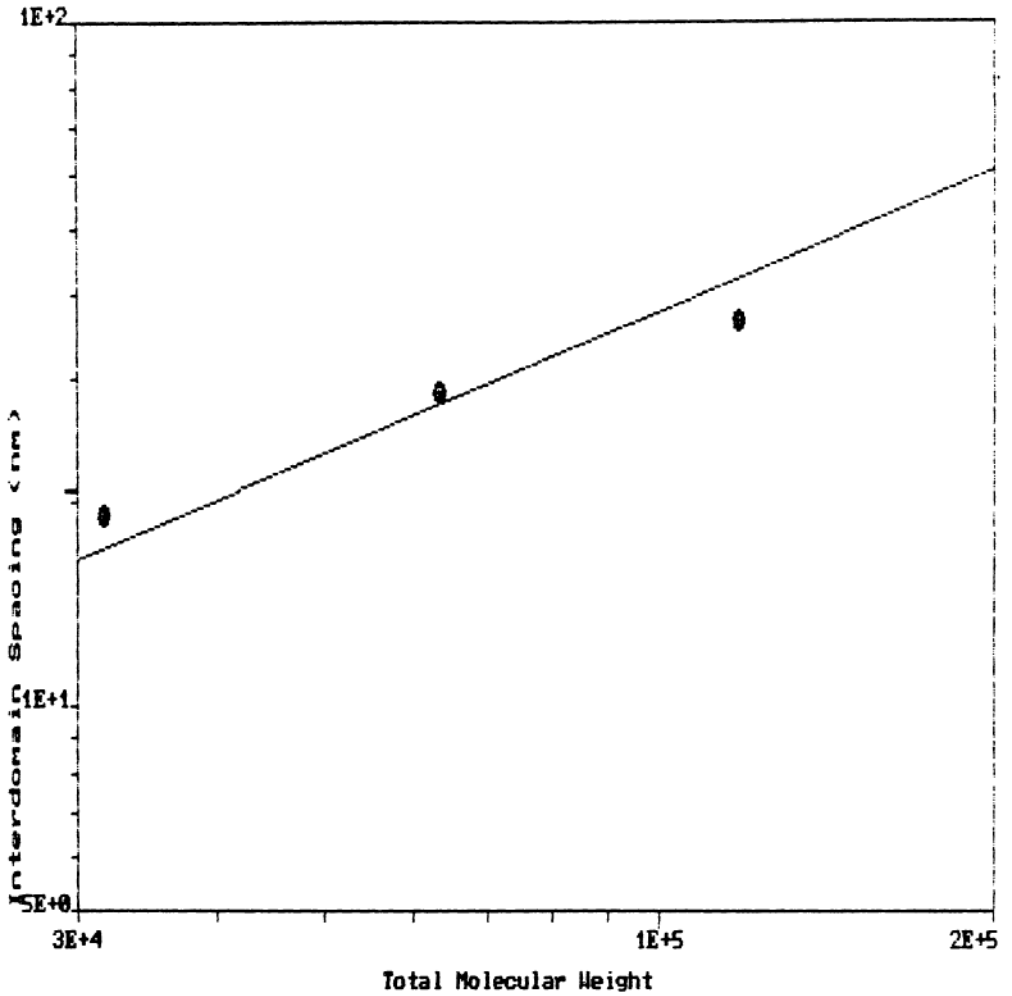

Figure 4.14c Log-log plot of domain radius vs graft molecular weight with 2/3 slope line.

molecular weight scaling relationship determined for the graft copolymers are well within experimentally determined values quoted in section 2.2.3 for spherical, cylindrical and lamellar diblock microstructures.

As the PSX block size increases for the similar compositions deviation from the 2/3 power is expected. As the number of grafts/backbone becomes less than unity (Table 4.4), the amount of homopolymer PMMA in the system increases. From this one would anticipate interdomain distance scaling behavior to approach the Gaussian chain in the bulk, scaling with molecular weight to the 1/2 power as the fraction of homopolymer increases. The magnitude of deviation from the 2/3 power law would be proportional to the amount of homopolymer in the system, asymptotically approaching the 1/2 power. Preliminary interdomain spacing estimates from TEM micrographs of 30/16 and 40/16 specimens support this proposed trend.

From interdomain spacing-molecular weight scaling relationships, the 16 Wt.% PSX graft copolymers followed the 2/3 power law when modelled as diblocks or triblocks based on $\langle M_n \rangle$ values determined by NMR. The agreement of the interdomain spacings to the 2/3 power law indicates the number average molecular weight between grafts is related to interdomain distances as suggested earlier. Since only the

absolute value of the interdomain distances will change for di- or triblock architecture, the type of phase behavior can not be delineated from the interdomain scaling relationships. Nevertheless, the breakdown in the long range ordering of the spherical domain structure was in consonance with the heterogeneous nature of the PMMA continuous phase indicated by compositional analysis. The well defined PSX grafts formed domains that closely followed the scaling relationships derived for di- and triblocks, as evidenced by the close correlation to the 2/3 power law.

4.3 PMMA-g-PSX 45 Wt.% Siloxane Series

Microstructural Analysis of Thin- and Thick-Cast Films

Similar microstructures were observed for the thick- and thin-cast films in the 5/45 sample (Figure 4.15). TEM photomicrographs of the thick- and thin-cast 1Ø/45 and 2Ø/45 graft copolymers (Figure 4.16 and 4.17 respectively) exhibited significantly different morphological textures. The similar microstructure observed in the 5/45 system cast with very slow solvent evaporation rate (thick -cast) suggests that the observed morphological texture of the thin-cast films are determined primarily from thermodynamic

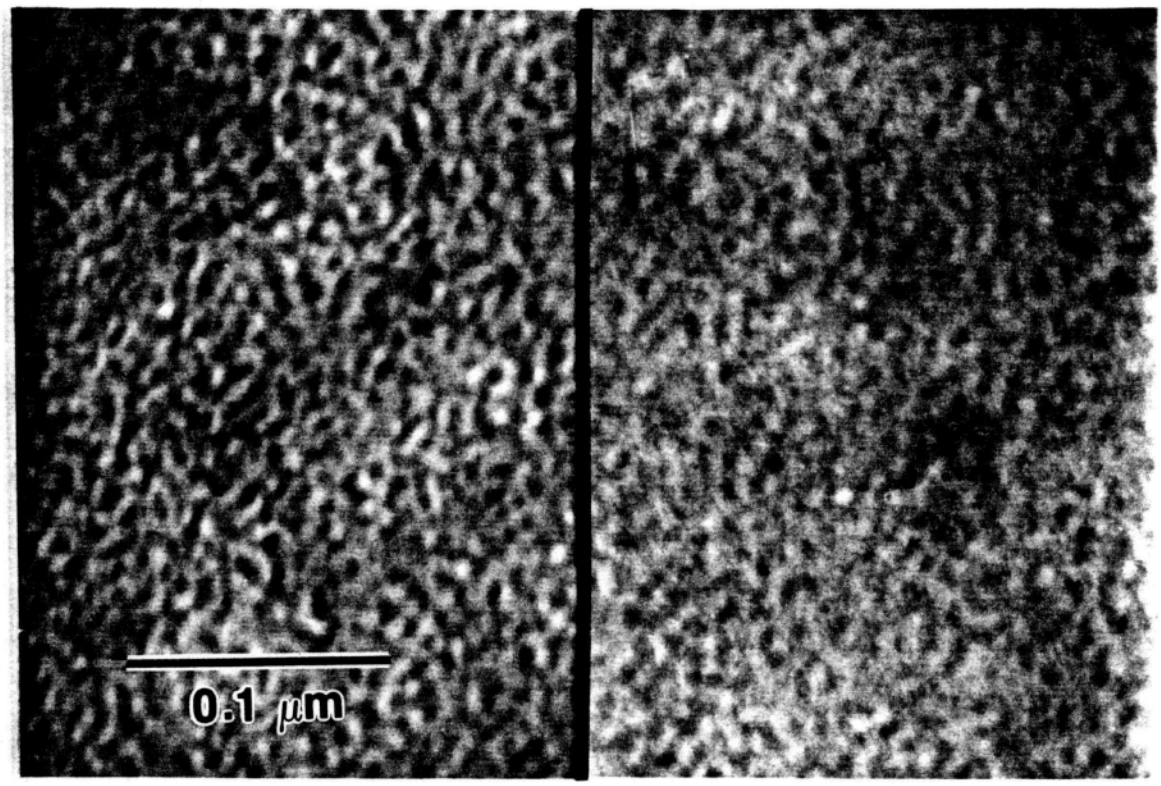

Figure 4.15 TEM micrographs of 5/45 PMMA-g-PSX thick-cast (right) and thin-cast (left) films.

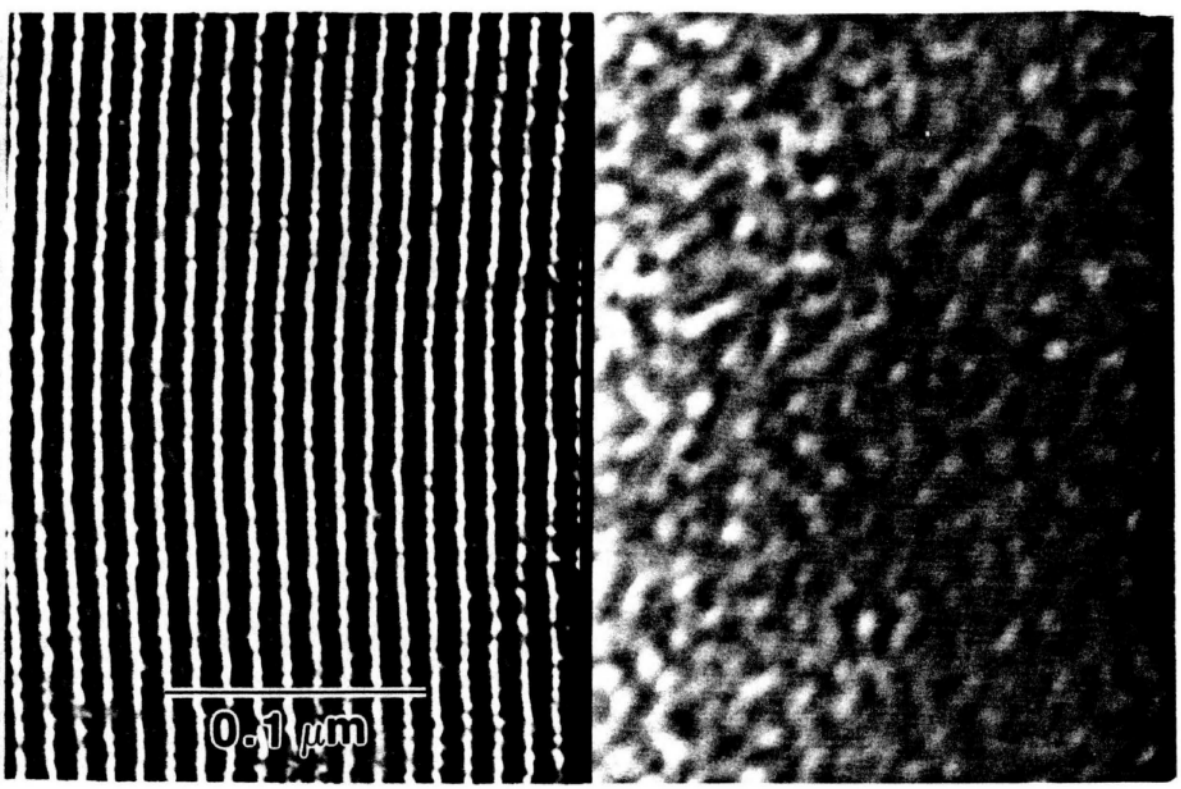

Figure 4.16 TEM micrographs of 10/45 PMMA-g-PSX thick-cast (right) and thin-cast (left) films.

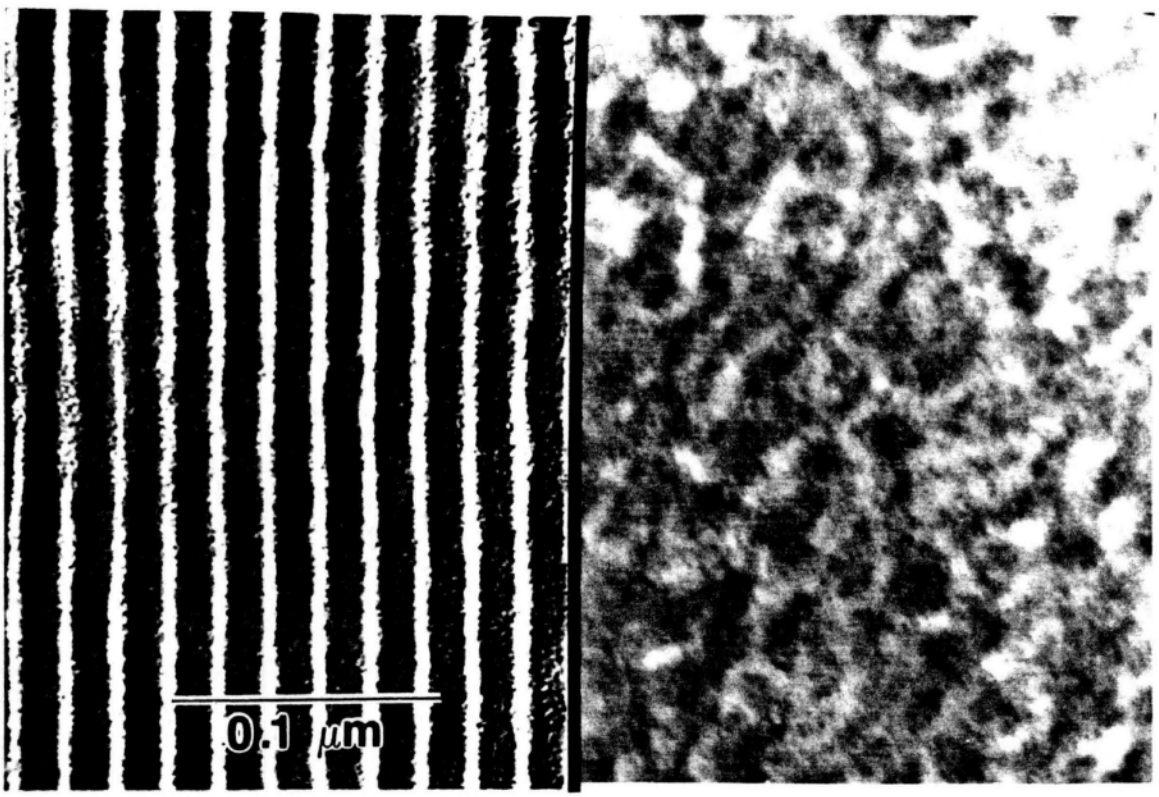

Figure 4.17 TEM micrographs of 20/45 PMMA-g-PSX thick-cast (right) and thin-cast (left) films.

and kinetic influences, and not any effects that result from the dynamic nature of the thin-casting process. The existence of a real structure is further supported by the increasing scale of the thin-cast microstructure with increasing graft molecular weight. That is, during microstructural formation (between concentrations C_2^* and C_3^*) the discrete structures seemed to equilibrate, or adjust their dimensions, in response to the larger graft molecular weight. Taking into account these observed differences in phase behavior, the variation between the thin- and thick-cast microstructures may be explained by the relatively short time elapsed between concentrations C_2^* and C_3^* resulting from the rapid evaporation of the solvent in thin-cast films.

Assuming the thin-cast microstructure is present at C_2^*, and microstructure at C_3^* is characterized by the thick-cast texture, the type of phase behavior between those critical concentrations may be delineated. This assumption is quite reasonable, since the difference in the time period between the critical concentrations for the two casting methods is several orders of magnitude (several seconds for the thin-cast films as opposed to 10-20 hours for the thick-cast films). As discussed in the section 2.2.5 of the literature review, two types of phase behavior are typically observed

between concentrations C_2^* and C_3^*. The 16 Wt.% PSX system and the 5/45 copolymer (actual compositions are listed in Table 4.3) exhibited only one type of microstructure in this concentration range and would then be considered Type I in behavior. However, the substantial differences observed in the microstructures for the 10/45 and 20/45 samples are indicative of a phase transition from disordered bicontinuous to well-ordered lamellar (10K) or cylindrical (20K) structures, thus exhibiting Type II behavior. Hence, during the initial stages of phase separation, all the graft molecular weights obtain a disordered bicontinuous morphology. Given enough time, the 10/45 and 20/45 will go through a phase transition and develop a well-ordered, sharply phase separated system. The thin-cast structures have excess interfacial volume resulting from the metastable state. This is particularly evident in the comparison of the 5/45 thin- and thick-cast films, in which the thin-cast case has "fuzzy" siloxane domains. The term disordered bicontinuous means that both components appear to be present in some areas as discrete phase, but in other area as the continuous phase. As mentioned before, a TEM image is a two dimensional projection of a three dimensional object. The fact that a significant amount of grey area exists in the micrographs of the disordered bicontinuous microstructure

indicates that the grey area are projections through both siloxane and PMMA phases. This is a problem when the thickness of the film is not greater than the scale of microstructure, and an image resembling a pure noise object is obtained. Film thicknesses are estimated to be between 20 and 40 nm, which is close to the scale of the microstructure examined. Thermal annealing of the 5/45 copolymer thick-cast film could induce more ordering into the system, and enable more insight into the equilibrium microstructure (which may resemble the ordered bicontinuous structures observed in the star block systems).

4.3.2 Quantitative Analysis and Microstructural Interpretation of Thick-cast Films

Due to the complex nature of the macromer graft systems, it is important to consider differences in the MWD and compositional distributions before an analysis of the phase behavior of the systems. From examination of the membrane osmometry, GPC, differential viscometer and isorefractive index analysis used in molecular weight analysis and SCFE results, several trends develop. First, the compositional distributions narrow as the graft molecular weight decreases for the same average composition.

Second, the copolymer MWD, and more importantly the PMMA backbone MWD tend to narrow with increasing graft molecular weight at similar compositions. Narrower composition and molecular weight distributions would indicate better agreement between the calculated number average graft/backbone and the real system. For the sake of simplicity, the behavior of the system will be analyzed on the basis of average values of composition and molecular weight, which seem to represent of the observed trends in the microphase separated behavior. Consequently, the only controlled variables used to describe differences in microstructural behavior are the number of grafts/backbone (block architecture) and graft molecular weight.

The effect of block architecture (number of grafts/backbone) on phase behavior is most dramatically illustrated in Figure 4.18 (45 Wt.% PSX PMMA-g-PSX graft copolymer series). As the number of grafts/backbone goes from 1.6 (2Ø/45) to 4.2 (1Ø/45) a cylindrical-to-lamellar phase transition occurs. For the 2Ø/45, specimen the well ordered cylinders had both axial (end view in Figure 4.18a) and longitudinal (Figure 4.18) orientations in the specimen, sectioned perpendicular to the plane of the thick-cast film. Sections taken perpendicular and parallel to the plane of the film were required for the positive identification of

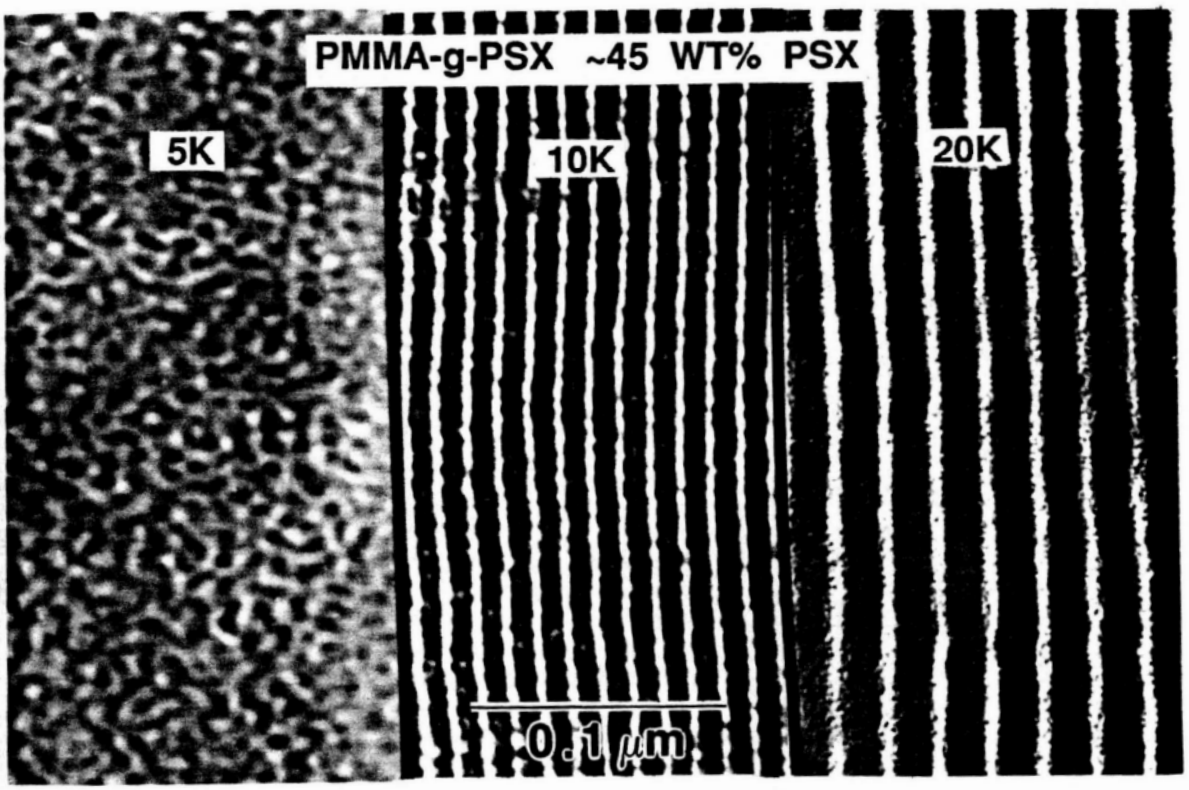

Figure 4.18 TEM micrographs of (from right to left) 5/45, 10/45 and 20/45 thick-cast samples.

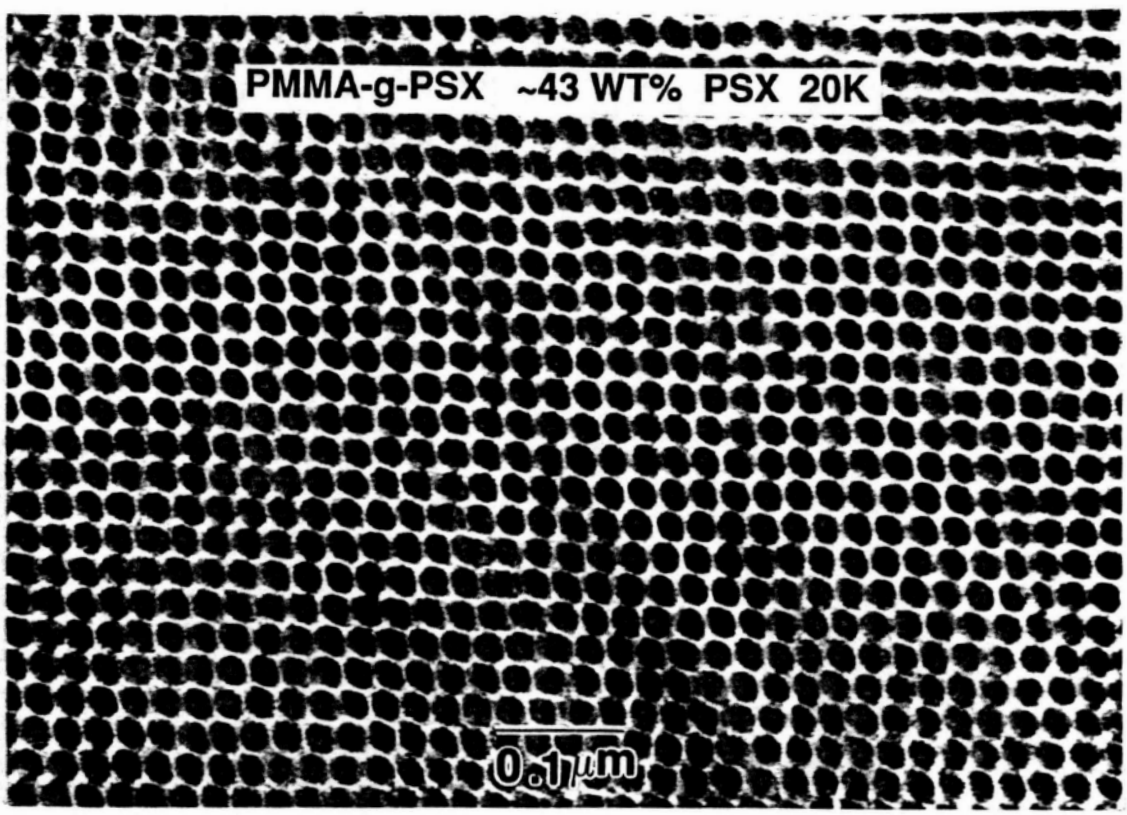

Figure 4.18a TEM micrograph of end view of the 5/45 cylindrical structure.

the lamellar microstructure of the 10/45 copolymer. The actual Wt.% PSX of the 10/45 is slightly higher than 45 Wt.% (actually 48 Wt.%). TEM analysis of a 10/42 specimen revealed a lamellar morphological texture, such that a phase transition due to the higher Wt.% PSX in the 10/45 specimen was ruled out. Another phase transition (lamellar-to-disordered bicontinuous) was observed as the number of grafts/backbone was increased from 4.2 to an average of 9.6.

The effect of the number of grafts/backbone on phase behavior may be rationalized in terms of the various factors involved with of the minimization of free energy. Generally, the energy minimization problem of the balancing of the entropic constraints (conformation restrictions resulting from junction placement and maintenance of uniform density) with the surface area to volume ratio considerations associated with diblock microphase separation will apply to macromer graft copolymers, with an additional facet which includes the conformational restrictions placed on the system by the number of grafts/backbone. It follows that contribution of these additional constraints to the overall free energy of the system, as determined by the number of grafts/backbone, will strongly influence the type of micro-structure thermodynamically favored.

The restrictions placed on the backbone by the placement of multiple grafts onto the backbone seem to be twofold. As the number of grafts/backbone increases for graft copolymers of similar molecular weights, the number of chemical junctions (that must reside in the interphase region) per backbone increases, resulting in an increased loss in the placement entropy for the backbone. Additionally the average distance between grafts decreases with increasing number of grafts/backbone. If the average molecular weight between grafts decreased enough, packing might be subject to similar excluded volume effects predicted and observed for the core of starblock copolymers. In other words, the backbone may be forced assume a radial orientation to reduce overcrowding effects of the grafts. This further restricts the PMMA chain conformations: additional conformational entropy is lost due to the increase in the number PMMA segments with both chain ends restricted.

Another quite interesting effect is observed in the 1Ø/45 and 2Ø/45 specimens. Even though broad molecular weight distributions are present, these systems exhibit quite uniform interdomain periods and highly ordered structures. This suggests that the chains are able to pack into the domain space so as to compensate for the broad

molecular weight distributions. Typically, highly ordered structures observed in di-and triblocks systems are thought to result from the well defined, simple topology and narrow MWD of these systems. Recently Hashimoto, et al.[89] showed that a 50/50 blend of diblocks of approximately the same composition and different molecular weights (one diblock being twice the molecular weight of the other) exhibited a lamellar microstructure with domain identity periods in between those observed for each respective pure diblock. It was suggested that the domains obtained spacings representative of the $\langle M_n \rangle$ value of the two blocks and the molecules packed in domain space such that they compensated for molecular distributions. These observation seems to be consistent with the uniformly spaced and well ordered microstructures observed for the 10/45 and 20/45 graft copolymers that have a broad MWD of the PMMA component.

The comparison of the 16 Wt.% PSX and 45 Wt.% PSX series reveals some interesting aspects of the phase behavior of the graft system. As was establish earlier, the spherical morphology of the 16 Wt.% series did not exhibit any periodicity. Since the cylindrical and lamellar structures of the 10/45 and the 20/45 did exhibit periodicity, it appears that at 50 volume % PSX develops a highly ordered array of cylindrical or lamellar microphases,

and forces the PMMA to uniformly fill the space between them. In contrast, the lower volume fraction (20 vol.%) seems to have the interdomain spacings determined by the broad MWD PMMA backbone, as illustrated by the disordered packing in the TEM micrographs and the absence of higher-order maxima in the SAXS spectra of the spherical domains. However, the interdomain distances do represent PMMA $\langle M_n \rangle$ values between the spherical domains as judged by the close agreement of the interdomain distance scaling relationships with the 2/3 power law.

When attempting quantitative measurement of interdomain identity periods of longitudinal views of cylindrical and lamellar morphological textures there are basically two factors to consider: (1) the projected spacings in the image will depend upon the angle of the plane of the structure to the microtome knife, and (2) the angle between the sectioned interface and the incident beam. Changing the angle of the interface from parallel to the beam should increase the spacing the secant of the tilt angle[78]. Furthermore, a beam passing through the specimen at angles other than normal to the plane of the structure results in decreased contrast (increased grey area between domains). Therefore, maximizing the contrast through variation of the tilt angle may be used as a qualitative method of determining proper orientation of

the specimen. The other factor is deformation of the sample during microtoming: it has been shown[7,8] that lamellae spacings changed with microtoming direction.

Quantitative analysis was performed on the end view of the cylindrical domains of the 20/45 sample. From the centers of mass calculated for each domain, interdomain distances were found to be 28.1 nm (+ or - 1.6 nm error from measurements). An interdomain identity period of 26.9 nm was determined from volume fractions calculations assuming a hexagonal packing for the cylinders. The general agreement between calculated and measured values indicates the cylinders are arranged in a hexagonal packed lattice.

4.4 Microstructural Differences in the Polyarylester-Siloxane Series With Varying Processing Conditions

The nomenclature adopted for the polyarylester-polysiloxane system is as follows; a perfectly alternating copolymer composed of an arylester block of approximately 5000 g/mol and a polydimethylsiloxane block 5000 g/mol will be referred to as 5/5 PA-PDSX. Likewise, a 5/5 PA-PFSX(50) represents a siloxane with 50% fluoropropyl groups and a 5/5

PA-PPSX(5Ø) has 5Ø% phenyl siloxane character. The chemical structures of each type of siloxane are in Figure 3.1. The TEM photomicrographs of the 5/5 PA-PDSX, 5/5 PA-PFSX(5Ø) and 5/5 PA-PPSX(5Ø) perfectly alternating copolymers, under the various processing conditions (thick-casting, compression molded and thin-casting) all exhibited bicontinuous microstructures. However, differences among the microstructure were observed depend upon the chemistry of the siloxane and the processing conditions.

4.4.1 Microstructural Analysis of Thick-Cast Samples With Varying Siloxane Character

For convenience a side by side comparison of the thick cast specimens are presented in Figure 4.19. The 5/5 PA-PDSX (Figures 4.19 and 4.2Øa) and 5/5 PA-PFSX(5Ø) (Figures 4.19 and 4.2Øb) thick-cast samples exhibited the highest degree short-range order (<6Ø nm). The regions of ordering in the 5/5 PA-PDSX and 5/5 PA-PFSX(5Ø) thick-cast samples are indicated by the arrows on the TEM micrographs. For the 5/5 PA-PDSX the region indicated is a radial arrangement on the order of 5Ø nm of alternating siloxane (dark phase) and arylester (light phase) domains. Similar structures are

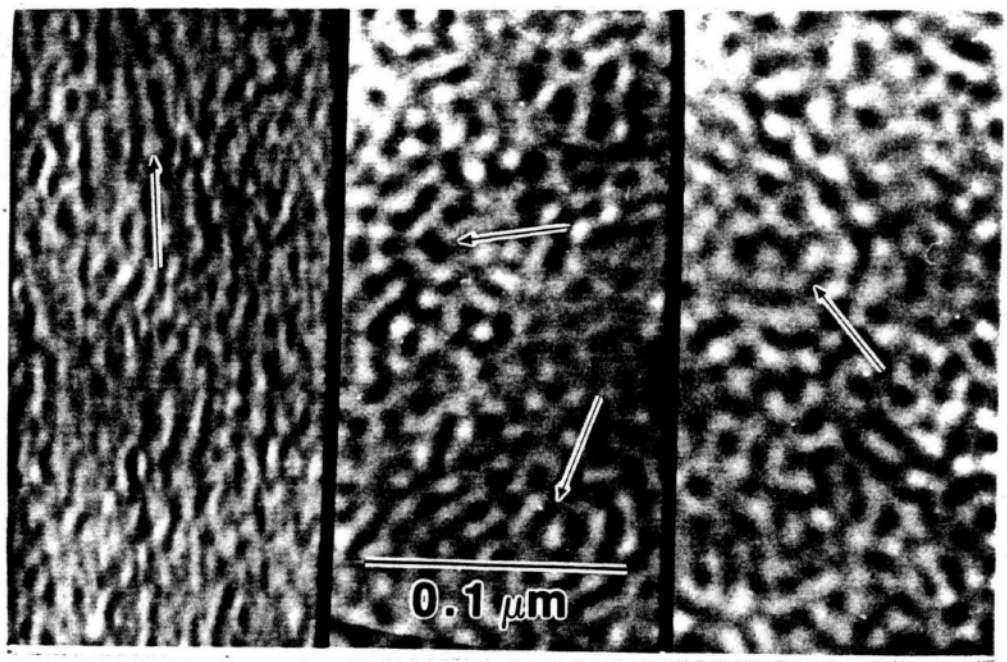

Figure 4.19 TEM micrograpahs of 5/5 PA-PDSX, 5/5 PA-PFSX(50) and 5/5 PA-PPSX(50) thick-cast (from right to left).

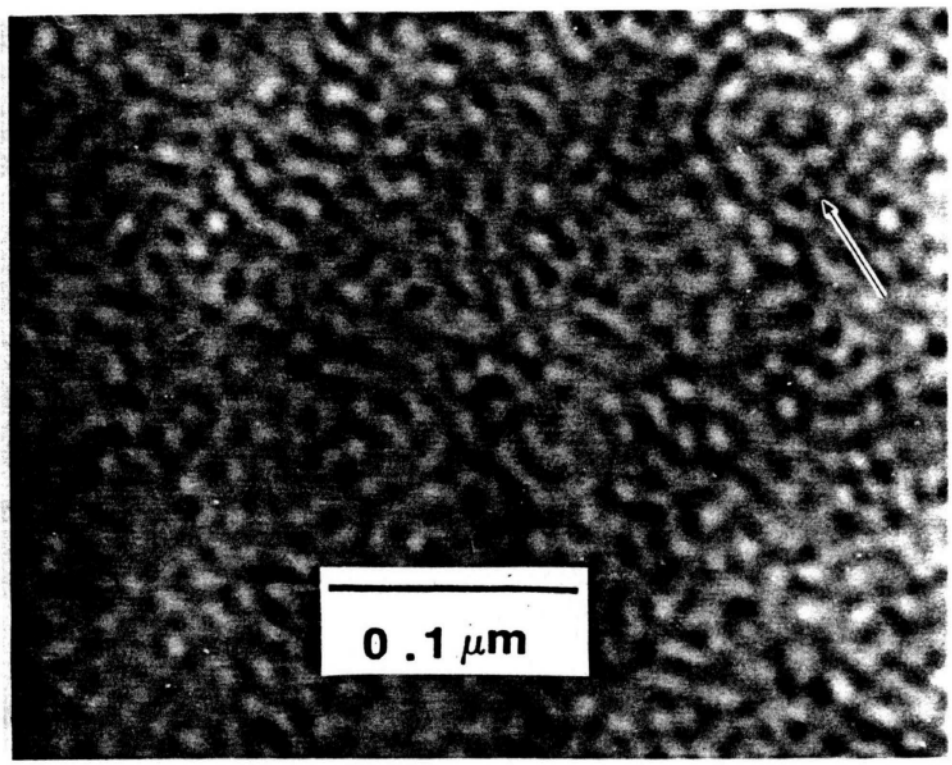

Figure 4.2Øa TEM micrograph of 5/5 PA-PDSX thick-cast film.

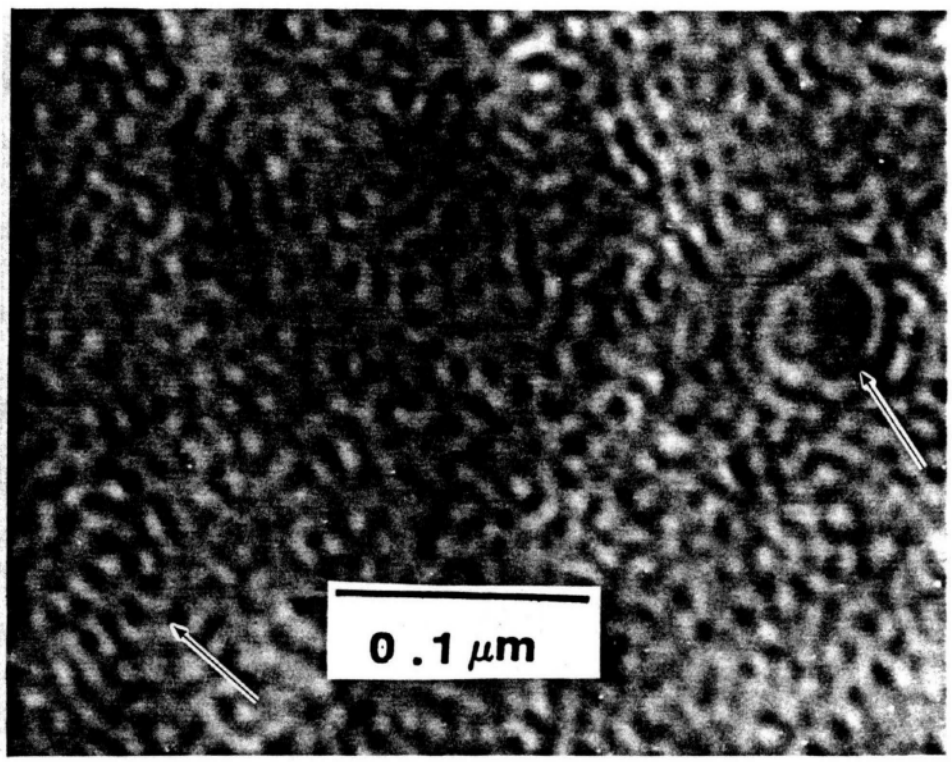

Figure 4.2Øb TEM micrograph of 5/5 PA-PFSX(5Ø) thick-cast film.

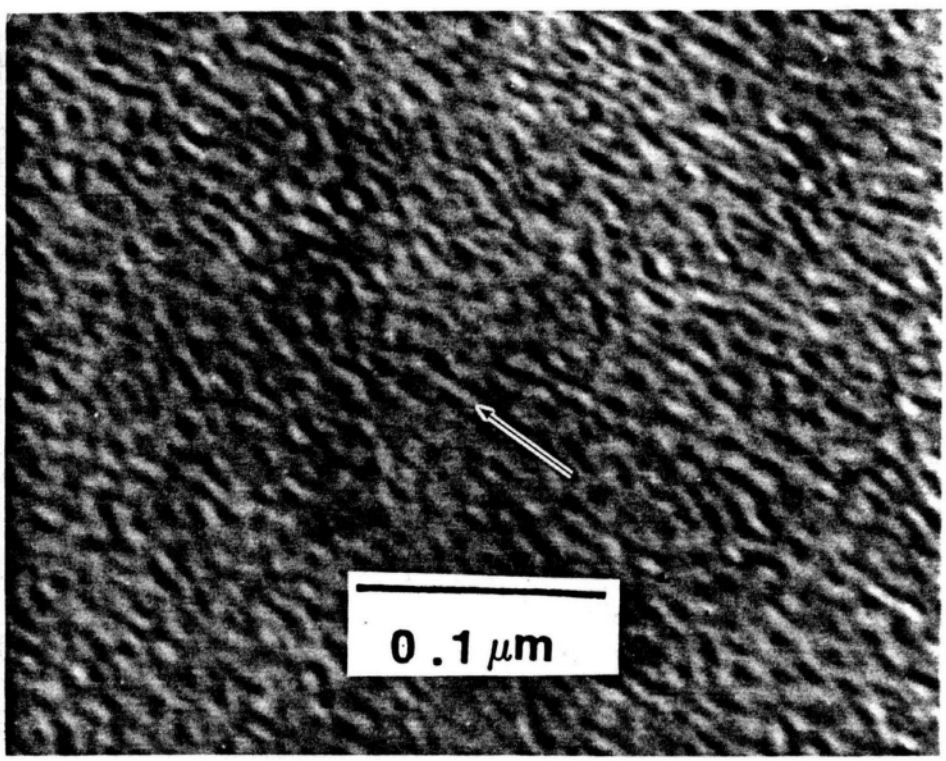

Figure 4.20c TEM micrograph of 5/5 PA-PPSX(50) thick-cast film.

shown in the 5/5 PA-PFSX(5Ø) thick-cast specimen. In contrast, examination of the thick-cast 5/5 PA-PPSX(5Ø) (Figure 4.19 and 4.2Øc) micrographs revealed no regions of short-range order, and smaller ester and siloxane domains than the 5/5 PA-PDSX and 5/5 PA-PFSX(5Ø). Additionally, the 5/5 PA-PPSX(5Ø) specimen seemed to have a uniaxial orientation of ellipsoidal domains.

A comparison of siloxane oligomer T_g and the T_g of the siloxane incorporated into the copolymer allows a relative assessment of compatibility of the different types of siloxane character with the arylester. For a completely miscible system, a single T_g that is proportional the weight percent of each component is typically observed. Extending this to microphase separated systems, generally a more compatible polymer (in this molecular weight range) will have greater interphase thickness or a greater interphase volume, therefore more phase mixing. For a component with a lower T_g mixing with a higher T_g component, the greater degree of mixing will inhibit the large-scale cooperative motion associated with the onset of T_g, thus raising the T_g of the lower T_g components.

From Table 3.1 and 3.2 the siloxane compatibility with the arylester phase generally increases with varying the siloxane character: PPSX, PFSX and PDSX respectively.

Additionally, the PPSX oligomer has a significantly higher T_g (-74°C) as compared to the PFSX (-1Ø4°C) and PDSX (-123°C) oligomers. Since compositions (volume fractions) are approximately equal for each sample, the increased compatibility and the decreased mobility (due to the stearic hinderance effects of the bulky phenyl substituent) of the PPSX alter the nature of the microphase separated behavior causing differences in the size and orientation observed in the morphology. Although, small differences in the T_g and compatibility with the arylester phase exist between the PDSX and PFSX, no significant microstructural differences were observed for the 5/5 PA-PDSX and 5/5 PA-PFSX(5Ø) specimens, suggesting that those small differences in compatibility do not significantly affect the microphase separation behavior.

4.4.2 Microstructural Differences in Compression-molded Specimens With Varying Siloxane Character

The regions of domain periodicity or alignment exhibited in the 5/5 PA-PDSX, 5/5 PA-PFSX(5Ø) and 5/5 PA-PPSX(5Ø) thick-cast films were not observed in the compression-molded (CM) samples (Figures 4.21a, b and c) of the same respective siloxane character. Aside from these

ordering differences between the thick-cast and compression-molded samples, the siloxane and arylester domains for all three types of siloxane character appeared distorted and unsymmetric when compared to the uniform spherically shaped domains in the 5/5 PA-PDSX and 5/5 PA-PFSX(5Ø) thick-cast films. Since the 5/5 PA-PPSX(5Ø) thick-cast structures were not as ordered as the other two types of thick-cast structures, differences between the thick-cast and compression molded microstructures in this system are much more subtle. The compression molded 5/5 PA-PPSX(5Ø) sample did not exhibit the same short range domain alignment and uniform shape as was observed in the thick-cast sample. From these results it is evident that compression-molded film (formed via rapid cooling from the melt under 1Ø,ØØØ psi) did not allow the same type of short range order observed in the thick-cast. Furthermore, the nonuniform shapes of the both the siloxane and arylester domains implies the phase separated structures may be deformed by either differences in the thermal contraction of the plates and polymer film or the pressure induced flow of the melt. Subsequently the sheared domains are trapped in metastable shapes as the film is cooled fairly rapidly below the arylester T_g. Implicit in this hypothesis is that the phase separation transition temperature was not exceeded during compression- molding. If

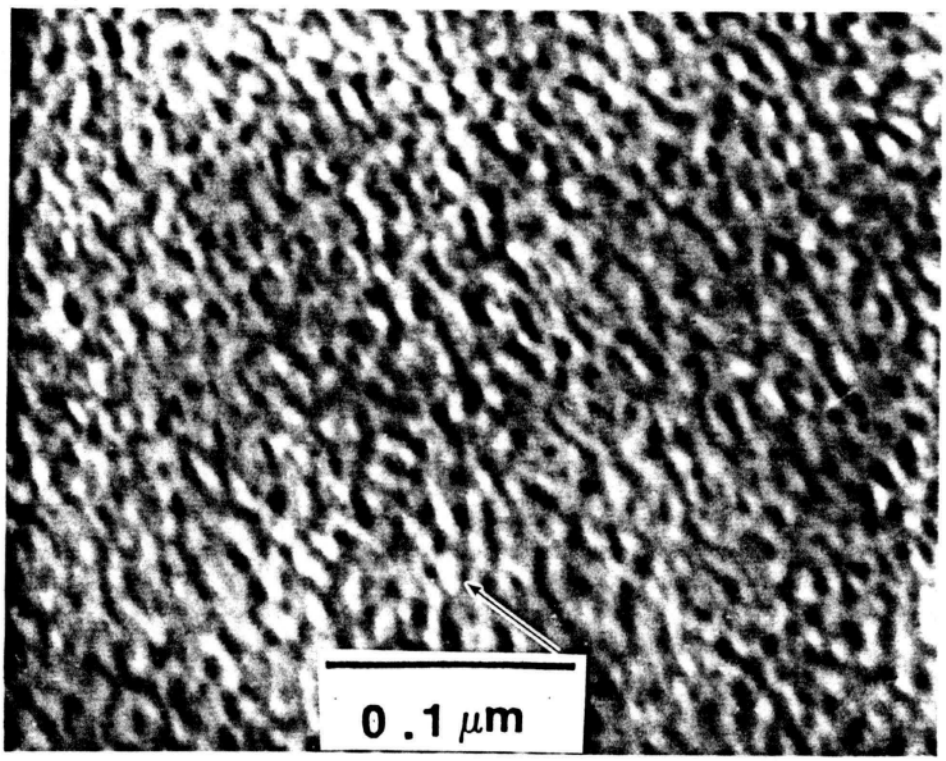

Figure 4.21a TEM micrograph of 5/5 PA-PDSX compression-molded film.

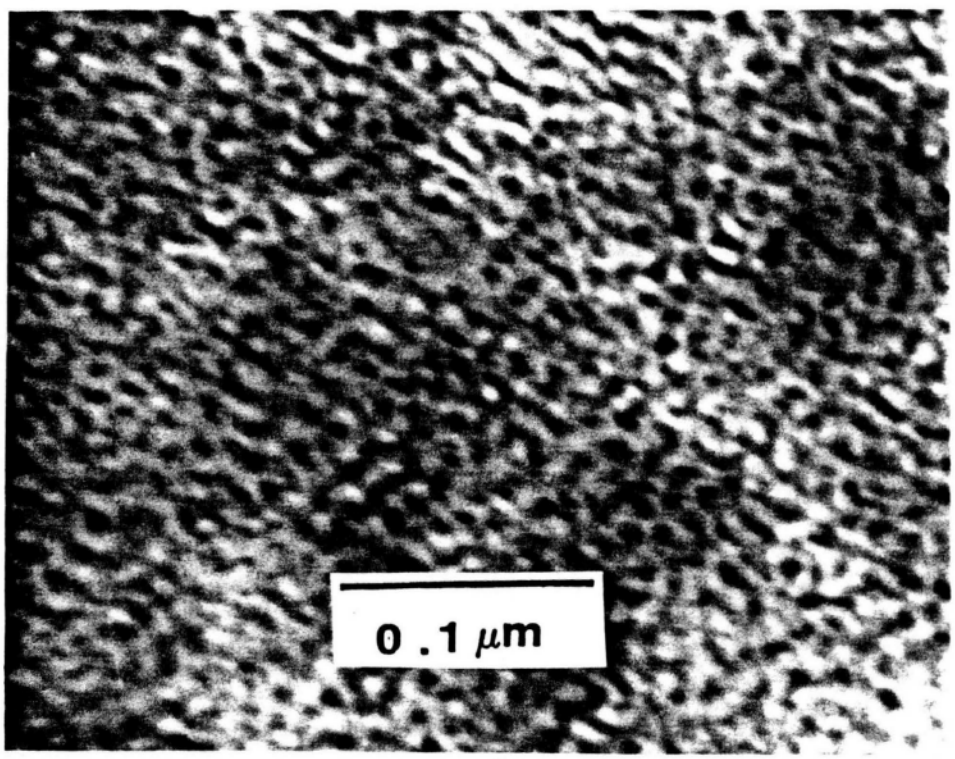

Figure 4.21b TEM micrograph of 5/5 PA-PFSX(5Ø) compression-molded film.

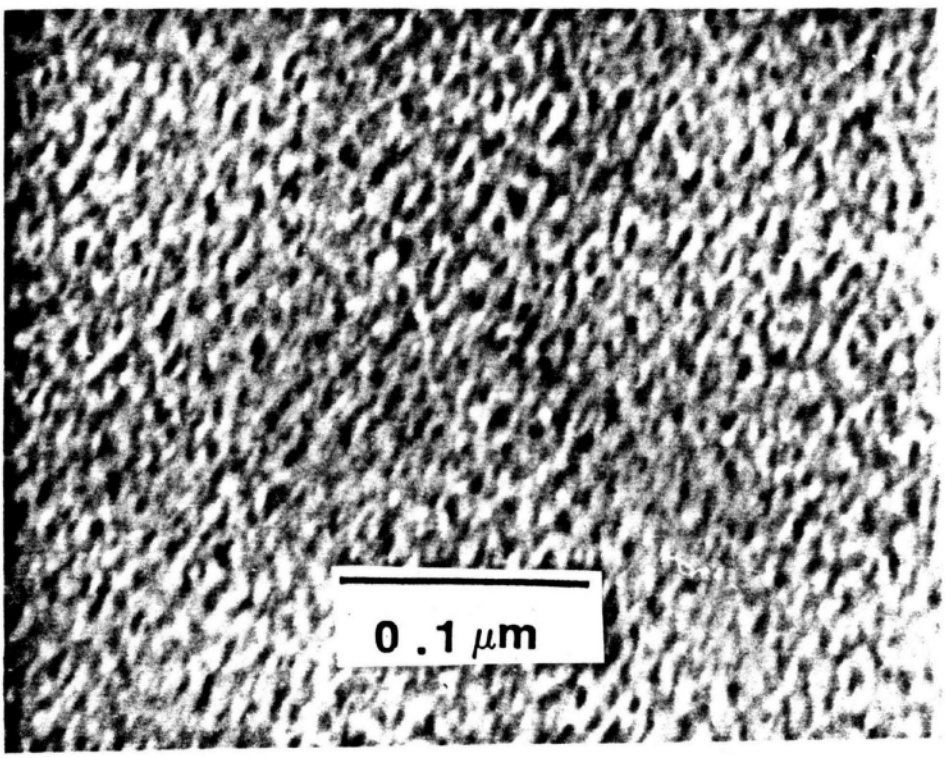

Figure 4.21c TEM micrograph of 5/5 PA-PFSX(5Ø) compression-molded film.

compatibility were significantly enhanced by the increase in temperature (nearing the phase separation transition), the fast cooling rate may also result in a metastable structure similar to the observed microstructure.

4.4.3 Microstructural Analysis of Thin-cast Samples With Varying Siloxane Character

TEM micrographs of the 5/5 PA-PDSX, 5/5 PA-PFSX(50) and 5/5 PA-PPSX(50) thin-cast films (Figures 4.22a, b and c respectively) show microstructural features similar to the thick-cast films. The phase structure of the thin-cast are less defined, signifying increased mixing of the phases as a result of the rapid evaporation rate. The only significant microstructural differences are that the regions of short range ordering observed in the thick-cast films are not present in the thin-cast films. Aside from the ordering, the basic microstructural features are preserved in the thin-cast films. This preservation of basic microstructural features of the thin-cast films suggest that valuable insight into the microstructural behavior of the arylester-siloxane may be gained from the thin-cast film TEM analysis.

The microstructural behavior trends discussed for the different processing conditions are enhanced by the side by

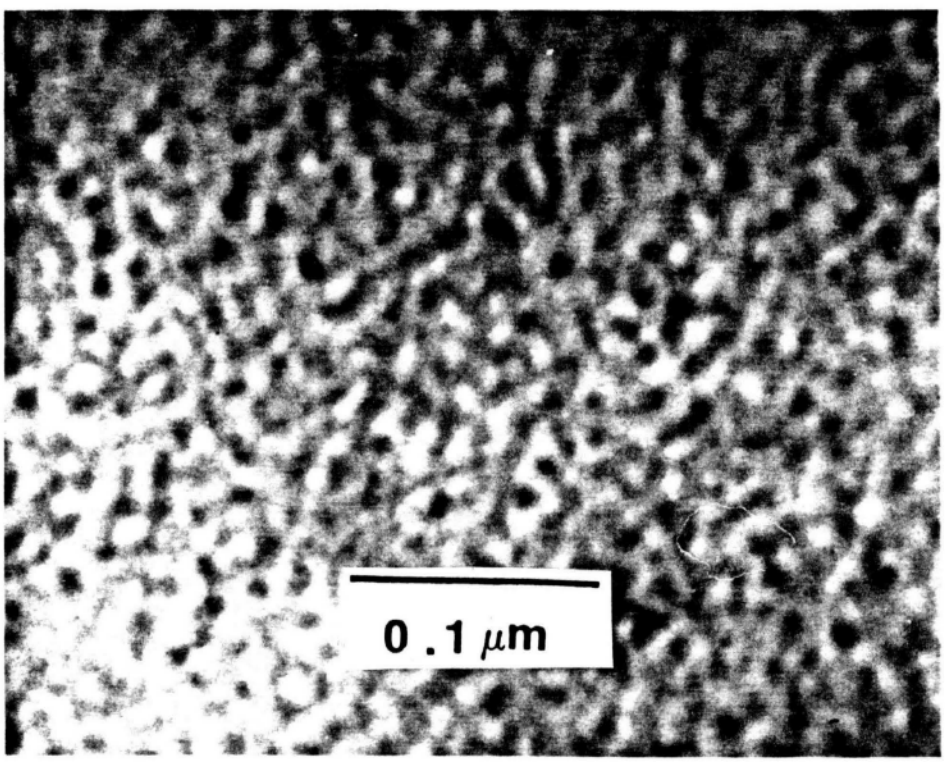

Figure 4.22a TEM micrograph of 5/5 PA-PDSX thin-cast film.

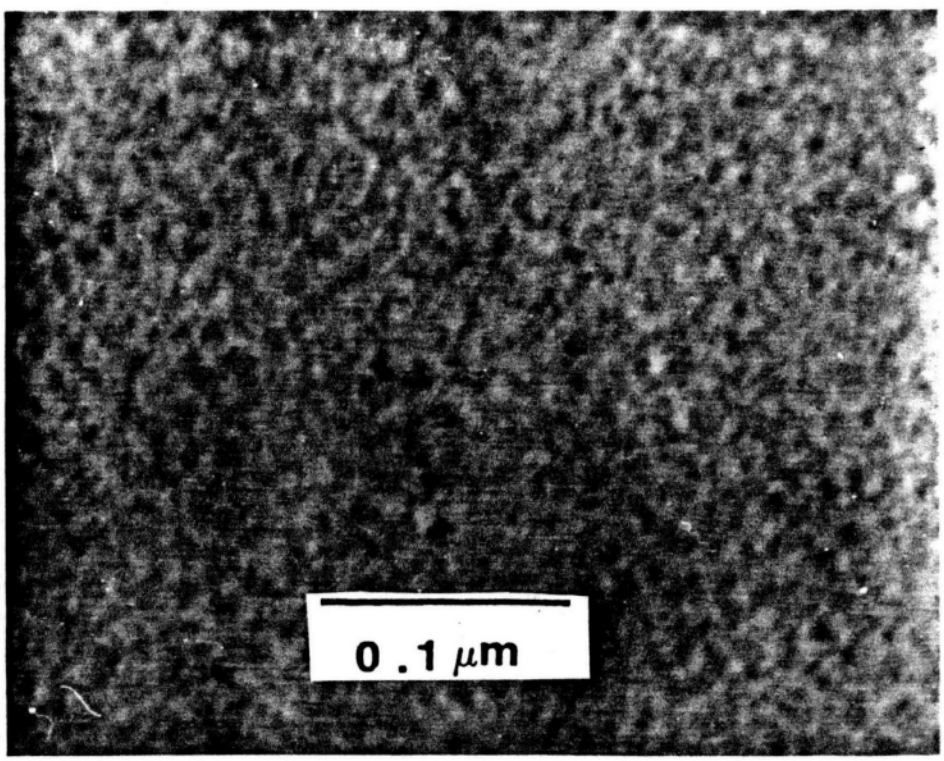

Figure 4.22b TEM micrograph of 5/5 PA-PFSX(5Ø) thin-cast film.

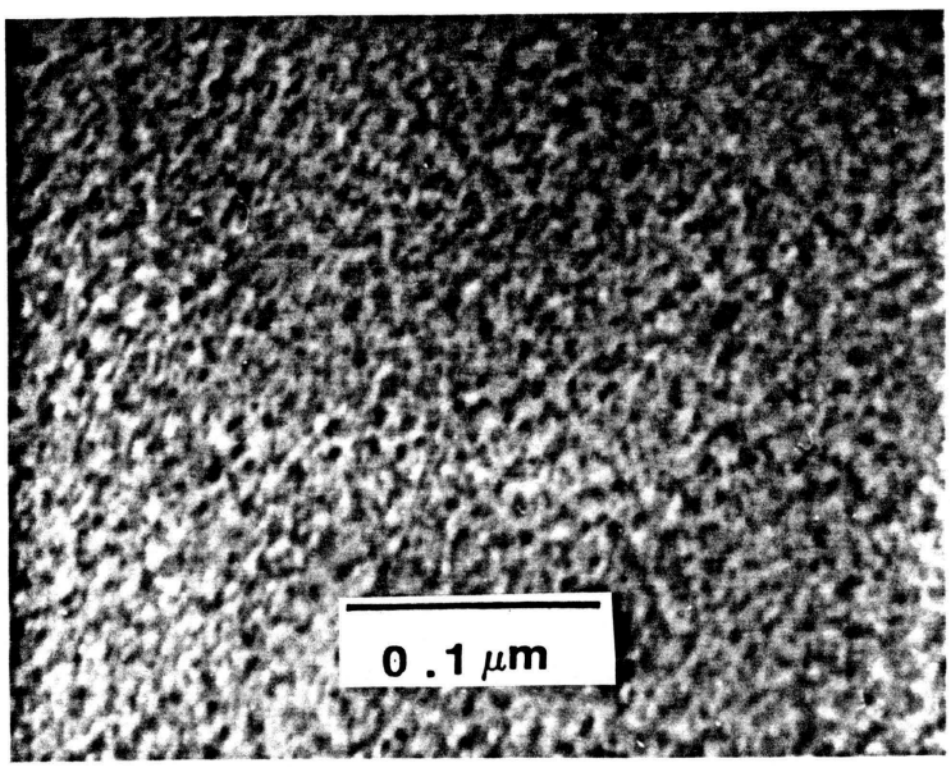

Figure 4.22c TEM micrograph of 5/5 PA-PPSX(5Ø) thin-cast film.

side comparison of the 5/5 PA-PDSX (Figure 4.23) system. Where the change from a short range ordered system with uniformly shaped domains in the thick-cast sample to the disorder and deformed or unsymmetrical domains in the compression molded sample is evident. As well, the presence of the same basic bicontinuous microstructure under all three type of processing conditions is clearly evident in Figure 4.23.

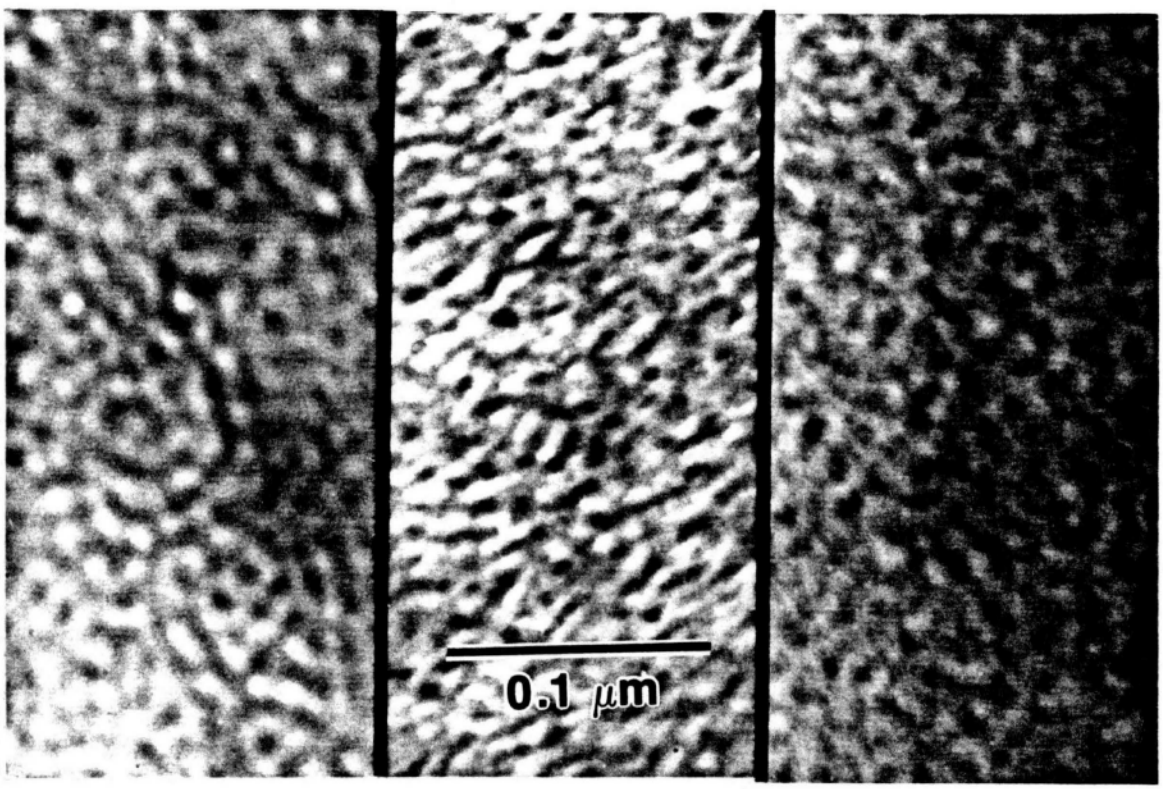

Figure 4.23 comparison of the 5/5 PA-PDSX thick-cast, compression-molded and thin-cast microstructure.

CHAPTER V

SUMMARY AND CONCLUSION

The use of TEM/EDX analysis of thin-cast films was proven effective in several important aspects of qualitative analysis. Homopolymer and oligomeric impurities, common to many copolymerizations, were effectively detected so that steps toward further purification of the polymer systems could be undertaken. It was shown that small changes in reaction conditions produced significant changes in the thin-cast microstructure, such that qualitative monitoring of reaction conditions was possible. Qualitative analysis was also shown to give an evaluation of work up procedures. By virtue of its ability to quickly and easily monitor and analyze of polymer synthesis and work up procedure, qualitative analysis proved useful as an interactive method in the evaluation of novel multiblock systems where novel synthetic methods or work up procedures were utilized.

In addition it was demonstrated that qualitative analysis of thin-cast films was a quick and easy method of determining blend compatibility, where domains (if present) may be chemically identified by EDX analysis. Intentionally blending a multiblock copolymer (about 10 Wt.%) with a homopolymer corresponding to one of the blocks allows easy

identification of the dark and light phase. The minority component (the copolymer) will contain both light and dark phases, hence matrix color will be representative of the homopolymer.

Computerized quantitative image analysis was utilized to obtain domain size and interdomain distance from TEM micrographs. Although some limitations existed, it was shown to be a less subjective method of quantitative determination microstructural dimensions.

For thick-cast films of PMMA-g-PSX (16 Wt.% PSX) the siloxane was found to form a spherical morphology, and the size of the spheres increased with graft molecular. A log-log plot of domain size vs graft molecular weight revealed that the domains scaled with molecular weight to the Ø.66 power in excellent agreement with the 2/3 power law derived for di- and triblock systems. The interdomain distances obtained from SAXS spectra most closely fit the spacings of a hexagonal close packed lattice determined from volume fraction calculation. However, the absence of higher order maxima in SAXS indicted that no significant amount of periodicity or global ordering was present. When the graft copolymer was modelled as a diblock or triblock, the interdomain distance-molecular weight scaling relationship were found to agree with the 2/3 power law, suggesting that interdomain distances scale with $\langle M_n \rangle$ of the PMMA.

Even though compositional and molecular weight analysis show that both the PMMA-g-PSX 16 and 45 Wt.% PSX series have broad PMMA distributions, the thick-cast 1Ø/45 and 2Ø/45 samples exhibited highly ordered lamellar and cylindrical structures respectively. Therefore, when a large enough volume fraction (about 5Ø% in the 45 Wt.% PSX series) of monodispersed PSX grafts form well-ordered structures, it forces the PMMA backbones to uniformly fill the space between PSX domains. In the PMMA-g-PSX 16 Wt.% PSX series, where the well defined siloxane grafts were present as a lower volume fraction (2Ø%) component, the broad PMMA distribution of the primary influence producing a disordered structure.

Block architecture had a dramatic effect on the morphological textures of the thick-cast PMMA-g-PSX 45 Wt.% PSX series. As the number of grafts/backbone was increased from about 1.5 (2Ø/45 sample) to 4 (1Ø/45 sample) a lamellar-to-cylindrical phase transition was observed. Upon further increase to approximately 1Ø (5/45 specimen) grafts/backbone, the lamellar-to-disordered bicontinuous transition was observed.

In the arylester-siloxane perfectly alternating block copolymer series both the 5/5 PA-PDSX and 5/5 PA-PFSX(5Ø) thick-cast specimens exhibited some short range ordering. The 5/5 PA-PPSX(5Ø) thick-cast sample had a microstructure

that showed a lower degree of order and a slightly smaller scale structure. The observed differences were attributed to the increased compatibility and restricted mobility of the PPSX. These results were corroborated by T_g measurements. The compatibility differences between the PDSX and the PSFX were not sufficient to cause any observable difference in the microstructures.

The high pressure and relatively fast cooling rate of the compression-molded samples affected ordering and shape of the domains. None of the compression-molded samples exhibited the degree of ordering of the corresponding thick-cast specimens. The domains of all the compression-molded samples were typically irregular shaped, possibly reflecting shearing during the flow under pressure of the compression-molding process.

Thin-cast microstructures of the arylester-siloxane and PMMA-g-PSX 16 Wt.% PSX series were similar with the thick-cast structures. Generally the thin-cast structures did not exhibit the same degree of ordering or uniformity as the thick-cast films, however the thin-cast PMMA-g-PSX 16 Wt.% PSX series structures did exhibit a wider distribution of sizes, but the measured average domain sizes of the thin-cast specimens were good agreement with the thick-cast structures. The thin-cast PMMA-g-PSX 45 Wt.% PSX series exhibited a disordered bicontinuous microstructure similar

to that observed in the 5/45 thick-cast film. From a comparison of the thick- and thin-cast films it is apparent that the 10/45 and 20/45 sample if given enough time, via slowing evaporation rate, they will go through a phase transition and form a well ordered lamellar and cylindrical microstructure at longer times.

The vita has been removed from the scanned document